The Dissertation Committee for Rongting Zhang
certifies that this is the approved version of the following dissertation:

# Hybrid Inverse Problems in Molecular Imaging

Committee:

Kui Ren, Supervisor

Yen-Hsi Tsai

Oscar Gonzalez

Omar Ghattas

George Biros

# Hybrid Inverse Problems in Molecular Imaging

**by**

**Rongting Zhang, B.S., M.A.**

**DISSERTATION**

Presented to the Faculty of the Graduate School of

The University of Texas at Austin

in Partial Fulfillment

of the Requirements

for the Degree of

**DOCTOR OF PHILOSOPHY**

THE UNIVERSITY OF TEXAS AT AUSTIN

May 2017

Dedicated to my parents.

# Acknowledgments

First, I would like to thank my advisor, Professor Kui Ren. It is very fortunate for me to have him as advisor. I have learned a great deal from his advice on both research and career during my years at UT Austin. It would be impossible for me to accomplish my research work and this dissertation without his guidance and help.

I would like to thank Prof. Richard Tsai, Prof. Oscar Gonzalez, Prof. Omar Ghattas and Prof. George Biros, for serving as my committee members. I have taken classes with Prof. Tsai, Prof Ghattas and Prof. Biros and I am very grateful for their mentorship during my study at UT Austin.

I am also very grateful to my colleagues Yimin Zhong and Patrick Bardsley for fruitful discussions and encouragement of my research work. It has been a pleasant experience working and studying with them. Especially, I would like to thank Yimin Zhong for various discussions on inverse problems, fast multipole methods and transport equations.

Many results presented in the dissertation are obtained collaboratively with Professor Kui Ren. The results in chapter 3 is based on a joint work with Professor Kui Ren and Yimin Zhong. I would like to thank them for allowing me to present the results in this dissertation.

I would also like to thank the Department of Mathematics for their

continued support through teaching assistantships. The graduate advisors, Prof. Thomas Chen and Prof. Dan Knopf and the administrative staff of the department, Elisa Bass, Sandra Catlett and Eva Hernandez, have provided me tremendous help on various issues during my years at UT Austin. I would like to thank them for everything they have done for me and for the department.

Finally, I thank my parents for their support and love. I would also like to thank Zhao Liu, Yuanzhong Xu, Ahmad Issa, Yunan Yang, Hui Yu, Xiaoxia Wu, Zheng Li, Shaohua Wan, Junlin Yi and all my other friends who accompanied, encouraged and helped me during the past six years.

# Hybrid Inverse Problems in Molecular Imaging

Publication No. _____

Rongting Zhang, Ph.D.
The University of Texas at Austin, 2017

Supervisor: Kui Ren

Hybrid inverse problems refer to inverse problems where two partial differential equations of different types are coupled. Such problems appear in modern hybrid imaging modalities where we attempt to combine two different imaging modalities together to achieve imaging abilities that could not be achieved by either of the two modalities alone.

This dissertation is devoted to the study of hybrid inverse problems in two molecular imaging modalities that are based on photoacoustics: the coupling of ultrasound imaging with optical tomography through photoacoustic effect to achieve high-resolution and high-contrast imaging of molecular functions of biological tissues.

The first inverse problem we study here is related to quantitative two-photon photoacoustic tomography (TP-PAT). The mathematical problem here is to reconstruct coefficients in a semilinear diffusion equation from interior

information on the solution of the PDE. We derive some uniqueness, non-uniqueness and stability results on the reconstruction problem under various circumstances. Moreover, we propose a few image reconstruction algorithms and perform numerical simulations using these algorithms to complement our theoretical analysis.

The second inverse problem we study here arise in quantitative fluorescence photoacoustic tomography (fPAT). The objective is to reconstruct optical coefficients in a system of radiative transport equations from interior data on the solution to the system. We study the question of uniqueness and stability of reconstructions and develop some direct and iterative image reconstruction methods for the reconstruction of the quantum efficiency and the fluorescent absorption coefficient. We also perform numerical studies on the inverse problems for media with different absorption and scattering properties.

# Table of Contents

# List of Figures

# Chapter 1

# Introduction

Inverse problems in optics and acoustics have been extensively studied in recent years. These problems have many applications in biomedical imaging where we are interested in learning physical properties of biological tissues from acoustic or optical measurements. Many imaging methods of interests in biomedical imaging are non-invasive in the sense that we would only have measurements outside or at the boundary of the domain.

Even though an ideal imaging modality would produce images that have both high resolution and high contrast, most traditional modalities are observed to only have one of the two desired properties when used independently. To achieve both high resolution and high contrast, a natural idea is to combine different imaging modalities with complementary properties. For example, optical tomography is a high-contrast and low-resolution imaging modality. It has high contrast as the optical properties of healthy and unhealthy tissues are observed to have a large difference. However, its spatial resolution is limited due to multiple scattering of light [13, 15]. Ultrasound imaging, however, exhibits much lower contrast, due to the fact that ultrasound speeds vary little between healthy and unhealthy tissues, but much

higher resolution, due to its ability to focusing accurately. Photoacoustic tomography is an imaging modality that that combines the advantage of optical tomography and ultrasound imaging.

## 1.1 Coupling Optics with Acoustics in PAT

Photoacoustic tomography (PAT) is a hybrid imaging modality based on the photo-acoustic effect, which couples optical and ultrasonic waves. In a PAT experiment, we send near infrared (NIR) light into the medium of interest. As optical radiation propagates, a fraction of its energy is absorbed and generates a local heating of the underlying medium. The medium expanses due to the temperature rise and then contracts when the remaining photons leave the medium. The mechanical expansion and contraction result in an acoustic signal that propagates through the domain of interest. Finally, ultrasonic transducers located at the boundary of the domain record the emitted pressure waves as a function of time. We then intend to infer from the ultrasonic measurements the optical properties of the medium, for instance the optical absorption and scattering coefficients.

It is generally believed that the propagation of near infra-red light in biological tissues can be accurately modeled by the radiative transport equation. Let $\Omega \in \mathbb{R}^d (d \geq 2)$ be the domain of interests and $\mathbb{S}^{d-1}$ be the unit sphere in $\mathbb{R}^d$. We denote by $X = \Omega \times \mathbb{S}^{d-1}$ the phase space and $\Gamma_\pm = \{(\mathbf{x}, \mathbf{v}) \in \partial\Omega \times \mathbb{S}^{d-1} | \pm \mathbf{n}(\mathbf{x}) \cdot \mathbf{v} > 0\}$ its boundary sets. We denote by $u(\mathbf{x}, \mathbf{v})$ the density of photons at location $\mathbf{x}$, traveling in direction $\mathbf{v} \in \mathbb{S}^{d-1}$. Then $u(\mathbf{x}, \mathbf{v})$ solves

the following radiative transport equation [12, 84]

$$\begin{aligned} -\mathbf{v}\cdot\nabla u + (\sigma_a+\sigma_s)u &= \sigma_s \int_{\mathbb{S}^{d-1}} \Theta(\mathbf{v},\mathbf{v}')u(\mathbf{x},\mathbf{v}')d\mathbf{v}', \quad \text{in } X \\ u(\mathbf{x},\mathbf{v}) &= g(\mathbf{x},\mathbf{v}), \qquad\qquad\qquad\qquad\quad \text{on } \Gamma_-. \end{aligned} \tag{1.1}$$

The coefficient $\sigma_a(\mathbf{x})$ and $\sigma_s(\mathbf{x})$ are respectively the absorption and scattering coefficients, and the scattering kernel $\Theta(\mathbf{v},\mathbf{v}')$ describes the probability that a photon traveling in direction $\mathbf{v}'$ gets scattered into direction $\mathbf{v}$.

The initial pressure field generated by the photoacoustic effect can be written as [43]:

$$H(\mathbf{x}) = \Xi(\mathbf{x})\sigma_a(\mathbf{x})K_I(u)(\mathbf{x}), \tag{1.2}$$

where $\Xi$ is the (*nondimensional*) Grüneisen coefficient that measures the photoacoustic efficiency of the underlying medium, and $K_I(u)(\mathbf{x}) = \int_{\mathbb{S}^{d-1}} u(\mathbf{x},\mathbf{v})d\mathbf{v}$ is local photon density at $\mathbf{x}\in\Omega$.

The initial pressure field generated from the photoacoustic effect, $H$, evolves in space and time following the acoustic wave equation [22, 43, 98]:

$$\begin{aligned} \frac{1}{c^2(\mathbf{x})}\frac{\partial^2 p}{\partial t^2} - \Delta p = 0, \qquad & \text{in } \mathbb{R}_+\times\mathbb{R}^d \\ p(0,\mathbf{x}) = H, \quad \frac{\partial p}{\partial t}(0,\mathbf{x}) = 0, \quad & \text{in } \mathbb{R}^d \end{aligned} \tag{1.3}$$

where $c(\mathbf{x})$ is the speed of the ultrasound in the medium. The data that we measure are the solutions to the wave equation (1.3) on the surface of the medium, $p_{|(0,t_{\max})\times\Sigma}$, $t_{\max}$ being large enough and $\Sigma\subset\partial\Omega$, for various excitation light sources.

## 1.2 Hybrid Inverse Problems in PAT

The inverse problem in PAT is to reconstruct optical absorption and scattering coefficients, as well as the Grüneisen coefficient from measured ultrasound signals. This is an inverse problem that involves both optics and acoustics. The problem is usually solved in two steps.

In the first step of PAT, the initial pressure field $H$ is inferred from the ultrasound measurements $p(t, \mathbf{x})|_{(0,t_{\max})\times\Sigma}$. This is a relatively well-known inverse source problem for the wave equation that has been extensively studied in the past [29, 40, 41, 51, 52, 57, 58, 64, 67, 74, 76, 78, 81, 98, 99, 100, 104]. In most of the settings considered, the sound speed is assumed to be known. When sound speed is constant, explicit formulas have been obtained for a large class of geometries of interest [42, 64, 67, 78]. When the sound speed is not constant but known, time reversal algorithms have good performance under non-trapping conditions [8, 58, 98, 105].

In the second step of PAT, which is often called quantitative photoacoustic tomography (QPAT), we intend to reconstruct optical properties ($\sigma_a$ and $\sigma_s$) and the Grüneisen coefficient $\Xi$ from the reconstruction result of the first step, the data $H$ in (1.2). This step has recently attracted significant attention from both mathematical [8, 9, 18, 19, 21, 22] and computational [23, 30, 31, 33, 45, 70, 93, 122, 123] perspectives. The reconstruction problem in this step is identical to diffuse optical tomography (DOT) problem except that here we have interior $H$ while in DOT we only have data on the boundary of the domain. The use of interior data improve the resolution of

the reconstruction significantly. This is the main advantage of photoacoustic tomography over diffuse optical tomography.

Let us remark that most of the past works on hybrid inverse problems in PAT have been done in diffusive regimes of light propagation. Let $U(\mathbf{x}) = K_I(u) \equiv \int_{\mathbb{S}^{d-1}} u(\mathbf{x}, \mathbf{v}) d\mathbf{v}$, where $u(\mathbf{x}, \mathbf{v})$ is solution to (1.1), $\gamma(\mathbf{x}) = \dfrac{1}{3(\sigma_a + \sigma_s)}$, then $U(\mathbf{x})$ solves approximately [34]:

$$\begin{aligned} \nabla \cdot (\gamma \nabla U) + \sigma_a U &= 0, \quad \text{in } \Omega \\ U(\mathbf{x}) &= g(\mathbf{x}), \quad \text{on } \partial\Omega \end{aligned} \tag{1.4}$$

when the underlying medium is strongly scattering but weakly absorbing. In this regime, equation (1.4) provides an alternative mathematical model for the second step of PAT reconstruction. The advantage of this model over the transport model (1.1) is that the diffusion equation is posed in physical space and therefore is computationally less expensive to solve than the transport model.

## 1.3 PAT in Molecular Imaging

The objective of this dissertation is to study hybrid inverse problems in two-photon abosorption photoacoustic tomography (TP-PAT) and fluorescence photoacoustic tomography (fPAT), two variants of PAT in the setting of molecular imaging where the goal is to image specific molecular functions inside biological tissues. In both cases, we prove uniqueness and stability results on the inverse problems in the quantitative steps and provide numerical simulations to complement the mathematical analysis.

The rest of the disseration is organized as follows.

In Chapter 2, we study two-photon quantitative PAT in diffusion regime where we are interested in recovering single-photon and two-photon absorption coefficients. We present some of the general properties of the semilinear diffusion equation. We then develop some uniqueness and stability results for reconstructing both a single coefficients and two coefficients. Uniqueness results for reconstructing the diffusion coefficient along with the two optical absorption coefficients under linearized setting are also obtained. Non-uniqueness result to recover Grüniesen coeffcient together with the aforementioned coefficients is also presented. We demonstrate the theoretical results with some numerical simulations based on synthetic data. The semilinear diffusion equation is discretized with a first-order finite element method on triangular meshes and solved using a quasi-Newton method based on the variational formulation. The inversion is performed with both direct methods and optimization methods. The results in this chapter is based on a joint work with Professor Kui Ren in [89].

In Chapter 3, we study quantitative PAT for fluorescence optical tomography in transport regime. The aim is to reconstruct fluorescent absorption coefficient and quantum efficiency. We develop some uniqueness and stability results on reconstructing both a single coefficient and two coefficients. We also present some numerical experiments based on synthetic data. The transport equation is discretized angularly with discrete ordinate method and spatially with a fist-order finite element method on triangular meshes. The inversions

are performed using direct methods and standard optimization algorithm. The results in this chapter is based on a joint work with Professor Kui Ren and Yimin Zhong in [90].

A summary of the disseration, as well as some perspectives on future work are presented in Chapter 4.

# Chapter 2

# Hybrid Inverse Problems in Two-Photon PAT

## 2.1 Introduction

Two-photon photoacoustic tomography (TP-PAT) [68, 69, 106, 108, 117, 118, 119, 121, 120] is an imaging modality that aims at reconstructing optical properties of heterogeneous media using the photoacoustic effect resulted from two-photon absorption. Here by two-photon absorption we mean the phenomenon that an electron transfers to an excited state after simultaneously absorbing two photons whose total energy exceed the electronic energy band gap. The main motivation for developing two-photon PAT is that two-photon optical absorption can often be tuned to be associated with specific molecular signatures, such as in stimulated Raman photoacoustic microscopy, to achieve label-free molecular imaging. Therefore, TP-PAT can be used to visualize particular cellular functions and molecular processes inside biological tissues.

The principle of TP-PAT is the same as that of the regular PAT [24, 32, 71, 110], except that the photoacoustic signals in TP-PAT are induced via two-photon absorption in addition to the usual single-photon absorption. In TP-PAT, we send near infra-red (NIR) photons into an optically absorbing and

scattering medium, for instance a piece of biological tissue, $\Omega \subseteq \mathbb{R}^n$ $(n \geq 2)$, where they diffuse. The density of the photons, denoted by $u(\mathbf{x})$, solves the following semilinear diffusion equation:

$$\begin{array}{rcll} -\nabla \cdot \gamma(\mathbf{x})\nabla u(\mathbf{x}) + \sigma(\mathbf{x})u(\mathbf{x}) + \mu(\mathbf{x})|u|u(\mathbf{x}) & = & 0, & \text{in } \Omega \\ u(\mathbf{x}) & = & g(\mathbf{x}), & \text{on } \partial\Omega \end{array} \tag{2.1}$$

where $\gamma(\mathbf{x})$ is the diffusion coefficient, $\sigma(\mathbf{x})$ and $\mu(\mathbf{x})$ are respectively the single-photon and the two-photon absorption coefficients, and the incoming NIR photon source is modelled by the function $g(\mathbf{x})$. The medium absorbs a portion of the incoming photons and heats up due to the absorbed energy. The heating then results in thermal expansion of the medium. The medium cools down after the photons exit. This cooling process results in contraction of the medium. The expansion-contraction of the medium generates ultrasound waves. The process is called the photoacoustic effect. The initial pressure field generated by the photoacoustic effect can be written as [22, 43]

$$H(\mathbf{x}) = \Xi(\mathbf{x})\Big[\sigma(\mathbf{x})u(\mathbf{x}) + \mu(\mathbf{x})|u|u(\mathbf{x})\Big], \qquad \mathbf{x} \in \Omega. \tag{2.2}$$

where $\Xi$ is the Grüneisen coefficient that describes the efficiency of the photoacoustic effect. This initial pressure field generated by single-photon and two-photon absorption processes evolves, in the form of ultrasound, according to the classical acoustic wave equation [22, 43].

The data we measure in TP-PAT are the ultrasound signals on the surface of the medium. From these measured data, we are interested in reconstructing information on the optical properties of the medium. The reconstruction is usually done in two steps. In the first step, we reconstruct

the initial pressure field $H$ in (2.2) from measured data. This step is the same as that in a regular PAT, and has been studied extensively in the past decade; see, for instance, [10, 27, 29, 40, 52, 57, 61, 63, 74, 81, 98] and references therein. In the second step of TP-PAT, we attempt to reconstruct information on the optical coefficients, for instance, the two-photon absorption coefficient $\mu$, from the result of the first step inversion, i.e. the internal datum $H$ in (2.2). This is called the quantitative step in the regular PAT [8, 15, 22, 20, 31, 44, 70, 72, 80, 88, 90, 94, 123].

It is clear from (2.1) that the two-photon absorption strength depends quadratically, not linearly, on the local photon density $u(\mathbf{x})$. It is generally believed that events of two-photon absorption in biological tissues can only happen when the local photon density is sufficiently high. In fact, the main difficulty in the development of TP-PAT is to be able to measure the ultrasound signal accurate enough such that the photoacoustic signal due to two-photon absorption is not completely buried by noise in the data. In recent years, many experimental research have been conducted where it is shown that the effect of two-photon absorption can be measured accurately; see, for instance, the study on the feasibility of TP-PAT on various liquid samples in [118, 119, 120] (solutions), [68, 120] (suspensions) and [69] (soft matter).

Despite various experimental study of TP-PAT, a thorough mathematical and numerical analysis of the inverse problems in the second step of TP-PAT is largely missing, not to mention efficient reconstruction algorithms. The objective of this study is therefore to pursue in these directions. In the rest

of the chapter, we first recall in Section 2.2 some fundamental mathematical results on the properties of solutions to the semilinear diffusion equation (2.1). We then develop in Section 2.3 the theory of reconstructing the absorption coefficients. In Section 2.4 we analyze the linearized problem of simultaneously reconstructing the absorption coefficients and the diffusion coefficient. Numerical simulations are provided in Section 2.5 to validate the mathematical analysis and demonstrate the quality of the reconstructions. Concluding remarks are offered in Section 2.6.

## 2.2 The Semilinear Diffusion Model

To prepare for the study of the inverse coefficient problems, we recall in this section some general results on the semilinear diffusion model (2.1). Thanks to the absolute value operator in the quadratic term $\mu|u|u$ in the equation, we can follow the standard theory of calculus of variation, as well as the theory of generalized solutions to elliptic equations in divergence form, to derive desired properties of the solution to the diffusion equation that we will need in the following sections. The results we collected here are mostly minor modifications/simplifications of classical results in [7, 14, 39, 46]. We refer interested readers to these references, and the references therein, for more technical details on these results.

We assume, in the rest of the chapter, that the domain $\Omega$ is smooth and satisfies the usual exterior cone condition [46]. We assume that all the coefficients involved are bounded in the sense that there exist positive constants

$\theta \in \mathbb{R}$ and $\Theta \in \mathbb{R}$ such that

$$0 < \theta \leq \Xi(\mathbf{x}), \gamma(\mathbf{x}), \sigma(\mathbf{x}), \mu(\mathbf{x}) \leq \Theta < \infty, \ \forall \mathbf{x} \in \bar{\Omega}. \tag{2.3}$$

Unless stated otherwise, we assume also that

$$(\gamma, \sigma, \mu) \in [W^{1,2}(\bar{\Omega})]^3, \text{ and, } g(x) \text{ is the restriction of a } \mathcal{C}^3(\bar{\Omega}) \text{ function on } \partial\Omega. \tag{2.4}$$

where $W^{1,2}(\Omega)$ denotes the usual Hilbert space of $L^2(\Omega)$ functions whose first weak derivative is also in $L^2(\Omega)$. Note thathere we used $W^{1,2}(\Omega)$ instead of $H^1(\Omega)$ to avoid confusion with the $H$ we used to denote the internal data in (2.2).

Technically speaking, in some of the results we obtained below, we can relax part of the above assumptions. However, we will address this issue at the moment. For convenience, we define the function $f(\mathbf{x}, z)$ and the linear operator $\mathcal{L}$,

$$f(\mathbf{x}, z) = \sigma(\mathbf{x})z + \mu(\mathbf{x})|z|z, \quad \text{and} \quad \mathcal{L}u = -\nabla \cdot \gamma \nabla u. \tag{2.5}$$

With our assumption above, it is clear that $\mathcal{L}$ is uniformly elliptic, and $f(\mathbf{x}, z)$ is continuously differentiable with respect to $z$ on $\bar{\Omega} \times \mathbb{R}$. Moreover, $f_z(\mathbf{x}, z) := \partial_z f(\mathbf{x}, z) = \sigma(\mathbf{x}) + 2\mu(\mathbf{x})|z| \geq \theta > 0$, $\forall z \in \mathbb{R}$.

We start by recalling the definition of weak solutions to the semilinear diffusion equation (2.1). We say that $u \in \mathcal{W} \equiv \{w | w \in W^{1,2}(\Omega) \text{ and } w_{|\partial\Omega} = g\}$ is a weak solution to (2.1) if

$$\int_\Omega \gamma(\mathbf{x}) \nabla u \cdot \nabla v + \sigma(\mathbf{x}) u(\mathbf{x}) v(\mathbf{x}) + \mu(\mathbf{x})|u| u(\mathbf{x}) v(\mathbf{x}) d\mathbf{x} = 0, \quad \forall v \in W_0^{1,2}(\Omega).$$

We first summarize the results on existence, uniqueness and regularity of the solution to (2.1) in the following lemma.

**Lemma 2.2.1.** *Let $(\gamma, \sigma, \mu)$ satisfy (2.3), and assume that $g \in \mathcal{C}^0(\partial\Omega)$. Then there is a unique weak solution $u \in W^{1,2}(\Omega)$ such that $u \in \mathcal{C}^\alpha(\Omega) \cap \mathcal{C}^0(\bar{\Omega})$ for some $0 < \alpha < 1$. If we assume further that $(\gamma, \sigma, \mu)$ and $g$ satisfy (2.4), then $u \in W^{3,2}(\Omega) \cap \mathcal{C}^0(\bar{\Omega})$.*

*Proof.* This result is scattered in a few places in [7, 14] (for instance [14, Theorem 1.6.6]). We provide a sketch of proof here. For any function $w \in \mathcal{W}$, we define the following functional associated with the diffusion equation (2.1):

$$I[w] = \int_\Omega L(\mathbf{x}, w, Dw) d\mathbf{x} = \int_\Omega \left[ \frac{1}{2}\gamma|\nabla w|^2 + \frac{1}{2}\sigma w^2 + \frac{1}{3}\mu|w|w^2 \right] d\mathbf{x}.$$

It is straightforward to verify that $I[w] : \mathcal{W} \to \mathbb{R}$ is strictly convex (thanks again to the absolute value in the third term) and differentiable on $\mathcal{W}$ with

$$I'[w]v = \int_\Omega \Big[ \gamma(\mathbf{x})\nabla w \cdot \nabla v + \sigma(\mathbf{x}) wv + \mu(\mathbf{x})|w|wv \Big] d\mathbf{x}.$$

We also verify that the function $L(\mathbf{x}, z, \mathbf{p})$ satisfies the following growth conditions:

$$\begin{aligned} |L(\mathbf{x}, z, \mathbf{p})| &\le C(1 + |z|^3 + |\mathbf{p}|^2), \\ |D_z L(\mathbf{x}, z, \mathbf{p})| &\le C(1 + |z|^2), \\ |D_{\mathbf{p}} L(\mathbf{x}, z, \mathbf{p})| &\le C(1 + |\mathbf{p}|), \end{aligned}$$

for all $\mathbf{x} \in \Omega$, $z \in \mathbb{R}$ and $\mathbf{p} \in \mathbb{R}^n$. It then follows from standard results in calculus of variations [7, 14, 39] that there exists a unique $u \in \mathcal{W}$ satisfies

$$I[u] = \min_{w \in \mathcal{W}} I[w],$$

and $u$ is the unique weak solution of (2.1). By Sobolev embedding, when $n = 2, 3$, there exists $q > n$, such that $u \in L^q(\Omega)$. This then implies that $f(\mathbf{x}, u) \in L^{q/2}(\Omega)$ with the assumption (2.3). Let us rewrite the diffusion equation (2.1) as

$$-\nabla \cdot (\gamma \nabla u) = f(\mathbf{x}, u), \quad \text{in } \Omega, \qquad u = g, \quad \text{on } \partial\Omega. \tag{2.6}$$

Following standard results in [39, 46], we conclude that $f \in L^{q/2}(\Omega)$ implies $u \in \mathcal{C}^{\alpha}(\Omega)$ for some $0 < \alpha < 1$, where $\alpha = \alpha(n, \Theta/\theta)$. Moreover, when $g \in \mathcal{C}^0(\partial\Omega)$, $u \in \mathcal{C}^0(\bar{\Omega})$. If we assume further that $(\gamma, \sigma, \mu)$ and $g$ satisfy (2.4), then $f \in W^{1,2}$ thanks to the fact that $u \in \mathcal{C}^0(\bar{\Omega})$. Equation (2.6) then implies that $u \in W^{3,2}(\Omega) \cap \mathcal{C}^0(\bar{\Omega})$ [39, 46]. □

We now recall the following comparison principle for the solutions to the semilinear diffusion equation (2.1).

**Proposition 2.2.2.** *(i) Let $u, v \in W^{1,2}(\Omega) \cap \mathcal{C}^0(\bar{\Omega})$ be functions such that $\mathcal{L}u + f(\mathbf{x}, u) \leq 0$ and $\mathcal{L}v + f(\mathbf{x}, v) \geq 0$ in $\Omega$, and $u \leq v$ on $\partial\Omega$. Then $u \leq v$ in $\Omega$. (ii) If, in addition, $\Omega$ satisfies the exterior cone condition or $u, v \in W^{2,2}(\Omega)$, then either $u \equiv v$ or $u < v$.*

*Proof.* For $t \in [0, 1]$, let $u_t = tu + (1-t)v$ and define $a(\mathbf{x}) = \displaystyle\int_0^1 f_z(u_t, \mathbf{x})dt$. It is then straightforward to check that $a(\mathbf{x}) \geq \theta > 0$ (since $f_z \geq \theta > 0$). With the assumption that $u \in \mathcal{C}^0(\bar{\Omega})$ and $v \in \mathcal{C}^0(\bar{\Omega})$, we conclude that $u_t$ is bounded from above when $t \in [0, 1]$. Therefore, $a(\mathbf{x}) \leq \Lambda < \infty$ for some $\Lambda > 0$. We

also verify that $f(u, \mathbf{x}) - f(v, \mathbf{x}) = a(\mathbf{x})(u - v)$. Let $w = u - v$, we have, from the assumptions in the proposition, that

$$\mathcal{L}w + a(\mathbf{x})w \leq 0, \quad \text{in } \Omega, \qquad w \leq 0, \quad \text{on } \partial\Omega.$$

Since $\mathcal{L} + a$ is uniformly elliptic, by the weak maximum principle for weak solutions [46, Theorem 8.1], $w \leq 0$ in $\Omega$. This then implies that $u \leq v$ in $\Omega$.

If we assume in addition that $u, v \in W^{2,2}(\Omega)$, we can use the strong maximum principle to conclude that $w \equiv 0$ if $w(0) = 0$ for some $x \in \Omega$. Therefore, either $w \equiv 0$, in which case $u = v$, or $w < 0$, in which case $u < v$. If $u, v \in W^{1,2}(\Omega)$ and $\Omega$ satisfies the exterior cone condition, we can use [46, Theorem 8.19] to draw the same conclusion. □

The above comparison principle leads to the following assertion on the solution to the semilinear diffusion equation (2.1).

**Proposition 2.2.3.** *Let $u_j$ be the solution to (2.1) with boundary condition $g_j$, $j = 1, 2$. Assume that $\gamma$, $\sigma$, $\mu$ and $\{g_j\}_{j=1}^2$ satisfy the assumptions in (2.3) and (2.4). Then the following statements hold: (i) if $g_j \geq 0$, then $u_j \geq 0$; (ii) $\sup_\Omega u_j \leq \sup_{\partial\Omega} g_j$; (iii) if $g_1 > g_2$, then $u_1(\mathbf{x}) > u_2(\mathbf{x})$ $\forall \mathbf{x} \in \Omega$.*

*Proof.* (i) follows from the comparison principle in Proposition 2.2.2 and the fact that $u \equiv 0$ is a solution to (2.1) with homogeneous Dirichlet condition $g = 0$. (ii) By (i), $u_j \geq 0$. Therefore $f(\mathbf{x}, u_j) \geq 0$. Therefore, we can have

$$-\nabla \cdot (\gamma \nabla u_j) = -f(\mathbf{x}, u_j) \leq 0, \quad \text{in } \Omega.$$

By the maximum principle, $\sup_\Omega u_j \leq \sup_{\partial\Omega} g_j$. (iii) is a direct consequence of part (ii) of Proposition 2.2.2. □

In the study of the inverse problems in the next sections, we sometimes need the solution to the semilinear diffusion equation to be bounded away from 0. We now prove the following result.

**Theorem 2.2.4.** *Let $u$ be the solution to (2.1) generated with source $g \geq \varepsilon > 0$ for some $\varepsilon$. Then there exists $\varepsilon' > 0$ such that $u \geq \varepsilon' > 0$.*

*Proof.* We follow the arguments in [5]. We again rewrite the PDE as

$$-\nabla \cdot \gamma \nabla u = -f(\mathbf{x}, u), \quad \text{in } \Omega, \qquad u = g, \quad \text{on } \partial\Omega.$$

Then by classical gradient estimates, see for instance [53, Proposition 2.20], we know that there exists $K > 0$, depending on $\gamma$, $|\nabla\gamma|$ and $\Omega$, such that

$$|u(\mathbf{x}) - u(\mathbf{x}_0)| \leq K|\mathbf{x} - \mathbf{x}_0|, \quad \forall \mathbf{x} \in \Omega, \quad \mathbf{x}_0 \in \partial\Omega.$$

Using the fact that $g \geq \varepsilon$, we conclude from this inequality that there exists a $d > 0$ such that

$$u(\mathbf{x}) \geq \varepsilon/2, \qquad \forall \mathbf{x} \in \Omega \backslash \Omega_d,$$

where $\Omega_d = \{\mathbf{x} \in \Omega : \ \text{dist}(\mathbf{x}, \partial\Omega) > d\}$. Therefore, $\sup_{\Omega_{d/2}} u \geq \varepsilon/2$.

Let $c(\mathbf{x}) = \sigma(\mathbf{x}) + \mu(\mathbf{x})|u(\mathbf{x})|$. Due to the fact that $u$ is nonnegative and bounded from above, we have that $0 < \theta \leq c(\mathbf{x}) \leq \Theta(1 + \sup_{\partial\Omega} |g|)$. We then have that $u$ solves

$$-\nabla \cdot \gamma \nabla u + cu = 0, \quad \text{in } \Omega, \qquad u = g, \quad \text{on } \partial\Omega.$$

By the Harnack inequality (see [46, Corollary 8.21]), we have that there exists constant $C$, depending on $d$, $\gamma$, $c$, $\Omega$, and $\Omega_{d/2}$, such that

$$C \inf_{\Omega_{d/2}} u \geq \sup_{\Omega_{d/2}} u.$$

Therefore, $\inf_{\Omega_{d/2}} u \geq \dfrac{\varepsilon}{2C}$. The claim then follows from

$$\inf_{\Omega} u \geq \min\{\inf_{\Omega_{d/2}} u, \inf_{\Omega\setminus\Omega_d} u\} \geq \frac{\varepsilon}{2}\min\{1/C, 1\} \equiv \varepsilon'.$$

□

We conclude this section by the following result on the differentiability of the datum $H$ with respect to the coefficients in the diffusion equation. This result justifies the linearization that we perform in Section 2.4.

**Proposition 2.2.5.** *The datum $H$ defined in (2.2) generated from an illumination $g \geq 0$ on $\partial\Omega$, viewed as the map*

$$H[\gamma,\sigma,\mu] : \begin{array}{ccc} (\gamma,\sigma,\mu) & \mapsto & \Xi(\sigma u + \mu|u|u) \\ W^{1,2}(\Omega)\times L^\infty(\Omega)\times L^\infty(\Omega) & \to & W^{1,2}(\Omega) \end{array} \tag{2.7}$$

*is Fréchet differentiable when the coefficients satisfies (2.3) and (2.4). The derivative at $(\gamma,\sigma,\mu)$ in the direction $(\delta\gamma,\delta\sigma,\delta\mu) \in W^{1,2}(\Omega)\times L^\infty(\Omega)\times L^\infty(\Omega)$ is given by*

$$\begin{pmatrix} H'_\gamma[\gamma,\sigma,\mu](\delta\gamma) \\ H'_\sigma[\gamma,\sigma,\mu](\delta\sigma) \\ H'_\mu[\gamma,\sigma,\mu](\delta\mu) \end{pmatrix} = \Xi \begin{pmatrix} \sigma v_1 + 2\mu u v_1 \\ \delta\sigma u + 2\mu|u|v_2 \\ \delta\sigma v_3 + 2\mu|u|v_3 + \delta\mu|u|u \end{pmatrix}, \tag{2.8}$$

*where $v_j$ $(1 \leq j \leq 3)$ is the solution to the diffusion equation*

$$-\nabla\cdot(\gamma\nabla v_j) + (\sigma + 2\mu|u|)v_j = S_j, \quad \text{in } \Omega, \qquad v_j = 0, \quad \text{on } \partial\Omega \tag{2.9}$$

*with*

$$S_1 = \nabla \cdot \delta\gamma \nabla u, \qquad S_2 = -\delta\sigma u, \qquad S_3 = -\delta\mu |u| u.$$

*Proof.* We show here only that $u$ is Fréchet differentiable with respect to $\gamma$, $\sigma$ and $\mu$. The rest of the result follows from the chain rule.

Let $(\delta\gamma, \delta\sigma, \delta\mu) \in W^{1,2}(\Omega) \times L^\infty(\Omega) \times L^\infty(\Omega)$ be such that $(\gamma', \sigma', \mu') = (\gamma + \delta\gamma, \sigma + \delta\sigma, \mu + \delta\mu)$ satisfies the bounds in (2.3). Let $u'$ be the solution to (2.1) with coefficients $(\gamma', \sigma', \mu')$, and define $\widetilde{u} = u' - u$. We then verify that $\widetilde{u}$ solves the following linear diffusion equation

$$\begin{aligned} -\nabla \cdot (\gamma \nabla \widetilde{u}) + \big[\sigma + \mu(u + u')\big]\widetilde{u} &= \nabla \cdot \delta\gamma \nabla u' - \delta\sigma u' - \delta\mu u'^2, && \text{in } \Omega \\ \widetilde{u} &= 0, && \text{on } \partial\Omega \end{aligned}$$

where we have used the fact that $u \geq 0$ and $u' \geq 0$ following Proposition 2.2.3 (since $g \geq 0$ on $\partial\Omega$). Note also that both $u$ and $u'$ are bounded from above by Proposition 2.2.3. Therefore, $\sigma + \mu(u + u')$ is bounded from above. Therefore, we have the following standard estimate [46]

$$\begin{aligned} \|\widetilde{u}\|_{W^{1,2}(\Omega)} &\leq \mathfrak{C}_1 \left( \|\delta\gamma \nabla u'\|_{L^2(\Omega)} + \|\delta\sigma u'\|_{L^2(\Omega)} + \|\delta\mu u'^2\|_{L^2(\Omega)} \right) \\ &\leq \mathfrak{C}_1' (\|\delta\gamma\|_{L^\infty(\Omega)} + \|\delta\sigma\|_{L^\infty(\Omega)} + \|\delta\mu\|_{L^\infty(\Omega)}). \end{aligned} \tag{2.10}$$

Let $\widetilde{\widetilde{u}} = u' - u - (v_1 + v_2 + v_3)$ with $v_1$, $v_2$ and $v_3$ solutions to (2.9). Then we verify that $\widetilde{\widetilde{u}}$ satisfies the equation

$$\begin{aligned} -\nabla \cdot (\gamma \nabla \widetilde{\widetilde{u}}) + \big[\sigma + 2\mu u\big]\widetilde{\widetilde{u}} &= \nabla \cdot \delta\gamma \nabla \widetilde{u} - \delta\sigma \widetilde{u} - \delta\mu (u' + u)\widetilde{u}, && \text{in } \Omega \\ \widetilde{\widetilde{u}} &= 0, && \text{on } \partial\Omega \end{aligned}$$

Therefore, we have the following standard estimate

$$\begin{aligned}\|\widetilde{\widetilde{u}}\|_{W^{1,2}(\Omega)} &\leq \mathfrak{C}_2 \left( \|\delta\gamma \nabla \widetilde{u}\|_{L^2(\Omega)} + \|\delta\sigma \widetilde{u}\|_{L^2(\Omega)} + \|\delta\mu \widetilde{u}^2\|_{L^2(\Omega)} \right) \\ &\leq \mathfrak{C}_2' \left( \|\delta\gamma\|_{L^\infty(\Omega)} \|\nabla \widetilde{u}\|_{L^2(\Omega)} + \|\delta\sigma\|_{L^\infty(\Omega)} \|\widetilde{u}\|_{L^2(\Omega)} + \|\delta\mu\|_{L^\infty(\Omega)} \|\widetilde{u}\|_{L^2(\Omega)} \right). \end{aligned} \tag{2.11}$$

We can thus combine (2.10) with (2.11) to obtain the bound

$$\|\widetilde{\widetilde{u}}\|_{W^{1,2}(\Omega)} \leq \mathfrak{C} \left( \|\delta\gamma\|^2_{L^\infty(\Omega)} + \|\delta\sigma\|^2_{L^\infty(\Omega)} + \|\delta\mu\|^2_{L^\infty(\Omega)} \right).$$

This concludes the proof. □

We observe from the above proof that differentiability of $H$ with respect to $\sigma$ and $\mu$ can be proven when viewed as a map $L^\infty(\Omega) \times L^\infty(\Omega) \to L^\infty(\Omega)$, following the maximum principles for solutions $\widetilde{u}$ and $\widetilde{\widetilde{u}}$. The same thing can not be done with respect to $\gamma$ since we can not control the term $\|\nabla \cdot \delta\gamma \nabla u'\|_{L^\infty(\Omega)}$ with $\|\delta\gamma\|_{L^\infty(\Omega)}$ without much more restrictive assumptions on $\delta\gamma$.

## 2.3 Reconstructing Absorption Coefficients

We now study inverse problems related to the semilinear diffusion model (2.1). We first consider the case of reconstructing the absorption coefficients, assuming that the Grüneisen coefficient $\Xi$ and the diffusion coefficient $\gamma$ are both *known*.

### 2.3.1 One coefficient with single datum

We now show that with one datum set, we can uniquely recover one of the two absorption coefficients.

**Proposition 2.3.1.** *Let $\Xi$ and $\gamma$ be given. Assume that $g \geq \varepsilon > 0$ for some $\varepsilon$. Let $H$ and $\widetilde{H}$ be the data sets corresponding to the coefficients $(\sigma, \mu)$ and $(\widetilde{\sigma}, \widetilde{\mu})$ respectively. Then $H = \widetilde{H}$ implies $(u, \sigma + \mu|u|) = (\widetilde{u}, \widetilde{\sigma} + \widetilde{\mu}|\widetilde{u}|)$ provided that all coefficients satisfy (2.3). Moreover, we have*

$$\|(\sigma + \mu|u|) - (\widetilde{\sigma} + \widetilde{\mu}|u|)\|_{L^\infty(\Omega)} \leq C\|H - \widetilde{H}\|_{L^\infty(\Omega)}, \tag{2.12}$$

*for some constant $C$.*

*Proof.* The proof is straightforward. Let $w = u - \widetilde{u}$. We check that $w$ solves

$$-\nabla \cdot (\gamma \nabla w) = -\frac{1}{\Xi}(H - \widetilde{H}), \quad \text{in } \Omega, \qquad w = 0, \quad \text{on } \partial\Omega. \tag{2.13}$$

Therefore $H = \widetilde{H}$ implies $w = 0$ which is simply $u = \widetilde{u}$. This in turn implies that $\dfrac{H}{u} = \dfrac{\widetilde{H}}{\widetilde{u}}$, that is $\sigma + \mu|u| = \widetilde{\sigma} + \widetilde{\mu}|\widetilde{u}|$. Note that the condition $g \geq \varepsilon > 0$ implies that $u, \widetilde{u} \geq \varepsilon' > 0$ for some $\varepsilon'$ following Theorem 2.2.4. This makes it safe to take the ratios $H/u$ and $\widetilde{H}/\widetilde{u}$, and to omit the absolute values on $u$ and $\widetilde{u}$.

To derive the stability estimate, we first observe that

$$|(\sigma + \mu|u|) - (\widetilde{\sigma} + \widetilde{\mu}|\widetilde{u}|)| = \frac{1}{\Xi}\left|\frac{H}{u} - \frac{\widetilde{H}}{\widetilde{u}}\right| = \left|\frac{H(\widetilde{u} - u) + (H - \widetilde{H})u}{\Xi u \widetilde{u}}\right|.$$

Using the fact that $u$ and $\widetilde{u}$ are both bounded away from zero, and the triangle inequality, we have, for some constants $c_1$ and $c_2$,

$$\|(\sigma+\mu|u|)-(\widetilde{\sigma}+\widetilde{\mu}|\widetilde{u}|)\|_{L^\infty(\Omega)} \le c_1\|\widetilde{u}-u\|_{L^\infty(\Omega)} + c_2\|H-\widetilde{H}\|_{L^\infty(\Omega)}. \quad (2.14)$$

On the other hand, classical theory of elliptic equations allows us to derive, from (2.13), the following bound, for some constant $c_3$,

$$\|u-\widetilde{u}\|_{L^\infty(\Omega)} \le c_3\|H-\widetilde{H}\|_{L^\infty(\Omega)}. \quad (2.15)$$

The bound in (2.12) then follows by combining (2.14) and (2.15). □

The above proof provides an explicit algorithm to reconstruct one of $\sigma$ and $\mu$ from one datum. Here is the procedure. We first solve

$$-\nabla\cdot(\gamma\nabla u) = -\frac{1}{\Xi}H, \quad \text{in } \Omega, \qquad u=g, \quad \text{on } \partial\Omega \quad (2.16)$$

for $u$ since $\Xi$ and $\gamma$ are known. We then reconstruct $\sigma$ as

$$\sigma = \frac{H}{\Xi u} - \mu|u|, \quad (2.17)$$

if $\mu$ is known, or reconstruct $\mu$ as

$$\mu = \frac{H}{\Xi u|u|} - \frac{\sigma}{|u|}, \quad (2.18)$$

if $\sigma$ is known.

The stability estimate (2.12) can be made more explicit when one of the coefficients involved is known. For instance, if $\mu$ is known, then we have

$$|\sigma-\widetilde{\sigma}| = \frac{1}{\Xi}\Big|\frac{H}{u}-\mu|u|-\Big(\frac{\widetilde{H}}{\widetilde{u}}-\mu|\widetilde{u}|\Big)\Big| = \frac{1}{\Xi}\Big|\frac{(H(\widetilde{u}-u)+(H-\widetilde{H})u}{u\widetilde{u}}-\mu(|u|-|\widetilde{u}|)\Big|.$$

This leads to, using the triangle inequality again,

$$\|\sigma - \widetilde{\sigma}\|_{L^\infty(\Omega)} \leq c_1' \|\widetilde{u} - u\|_{L^\infty(\Omega)} + c_2' \|H - \widetilde{H}\|_{L^\infty(\Omega)}.$$

Combining this bound with (2.15), we have

$$\|\sigma - \widetilde{\sigma}\|_{L^\infty(\Omega)} \leq C' \|H - \widetilde{H}\|_{L^\infty(\Omega)}, \tag{2.19}$$

for some constant $C'$. In the same manner, we can derive

$$\|\mu - \widetilde{\mu}\|_{L^\infty(\Omega)} \leq C'' \|H - \widetilde{H}\|_{L^\infty(\Omega)}, \tag{2.20}$$

for the reconstruction of $\mu$ if $\sigma$ is known in advance.

### 2.3.2 Two coefficients with two data sets

We see from the previous result that we can reconstruct $\sigma + \mu|u|$ when we have one datum. If we have data generated from two different sources $g_1$ and $g_2$, then we can reconstruct $\sigma + \mu|u_1|$ and $\sigma + \mu|u_2|$ where $u_1$ and $u_2$ are the solutions to the diffusion equation (2.1) corresponding to $g_1$ and $g_2$ respectively. If we can choose $g_1$ and $g_2$ such that $|u_2| - |u_1| \neq 0$ anywhere, we can uniquely reconstruct the pair $(\sigma, \mu)$. This is the idea we have in the following result.

**Proposition 2.3.2.** *Let $\Xi$ and $\gamma$ be given. Let $(H_1, H_2)$ and $(\widetilde{H}_1, \widetilde{H}_2)$ be the data sets corresponding to the coefficients $(\sigma, \mu)$ and $(\widetilde{\sigma}, \widetilde{\mu})$ respectively that are generated with the pair of sources $(g_1, g_2)$. Assume that $g_i \geq \varepsilon > 0$, $i = 1, 2$, and $g_1 - g_2 \geq \varepsilon' > 0$ for some $\varepsilon$ and $\varepsilon'$. Then $(H_1, H_2) = (\widetilde{H}_1, \widetilde{H}_2)$ implies*

$(\sigma, \mu) = (\widetilde{\sigma}, \widetilde{\mu})$ *provided that all coefficients involved satisfy* (2.3). *Moreover, we have*

$$\|\sigma - \widetilde{\sigma}\|_{L^\infty(\Omega)} + \|\mu - \widetilde{\mu}\|_{L^\infty(\Omega)} \leq \widetilde{C} \left( \|H_1 - \widetilde{H}_1\|_{L^\infty(\Omega)} + \|H_2 - \widetilde{H}_2\|_{L^\infty(\Omega)} \right), \tag{2.21}$$

*for some constant* $\widetilde{C}$.

*Proof.* Let $w_i = u_i - \widetilde{u}_i$, $i = 1, 2$. Then $w_i$ solves

$$-\nabla \cdot (\gamma \nabla w_i) = -\frac{1}{\Xi}(H_i - \widetilde{H}_i), \quad \text{in } \Omega, \qquad w_i = 0, \quad \text{on } \partial\Omega. \tag{2.22}$$

Therefore $H_i = \widetilde{H}_i$ implies $u_i = \widetilde{u}_i$ and

$$\sigma + \mu |u_i| = \widetilde{\sigma} + \widetilde{\mu} |u_i|.$$

Collecting the results for both data sets, we have

$$\begin{pmatrix} 1 & |u_1| \\ 1 & |u_2| \end{pmatrix} \begin{pmatrix} \sigma \\ \mu \end{pmatrix} = \begin{pmatrix} 1 & |u_1| \\ 1 & |u_2| \end{pmatrix} \begin{pmatrix} \widetilde{\sigma} \\ \widetilde{\mu} \end{pmatrix}. \tag{2.23}$$

When $g_1$ and $g_2$ satisfy the requirements stated in the proposition, we have $u_1 - u_2 \geq \varepsilon' > 0$ for some $\varepsilon'$. Therefore, the matrix $\begin{pmatrix} 1 & |u_1| \\ 1 & |u_2| \end{pmatrix}$ is invertible. We can then remove this matrix in (2.23) to show that $(\sigma, \mu) = (\widetilde{\sigma}, \widetilde{\mu})$.

To get the stability estimate in (2.21), we first verify that

$$(\sigma - \widetilde{\sigma}) + (\mu - \widetilde{\mu})|u_i| = \frac{H_i}{u_i} - \frac{\widetilde{H}_i}{\widetilde{u}_i} - \widetilde{\mu}(|u_i| - |\widetilde{u}_i|), \qquad i = 1, 2.$$

This leads to,

$$\begin{pmatrix} 1 & |u_1| \\ 1 & |u_2| \end{pmatrix} \begin{pmatrix} \sigma - \widetilde{\sigma} \\ \mu - \widetilde{\mu} \end{pmatrix} = \begin{pmatrix} \dfrac{H_1}{u_1} - \dfrac{\widetilde{H}_1}{\widetilde{u}_1} - \widetilde{\mu}(|u_1| - |\widetilde{u}_1|) \\ \dfrac{H_2}{u_2} - \dfrac{\widetilde{H}_2}{\widetilde{u}_2} - \widetilde{\mu}(|u_2| - |\widetilde{u}_2|) \end{pmatrix}.$$

Therefore, we have

$$\begin{pmatrix} \sigma - \widetilde{\sigma} \\ \mu - \widetilde{\mu} \end{pmatrix} = \begin{pmatrix} 1 & |u_1| \\ 1 & |u_2| \end{pmatrix}^{-1} \begin{pmatrix} \dfrac{H_1(\widetilde{u}_1 - u_1) + (H_1 - \widetilde{H}_1)u_1}{u_1\widetilde{u}_1} - \widetilde{\mu}(|u_1| - |\widetilde{u}_1|) \\ \dfrac{H_2(\widetilde{u}_2 - u_2) + (H_2 - \widetilde{H}_2)u_2}{u_2\widetilde{u}_2} - \widetilde{\mu}(|u_2| - |\widetilde{u}_2|) \end{pmatrix}.$$

It then follows that

$$\begin{aligned} &\|\sigma - \widetilde{\sigma}\|_{L^\infty(\Omega)} + \|\mu - \widetilde{\mu}\|_{L^\infty(\Omega)} \\ &\leq c\left(\|H_1 - \widetilde{H}_1\|_{L^\infty(\Omega)} + \|H_2 - \widetilde{H}_2\|_{L^\infty(\Omega)} + \|u_1 - \widetilde{u}_1\|_{L^\infty(\Omega)} + \|u_2 - \widetilde{u}_2\|_{L^\infty(\Omega)}\right). \end{aligned} \tag{2.24}$$

Meanwhile, we have, from (2.22),

$$\|u_i - \widetilde{u}_i\|_{L^\infty(\Omega)} \leq c'\|H_i - \widetilde{H}_i\|_{L^\infty(\Omega)}, \quad i = 1, 2. \tag{2.25}$$

The bound in (2.21) then follows from (2.24) and (2.25). □

## 2.4 Reconstructing Absorption and Diffusion Coefficients

We now study inverse problems where we intend to reconstruct more than the absorption coefficients. We start with a non-uniqueness result on the simultaneous reconstruction of all four coefficients $\Xi$, $\gamma$, $\sigma$, and $\mu$.

### 2.4.1 Non-uniqueness in reconstructing $(\Xi, \gamma, \sigma, \mu)$

Let us assume for the moment that $\gamma^{1/2} \in \mathcal{C}^2(\Omega)$. We introduce the following Liouville transform

$$v = \sqrt{\gamma}u. \tag{2.26}$$

We then verify that the semilinear diffusion equation (2.1) is transformed into the following equation under the Liouville transform:

$$\Delta v - \left( \frac{\Delta \gamma^{1/2}}{\gamma^{1/2}} + \frac{\sigma}{\gamma} + \frac{\mu}{\gamma^{3/2}} |v| \right) v = 0, \quad \text{in } \Omega, \qquad v = \gamma^{1/2} g, \quad \text{on } \partial\Omega \tag{2.27}$$

and the datum $H$ is transformed into

$$H(\mathbf{x}) = \Xi(\mathbf{x}) \left( \frac{\sigma}{\gamma^{1/2}} v(\mathbf{x}) + \frac{\mu}{\gamma} v^2(\mathbf{x}) \right). \tag{2.28}$$

Let us now define the following functionals:

$$\alpha = \frac{\Delta \gamma^{1/2}}{\gamma^{1/2}} + \frac{\sigma}{\gamma}, \qquad \beta = \frac{\mu}{\gamma^{3/2}}, \qquad \zeta_1 = \Xi \frac{\sigma}{\gamma^{1/2}}, \qquad \zeta_2 = \Xi \frac{\mu}{\gamma}. \tag{2.29}$$

The following result says that once $(\alpha, \beta, \zeta_1)$ or $(\alpha, \beta, \zeta_2)$ is known, introducing new data would not bring in new information.

**Theorem 2.4.1.** *Let $\gamma^{1/2}|_{\partial\Omega}$ be given and assume that $\gamma^{1/2} \in \mathcal{C}^2(\Omega)$. Assume that either $(\alpha, \beta, \zeta_1)$ or $(\alpha, \beta, \zeta_2)$ is known, and $H$ is among the data used to determine them. Then for any given new illumination $\widetilde{g}$, the corresponding datum $\widetilde{H}$ is uniquely determined by $(\widetilde{g}, H)$.*

*Proof.* Let us first rewrite the datum as $H = \zeta_1 v + \zeta_2 v^2$. When $\alpha$ and $\beta$ are known, we know the solution $v$ of (2.27) for any given $g$. If $\zeta_1$ is also known, we know also $\zeta_1 v$. We therefore can form the ratio

$$\frac{\widetilde{H} - \zeta_1 \widetilde{v}}{H - \zeta_1 v} = \frac{\zeta_2 \widetilde{v}^2}{\zeta_2 v^2} = \frac{\widetilde{v}^2}{v^2}.$$

We then find $\widetilde{H}$ as $\widetilde{H} = \dfrac{\widetilde{v}^2}{v^2}(H - \zeta_1 v) + \zeta_1 \widetilde{v}$. If $\zeta_1$ is not known but $\zeta_2$ is known, we can form the ratio

$$\frac{\widetilde{H} - \zeta_2 \widetilde{v}^2}{H - \zeta_2 v^2} = \frac{\zeta_1 \widetilde{v}}{\zeta_1 v} = \frac{\widetilde{v}}{v}.$$

This gives $\widetilde{H} = \dfrac{\widetilde{v}}{v}(H - \zeta_2 v^2) + \zeta_2 \widetilde{v}^2$. The proof is complete. □

The above theorem says that we can at most reconstruct the triplet $(\alpha, \beta, \zeta_1)$ or the triplet $(\alpha, \beta, \zeta_2)$. Neither triplet would allow the unique determination of the four coefficients $(\Xi, \gamma, \sigma, \mu)$. Once one of the triplets is determined, adding more data is not helpful in terms of uniqueness of reconstructions.

Similar non-uniqueness results were proved in the case of the regular PAT [19, 20]. In that case, it was also shown that if the Grüneisen coefficient $\Xi$ is known, for instance from multi-spectral measurements [21, 72], one can uniquely reconstruct the absorption coefficient and the diffusion coefficient simultaneously. In the rest of this section, we consider this case, that is, $\Xi$ is known, for our TP-PAT model.

### 2.4.2 Linearized reconstruction of $(\gamma, \sigma, \mu)$

We study the problem of reconstructing $(\gamma, \sigma, \mu)$, assuming $\Xi$ is known, in linearized setting following the general theory of overdetermined elliptic systems developed in [36, 95]. For the sake of the readability of the presentation below, we collect some necessary terminologies in the theory of overdetermined elliptic systems in Appendix A. We refer interested readers to [17, 65, 114] for overviews of the theory in the context of hybrid inverse problems and references therein for more technical details on the theory. Our presentation below follows mainly [17].

We linearize the nonlinear inverse problem around background coefficients $(\gamma, \sigma, \mu)$, assuming that we have access to data collected from $J$ different illumination sources $\{g_j\}_{j=1}^J$. We denote by $(\delta\gamma, \delta\sigma, \delta\mu)$ the perturbations to the coefficients. Let $u_j$ be the solution to (2.1) with source $g_j$ and the background coefficients. We then denote by $\delta u_j$ the perturbation to solution $u_j$. Following the calculations in Proposition 2.2.5, we have, for $1 \leq j \leq J$, in $\Omega$,

$$-\nabla \cdot (\delta\gamma \nabla u_j) - \nabla \cdot (\gamma \nabla \delta u_j) + \delta\sigma u_j + \delta\mu |u_j| u_j + (\sigma + 2\mu |u_j|)\delta u_j = 0, \tag{2.30}$$

$$\delta\sigma u_j + \delta\mu |u_j| u_j + (\sigma + 2\mu |u_j|)\delta u_j = \delta H_j / \Xi, \tag{2.31}$$

To simplify our analysis, we rewrite the above system into, $1 \leq j \leq J$,

$$-\nabla \cdot (\delta\gamma \nabla u_j) - \nabla \cdot (\gamma \nabla \delta u_j) \quad = -\delta H_j / \Xi, \quad \text{in } \Omega \tag{2.32}$$

$$u_j \delta\sigma + |u_j| u_j \delta\mu + (\sigma + 2\mu |u_j|)\delta u_j \quad = +\delta H_j / \Xi, \quad \text{in } \Omega \tag{2.33}$$

This is a system of $2J$ differential equations for $J+3$ unknowns $\{\delta\gamma, \delta\sigma, \delta\mu, \delta u_1, \ldots, \delta u_J\}$.

To supplement the above system with appropriate boundary conditions, we first observe that the boundary conditions for the solutions $\{\delta u_j\}_{j=1}^J$ are given already. They are homogeneous Dirichlet conditions since $g$ does not change when the coefficients change. The boundary conditions for $(\delta\gamma, \delta\sigma, \delta\mu)$ are what need to be determined. In the case of single-photon PAT, it has been shown that one needs to have $\gamma_{|\partial\Omega}$ *known* to have uniqueness in the reconstruction [19, 88]. This is also expected in our case. We therefore take

$\delta\gamma_{|\partial\Omega} = \phi_1$ for some known $\phi_1$. The boundary conditions for $\sigma$ and $\mu$ are given by the data. In fact, on the boundary, $u = g$. Therefore, we have, from (2.33) which holds on $\partial\Omega$, that

$$g_j\delta\sigma + |g_j|g_j\delta\mu = \delta H_j/\Xi, \qquad \text{on } \partial\Omega.$$

If we have two perturbed data sets $\{\delta H_1, \delta H_2\}$ with $g_1$ and $g_2$ sufficiently different, we can then uniquely reconstruct $(\delta\sigma_{|\partial\Omega}, \delta\mu_{|\partial\Omega})$:

$$\delta\sigma_{|\partial\Omega} = \frac{\delta H_1|g_2|g_2 - \delta H_2|g_1|g_1}{\Xi g_1 g_2(|g_2| - |g_1|)} \equiv \phi_2, \qquad \delta\mu_{|\partial\Omega} = \frac{\delta H_2 g_1 - \delta H_1 g_2}{\Xi g_1 g_2(|g_2| - |g_1|)} \equiv \phi_3.$$

Therefore, we have the following Dirichlet boundary condition for the unknowns

$$(\delta\gamma, \delta\sigma, \delta\mu, \delta u_1, \ldots, \delta u_J) = (\phi_1, \phi_2, \phi_3, 0, \cdots, 0). \tag{2.34}$$

Let us introduce $v = (\delta\gamma, \delta\sigma, \delta\mu, \delta u_1, \ldots, \delta u_J)$, $\mathcal{S} = (-\delta H_1, \delta H_1, \ldots, -\delta H_J, \delta H_J)/\Xi$, $\phi = (\phi_1, \phi_2, \phi_3, 0, \cdots, 0)$. We can then write the linearized system of equations (2.32)-(2.33) and the corresponding boundary conditions into the form of

$$\mathcal{A}(\mathbf{x}, D)v = \mathcal{S}, \quad \text{in } \Omega \qquad \mathcal{B}(\mathbf{x}, D)v = \phi, \quad \text{on } \partial\Omega \tag{2.35}$$

where $\mathcal{A}$ is a matrix differential operator of size $M \times N$, $M = 2J$ and $N = 3+J$, while $\mathcal{B}$ is the identity operator. The symbol of $\mathcal{A}$ is given as

$$\mathcal{A}(\mathbf{x}, \mathbf{i}\boldsymbol{\xi}) = \begin{pmatrix} -\mathbf{i}\mathbf{V}_1\cdot\boldsymbol{\xi} - \Delta u_1 & 0 & 0 & \gamma|\boldsymbol{\xi}|^2 - \mathbf{i}\boldsymbol{\xi}\cdot\nabla\gamma & \ldots & 0 \\ 0 & u_1 & |u_1|u_1 & \sigma + 2\mu|u_1| & \ldots & 0 \\ \vdots & \vdots & \vdots & \vdots & \vdots & \vdots \\ -\mathbf{i}\mathbf{V}_J\cdot\boldsymbol{\xi} - \Delta u_J & 0 & 0 & 0 & \ldots & \gamma|\boldsymbol{\xi}|^2 - \mathbf{i}\boldsymbol{\xi}\cdot\nabla\gamma \\ 0 & u_J & |u_J|u_J & 0 & \ldots & \sigma + 2\mu|u_J| \end{pmatrix}, \tag{2.36}$$

with $\mathbf{V}_j = \nabla u_j,\ 1 \le j \le J$ and $\boldsymbol{\xi} \in \mathbb{S}^{n-1}$.

It is straightforward to check that if we take the associated Douglis-Nirenberg numbers as

$$\{s_i\}_{i=1}^{2J} = (0, -2, \dots, 0, -2), \qquad \{t_j\}_{j=1}^{J+3} = (1, 2, 2, 2, \dots, 2), \tag{2.37}$$

the principal part of $\mathcal{A}$ is simply $\mathcal{A}$ itself with the $-\mathbf{i}\boldsymbol{\xi} \cdot \nabla\gamma$ and $-\Delta u_j$ $(1 \le j \le J)$ terms removed.

In three-dimensional case, we can establish the following result.

**Theorem 2.4.2.** *Let $n = 3$. Assume that the background coefficients $\gamma \in \mathcal{C}^4(\Omega)$, $\sigma \in \mathcal{C}^2(\Omega)$, and $\mu \in \mathcal{C}^1(\Omega)$ satisfy the bounds in (2.3). Then, there exists a set of $J \ge n+1$ illuminations $\{g_j\}_{j=1}^J$ such that $\mathcal{A}$ is elliptic. Moreover, the corresponding elliptic system $(\mathcal{A}, \mathcal{B})$, with boundary condition (2.34), satisfies the Lopatinskii criterion.*

*Proof.* Let us first rewrite the principal symbol $\mathcal{A}_0$ as

$$\mathcal{A}_0(\mathbf{x}, \mathbf{i}\boldsymbol{\xi}) = \begin{pmatrix} -\mathbf{i}\mathbf{V}_1 \cdot \boldsymbol{\xi} & 0 & 0 & \gamma|\boldsymbol{\xi}|^2 & \dots & 0 \\ \mathbf{i}\frac{\mathbf{V}_1 \cdot \boldsymbol{\xi}}{\gamma|\boldsymbol{\xi}|^2}(\sigma + 2\mu|u_1|)u_1 & u_1 & |u_1|u_1 & 0 & \dots & 0 \\ \vdots & \vdots & \vdots & \vdots & \vdots & \vdots \\ -\mathbf{i}\mathbf{V}_J \cdot \boldsymbol{\xi} & 0 & 0 & 0 & \dots & \gamma|\boldsymbol{\xi}|^2 \\ \mathbf{i}\frac{\mathbf{V}_J \cdot \boldsymbol{\xi}}{\gamma|\boldsymbol{\xi}|^2}(\sigma + 2\mu|u_J|)u_J & u_J & |u_J|u_J & 0 & \dots & 0 \end{pmatrix}.$$

It is then straightforward to check that $\mathcal{A}_0(\mathbf{x}, \mathbf{i}\boldsymbol{\xi})$ is of full-rank as long as the following sub-matrix is of full-rank:

$$\widetilde{\mathcal{A}}_0(\mathbf{x}, \mathbf{i}\boldsymbol{\xi}) = \begin{pmatrix} \mathbf{i}\frac{\mathbf{V}_1 \cdot \boldsymbol{\xi}}{\gamma|\boldsymbol{\xi}|^2}(\sigma + 2\mu|u_1|)u_1 & u_1 & |u_1|u_1 \\ \vdots & \vdots & \vdots \\ \mathbf{i}\frac{\mathbf{V}_J \cdot \boldsymbol{\xi}}{\gamma|\boldsymbol{\xi}|^2}(\sigma + 2\mu|u_J|)u_J & u_J & |u_J|u_J \end{pmatrix}.$$

To simplify the calculation, we introduce $\Sigma_j = \sigma + 2\mu|u_j|$, $\widehat{F}_j = \mathbf{V}_j \cdot \boldsymbol{\xi}$. We also eliminate the non-zero common factor $\dfrac{\mathfrak{i}}{\gamma|\boldsymbol{\xi}|^2}$ from the first column and $u_j$ from each row. Without loss of generality, we check the determinant of first 3 (since $J \geq n+1 = 4$) rows of the simplified version of the submatrix $\tilde{\mathcal{A}}_0(\mathbf{x}, \mathfrak{i}\boldsymbol{\xi})$. This determinant is given as

$$\begin{aligned}
&\det(\widetilde{\mathcal{A}}_0) = \widehat{F}_1 \frac{\Sigma_1}{u_1}(|u_3| - |u_2|) + \widehat{F}_2 \frac{\Sigma_2}{u_2}(|u_1| - |u_3|) + \widehat{F}_3 \frac{\Sigma_3}{u_3}(|u_2| - |u_1|) \\
&= \frac{\Sigma_1\Sigma_2\Sigma_3}{u_1u_2u_3}\left(\widehat{F}_1 \frac{u_3u_2(|u_3| - |u_2|)}{\Sigma_3\Sigma_2} + \widehat{F}_2 \frac{u_1u_3(|u_1| - |u_3|)}{\Sigma_1\Sigma_3} + \widehat{F}_3 \frac{u_2u_1(|u_2| - |u_1|)}{\Sigma_2\Sigma_1}\right).
\end{aligned}$$

With the assumptions on the background coefficients, we can take $u_j$ to be the complex geometric optics solution constructed following Theorem 2.6.6 (in Appendix B) for $\boldsymbol{\rho}_j$ with boundary condition $g_j$. Then we have

$$\begin{aligned}
\widehat{F}_k \frac{u_iu_j(|u_i| - |u_j|)}{\Sigma_i\Sigma_j} &= \frac{u_iu_j(|u_i| - |u_j|)}{\Sigma_i\Sigma_j} \nabla u_k \cdot \boldsymbol{\xi} \\
&= u_iu_ju_k \frac{(|u_i| - |u_j|)}{\Sigma_i\Sigma_j}(\boldsymbol{\rho}_k + O(1)) \cdot \boldsymbol{\xi}.
\end{aligned}$$

This gives us,

$$\det(\widetilde{\mathcal{A}}_0) \sim \Big(\Sigma_1(|u_2| - |u_3|)\boldsymbol{\rho}_1 + \Sigma_2(|u_3| - |u_1|)\boldsymbol{\rho}_2 + \Sigma_3(|u_1| - |u_2|)\boldsymbol{\rho}_3\Big) \cdot \boldsymbol{\xi}. \quad (2.38)$$

Let us define $\alpha_k = \Sigma_k(|u_i| - |u_j|)$ with $(k, i, j) \in \{(1,2,3), (2,3,1), (3,1,2)\}$. Then we have $\alpha_1 + \alpha_2 + \alpha_3 = 0$. Let $(\mathbf{e}_1, \mathbf{e}_2, \mathbf{e}_3)$ an orthonormal basis for $\mathbb{R}^3$. Then $\boldsymbol{\xi} = \sum_{k=1}^3 c_k\mathbf{e}_k$ with $|c_1|^2 + |c_2|^2 + |c_3|^2 = 1$. We take

$$\begin{aligned}
\boldsymbol{\rho}_1 &= \beta_1\big(\tau_1\mathbf{e}_1 + \mathfrak{i}\widetilde{\tau}_1\mathbf{e}_2\big), \\
\boldsymbol{\rho}_2 &= \beta_2\big(\tau_2\mathbf{e}_2 + \mathfrak{i}\widetilde{\tau}_2\mathbf{e}_3\big), \\
\boldsymbol{\rho}_3 &= \beta_3\big(\tau_3\mathbf{e}_3 + \mathfrak{i}\widetilde{\tau}_3\mathbf{e}_1\big),
\end{aligned}$$

where $|\tau_k| = |\widetilde{\tau}_k|$, $\forall 1 \le k \le 3$. It is straightforward to verify that $\boldsymbol{\rho}_k \cdot \boldsymbol{\rho}_k = 0$, $|\boldsymbol{\rho}_k| = \sqrt{2}|\tau_k||\beta_k|$ for all $1 \le k \le 3$. We now deduce from (2.38) that $\det(\widetilde{\mathcal{A}}_0) \sim \square_{\mathcal{R}} + \mathrm{i}\square_{\mathcal{I}}$ where

$$\square_{\mathcal{R}} = \alpha_1\tau_1\beta_1c_1 + \alpha_2\tau_2\beta_2c_2 + \alpha_3\tau_3\beta_3c_3, \qquad \square_{\mathcal{I}} = \alpha_1\widetilde{\tau}_1\beta_1c_2 + \alpha_2\widetilde{\tau}_2c_3 + \alpha_3\widetilde{\tau}_3\beta_3c_1.$$

Take $\beta_1 = \beta_2 = \beta_3$, $\tau_k = \widetilde{\tau}_k = 1$, $1 \le k \le 3$. Then $\det(\mathcal{A}_0) \neq 0$ unless $c_1 = c_2 = c_3$. [ This is because if $\det(\mathcal{A}_0) = 0$, we have $\square_{\mathcal{R}} = 0$, $\square_{\mathcal{I}} = 0$, and $a_1 + a_2 + a_3 = 0$. That is

$$\begin{pmatrix} 1 & 1 & 1 \\ c_1 & c_2 & c_3 \\ c_2 & c_3 & c_1 \end{pmatrix} \begin{pmatrix} \alpha_1 \\ \alpha_2 \\ \alpha_3 \end{pmatrix} = \begin{pmatrix} 0 \\ 0 \\ 0 \end{pmatrix}.$$

This contradicts the construction of $\{\alpha_k\}_{k=1}^3$]. Let us now take

$$\boldsymbol{\rho}_4 = 2\boldsymbol{\rho}_3.$$

Then the submatrix formed by $u_1$, $u_2$ and $u_4$ will have full rank when $c_1 = c_2 = c_3$. Therefore the submatrix formed by $u_1$, $u_2$, $u_3$ and $u_4$ is of full rank for any $\boldsymbol{\xi}$.

To show that $(\mathcal{A}, \mathcal{B})$ satisfies the Lopatinskii criterion given in Definition 2.6.4 for a set of well chosen $u_j$, we first observe that since $\mathcal{B} = \mathcal{I}$, we have, from the definition in (2.55),

$$\{\eta_j\}_{j=1}^{J+3} = \{-1, \cdots, -1\} \tag{2.39}$$

with the selection of the Douglis-Nirenberg numbers $\{s_i\}_{i=1}^{2J}$ and $\{t_j\}_{j=1}^{J+3}$ in (2.37), and the principal part of $\mathcal{B}$ has components $\mathcal{B}_{0,11} = 1$ and $\mathcal{B}_{0,k\ell} = 0$ otherwise.

Therefore, the system of differential equations in (2.56) and (2.57) takes the following form

$$(\mathbf{V}_j \cdot \boldsymbol{\zeta} - \mathrm{i}\mathbf{V}_j \cdot \boldsymbol{\nu}\frac{d}{dz})\delta\gamma(z) - \gamma(-|\boldsymbol{\zeta}|^2 + \frac{d^2}{dz^2})\delta u_j(z) = 0, \quad z > 0 \tag{2.40}$$

$$u_j\delta\sigma(z) + |u_j|u_j\delta\mu(z) + (\sigma + 2\mu|u_j|)\delta u_j(z) = 0, \quad z > 0 \tag{2.41}$$

$$\delta\gamma = 0, \quad z = 0 \tag{2.42}$$

where $\gamma$, $\sigma$, $\mu$, $u_j$ and $\mathbf{V}_j$ $(1 \leq j \leq J$, are all evaluated at $\mathbf{y} \in \partial\Omega$. We first deduce from (2.41) that, for $1 \leq j \leq J$,

$$\delta u_j = -\frac{u_j}{\Sigma_j}\delta\sigma - \frac{|u_j|u_j}{\Sigma_j}\delta\mu, \quad z > 0.$$

Plugging this into (2.40), we obtain that, for $1 \leq j \leq J$,

$$(\mathbf{V}_j \cdot \boldsymbol{\zeta} - \mathrm{i}\mathbf{V}_j \cdot \boldsymbol{\nu}\frac{d}{dz})\delta\gamma + \gamma(-|\boldsymbol{\zeta}|^2 + \frac{d^2}{dz^2})\left(\frac{u_j}{\Sigma_j}\delta\sigma + \frac{|u_j|u_j}{\Sigma_j}\delta\mu\right) = 0, \quad z > 0.$$

Without loss of generality, we consider the system formed by $u_1, u_2, u_3$. Let $\widetilde{F}_j = \mathbf{V}_j \cdot \boldsymbol{\nu}$, $p_j = \frac{u_j}{\Sigma_j}$ and $q_j = \frac{u_j^2}{\Sigma_j}$. We look for eigenvalues of the system as the root of

$$\det\begin{pmatrix} \widehat{F}_1 - \mathrm{i}\lambda\widetilde{F}_1 & p_1\gamma(\lambda^2 - |\boldsymbol{\zeta}|^2) & q_1\gamma(\lambda^2 - |\boldsymbol{\zeta}|^2) \\ \widehat{F}_2 - \mathrm{i}\lambda\widetilde{F}_2 & p_2\gamma(\lambda^2 - |\boldsymbol{\zeta}|^2) & q_2\gamma(\lambda^2 - |\boldsymbol{\zeta}|^2) \\ \widehat{F}_3 - \mathrm{i}\lambda\widetilde{F}_3 & p_3\gamma(\lambda^2 - |\boldsymbol{\zeta}|^2) & q_3\gamma(\lambda^2 - |\boldsymbol{\zeta}|^2) \end{pmatrix} = 0.$$

We observe first that the above equation admits two *repeated* roots $\lambda_{2,3} = \pm|\boldsymbol{\zeta}|$. Besides that, we have another root

$$\lambda_1 = -\mathrm{i}\frac{\widehat{F}_1(p_2q_3 - p_3q_2) + \widehat{F}_2(p_3q_1 - p_1q_3) + \widehat{F}_3(p_1q_2 - p_2q_1)}{\widetilde{F}_1(p_2q_3 - p_3q_2) + \widetilde{F}_2(p_3q_1 - p_1q_3) + \widetilde{F}_3(p_1q_2 - p_2q_1)}.$$

Moreover, the eigenvectors corresponding to $\lambda_{2,3}$ are of the form

$$\boldsymbol{\pi}_{2,3} = \begin{pmatrix} 0 \\ x \\ y \end{pmatrix}$$

with $x$ and $y$ arbitrary. Therefore, $\delta\gamma(z) = ce^{i|\lambda_1|z}$. Using the boundary condition $\delta\gamma(0) = 0$ and the decay condition $\delta\gamma(z) \to 0$ as $z \to \infty$, we conclude that $\delta\gamma(z) \equiv 0$. This in turn implies, from (2.41), that $\delta\sigma(z) \equiv 0$ and $\delta\mu(z) \equiv 0$. The proof is complete. □

For the set of Douglis-Nirenberg numbers $\{s_i\}$ and $\{t_j\}$ in (2.37), as well as the parameters $\{\eta_k\}$ given in (2.39), we defined the function space, parameterized by $\ell > n + \frac{1}{2}$,

$$\mathcal{W}_\ell = W^{\ell-s_1,2}(\Omega) \times \ldots \times W^{\ell-s_{2J},2}(\Omega) \times W^{\ell-\eta_1-\frac{1}{2},2}(\partial\Omega) \times \ldots W^{\ell-\eta_3-\frac{1}{2},2}(\partial\Omega).$$

We have the following uniqueness and stability result.

**Theorem 2.4.3.** *Under the same conditions of Theorem 2.4.2, let* $\{\delta H_j\}_{j=1}^J$ *and* $\{\widetilde{\delta H_j}\}_{j=1}^J$ *be the data sets generated with* $(\delta\gamma, \delta\sigma, \delta\mu)$ *and* $(\widetilde{\delta\gamma}, \widetilde{\delta\sigma}, \widetilde{\delta\mu})$ *respectively. Assume that the data are such that* $(\mathcal{S}, \phi) \in \mathcal{W}_\ell$ *and* $(\widetilde{\mathcal{S}}, \widetilde{\phi}) \in \mathcal{W}_\ell$. *Then there exists a set of* $J \geq n + 1$ *boundary illuminations,* $\{g_j\}_{j=1}^J$, *such that* $\{\delta H_j\}_{j=1}^J = \{\widetilde{\delta H_j}\}_{j=1}^J$ *(resp.* $(\mathcal{S}, \phi) = (\widetilde{\mathcal{S}}, \widetilde{\phi})$*) implies* $(\delta\gamma, \delta\sigma, \delta\mu) = (\widetilde{\delta\gamma}, \widetilde{\delta\sigma}, \widetilde{\delta\mu})$ *(resp.* $v = \tilde{v}$*) if* $\delta\gamma_{|\partial\Omega} = \widetilde{\delta\gamma}_{|\partial\Omega}$. *Moreover, the following stability estimate holds:*

$$\sum_{j=1}^{J+3} \|v_j - \widetilde{v}_j\|_{W^{\ell+t_j,2}(\Omega)} \leq C\Big(\sum_{i=1}^{2J} \|\mathcal{S}_i - \widetilde{\mathcal{S}}_i\|_{W^{\ell-s_i,2}(\Omega)} + \sum_{k=1}^{3} \|\phi_k - \widetilde{\phi}_k\|_{W^{\ell-\eta_k-\frac{1}{2},2}(\partial\Omega)}\Big), \tag{2.43}$$

*for all* $\ell > n + \frac{1}{2}$.

*Proof.* We start with the uniqueness result. Let $\delta H_j = 0$, $1 \leq j \leq 3$, we then have that

$$u_j \delta\sigma + |u_j| u_j \delta\mu + (\sigma + 2\mu|u_j|)\delta u_j = 0, \quad 1 \leq j \leq 3.$$

We can eliminate the variables $\delta\sigma$ and $\delta\mu$ to have, with $\mathcal{E} = \{(1,2,3),(2,3,1),(3,1,2)\}$,

$$\sum_{(i,j,k)\in\mathcal{E}} u_i u_j (u_j - u_i)(\sigma + 2\mu|u_k|)\delta u_k = 0. \tag{2.44}$$

Let $G$ be the Green function corresponding to the operator $-\nabla\cdot\gamma\nabla$ with the homogeneous Dirichlet boundary condition. We can then write (2.44) as, using $\delta\gamma_{|\partial\Omega} = 0$ as well as $\delta u_{j|\partial\Omega} = 0$,

$$\sum_{(i,j,k)\in\mathcal{E}} u_i u_j (u_j - u_i)(\sigma + 2\mu|u_k|) \int_\Omega \delta\gamma(\mathbf{y}) \nabla u_k(\mathbf{y}) \cdot \nabla G(\mathbf{x};\mathbf{y}) d\mathbf{y} = 0.$$

Take $u_k$ to be the complex geometric optics solution we constructed in Theorem 2.6.6 with complex vector $\boldsymbol{\rho}_k$, using the fact that $u_k \sim e^{\boldsymbol{\rho}_k\cdot\mathbf{x}}(1+\varphi_k)$ (and $\varphi_k$ decays as $|\boldsymbol{\rho}_k|^{-1}$) and $\nabla u_k = u_k(\boldsymbol{\rho}_k + O(1))$, we can rewrite the above equation as, for $|\boldsymbol{\rho}_k|$ sufficiently large,

$$\sum_{(i,j,k)\in\mathcal{E}} u_i u_j (u_j - u_i)(\sigma + 2\mu|u_k|) \int_\Omega \delta\gamma(\mathbf{y}) u_k(\mathbf{y}) \boldsymbol{\rho}_k \cdot \nabla G(\mathbf{x};\mathbf{y}) d\mathbf{y} = 0.$$

Even though it is not necessary here, but if we select $\boldsymbol{\rho}_k$ such that $\Re\boldsymbol{\rho}_k < 0$ and $|\Re\boldsymbol{\rho}_k|$ is sufficiently large, then we can simplify the above equation further to

$$\int_\Omega \delta\gamma(\mathbf{y}) \mathbf{v}(\mathbf{x};\mathbf{y}) \cdot \nabla G(\mathbf{x};\mathbf{y}) d\mathbf{y} = 0. \tag{2.45}$$

with $\mathbf{v}$ the vector given by

$$\mathbf{v} = \sum_{(i,j,k)\in\mathcal{E}} \sigma(\mathbf{x})\Big(u_i u_j(u_j - u_i)\Big)(\mathbf{x})u_k(\mathbf{y})\boldsymbol{\rho}_k. \tag{2.46}$$

We now need the following lemma.

**Lemma 2.4.4.** *Let* $\mathbf{v}$ *be such that: (i) there exists* $\mathfrak{c} > 0$ *such that* $|\mathbf{v}| \geq \mathfrak{c} > 0$ *for a.e.* $\mathbf{x} \in \Omega$*; and (ii)* $\mathbf{v} \in [W^{1,\infty}(\Omega)]^n$ *at least. Then* (2.45) *implies that* $\delta\gamma \equiv 0$.

*Proof.* Let $u$ be the solution to

$$-\nabla\cdot\gamma\nabla u - \nabla\cdot(\delta\gamma\mathbf{v}) = 0, \quad \text{in } \Omega, \qquad u = 0, \quad \text{on } \partial\Omega \tag{2.47}$$

Then

$$u(\mathbf{x}) = \int_\Omega \delta\gamma(\mathbf{y})\mathbf{v}(\mathbf{x};\mathbf{y})\cdot\nabla G(\mathbf{x};\mathbf{y})d\mathbf{y}.$$

Therefore (2.45) implies that $u \equiv 0$. Therefore

$$-\nabla\cdot\delta\gamma\mathbf{v} = 0, \quad \text{in } \Omega, \qquad \delta\gamma = 0, \quad \text{on } \partial\Omega. \tag{2.48}$$

This is a transport equation for $\delta\gamma$ that admits the unique solution $\delta\gamma \equiv 0$ with the vector field $\mathbf{v}$ satisfying the assumed requirements; see for instance [19, 25, 28, 35, 54] and references therein. □

It is straightforward to check that we can select $\{\boldsymbol{\rho}_j\}_{j=1}^3$ such that the vector field $\mathbf{v}$ defined in (2.46) satisfies the requirement in Lemma 2.4.4. We then conclude that $\delta\gamma \equiv 0$.

The conditions assumed on the background coefficients ensure the ellipticity of the system as proven in Theorem 2.4.2. The stability result then follows from (2.58); see more discussions in [17] and references therein. Note that the simplification inthe last term in (2.43) is due to the fact that $\phi_k = \widetilde{\phi}_k = 0$ when $4 \leq k \leq J+3$. Note also that the following simplification can be made in (2.43):

$$\sum_{i=1}^{2J} \|\mathcal{S}_i - \widetilde{\mathcal{S}}_i\|_{W^{\ell-s_i,2}(\Omega)} \leq 2 \sum_{i=1}^{J} \|\delta H_j - \widetilde{\delta H}_j\|_{W^{\ell+2,2}(\Omega)}.$$

The proof is complete. □

## 2.5 Numerical Simulations

We present in this section some preliminary numerical reconstruction results using synthetic internal data. We restrict ourselves to two-dimensional settings only to simplify the computation. The spatial domain of the reconstruction is the square $\Omega = (1,1)^2$. All the equations in $\Omega$ are discretized with a first-order finite element method on triangular meshes. In all the simulations in this section, reconstructions are performed on a finite element mesh with about 6000 triangular elements. The nonlinear system resulted from the discretization of the diffusion equation (2.1) is solved using a quasi-Newton method as implemented in [86].

To generate synthetic data for inversion, we solve (2.1) using the true coefficients. We performed reconstructions using both noiseless and noisy synthetic data. For the noisy data, we added additive random noise to the data

by simply multiplying each datum by $(1 + \sqrt{3}\epsilon \times 10^{-2}\texttt{random})$ with `random` a uniformly distributed random variable taking values in $[1, 1]$, $\epsilon$ being the noise level (i.e. the size of the variance in percentage).

We will focus on the reconstruction of the absorption coefficients $\sigma$ and $\mu$. We present reconstruction results from two different numerical methods.

**Direct Algorithm.** The first method we use is motivated from the method of proofs of Propositions 2.3.1 and 2.3.2. When we have $J \geq 2$ data sets $\{H_j\}_{j=1}^J$ from $J$ illuminations $\{g_j\}_{j=1}^J$, we first reconstruct, for each $j$, $u_j^*$ as the solutions to

$$-\nabla \cdot (\gamma \nabla u_j^*) = -\frac{H_j^*}{\Xi} \quad \text{in } \Omega, \qquad u_j^* = g_j \quad \text{on } \partial\Omega.$$

We then reconstruct $\sigma + \mu|u_j^*| = \frac{H_j}{\Xi u_j^*}$. Collecting this quantity from all data, we have, for each point $\mathbf{x} \in \Omega$,

$$\begin{pmatrix} 1 & |u_1^*| \\ \vdots & \vdots \\ 1 & |u_J^*| \end{pmatrix} \begin{pmatrix} \sigma \\ \mu \end{pmatrix} = \begin{pmatrix} \frac{H_1^*}{\Xi u_1^*} \\ \vdots \\ \frac{H_J^*}{\Xi u_J^*} \end{pmatrix}.$$

We then reconstruct $(\sigma, \mu)$ by solving this small linear system, in least square sense, at each point $\mathbf{x} \in \Omega$. Therefore, the main computational cost of this algorithm lies in the numerical solution of the $J$ linear equations for $\{u_j^*\}$.

**Least-Square Algorithm.** The second reconstruction method that we will use is based on numerical optimization. This method searches for the unknown

coefficient by minimizing the objective functional

$$\Phi(\sigma,\mu) \equiv \frac{1}{2}\sum_{j=1}^{J}\int_{\Omega}(\Xi\sigma u_j + \Xi\mu|u_j|u_j - H_j^*)^2 d\mathbf{x} + \kappa R(\sigma,\mu), \tag{2.49}$$

where we use the functional $R(\sigma,\mu) = \frac{1}{2}\left(\int_\Omega |\nabla\sigma|^2 d\mathbf{x} + \int_\Omega |\nabla\mu|^2 d\mathbf{x}\right)$ together with the parameter $\kappa$ to add regularization mechanism in the reconstructions. We use the BFGS quasi-Newton method that we developed in [86] to solve this minimization problem. It is straightforward to check, following Proposition 2.2.5, that the gradient of the functional $\Phi(\sigma,\mu)$ with respect to $\sigma$ and $\mu$ are given respectively by

$$\Phi'_\sigma[\sigma,\mu](\delta\sigma) = \int_\Omega \left\{\sum_{j=1}^{J}\Big[z_j\Xi u_j + v_j u_j\Big]\delta\sigma + \kappa\nabla\sigma\cdot\nabla\delta\sigma\right\} d\mathbf{x} \tag{2.50}$$

$$\Phi'_\mu[\sigma,\mu](\delta\mu) = \int_\Omega \left\{\sum_{j=1}^{J}\Big[z_j\Xi|u_j|u_j + v_j|u_j|u_j\Big]\delta\mu + \kappa\nabla\mu\cdot\nabla\delta\mu\right\} d\mathbf{x} \tag{2.51}$$

where $z_j = \Xi(\sigma u_j + \mu|u_j|u_j) - H_j^*$ and $v_j$ solves

$$-\nabla\cdot\gamma\nabla v_j + (\sigma + 2\mu|u_j|)v_j = -z_j\Xi(\sigma+2\mu|u_j|), \quad \text{in } \Omega, \qquad v_j = 0, \quad \text{on } \partial\Omega \tag{2.52}$$

Therefore, in each iteration of the optimization algorithm, we need to solve $J$ semilinear diffusion equations for $\{u_j\}_{j=1}^J$ and then $J$ adjoint linear elliptic equations for $\{v_j\}_{j=1}^J$ to evaluate the gradients of the objective function with respect to the unknowns.

**Experiment I.** We start with a set of numerical experiments on the reconstruction of the two-photon absorption coefficient $\mu$ assuming that the single-photon absorption coefficient $\sigma$ is known. We use data collected from four

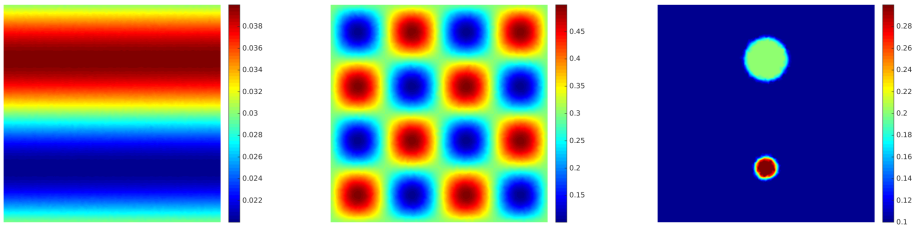


Figure 2.1: The true coefficients, $\gamma$ (left), $\sigma$ (middle), $\mu$ (right), used to generate synthetic data for the reconstructions.

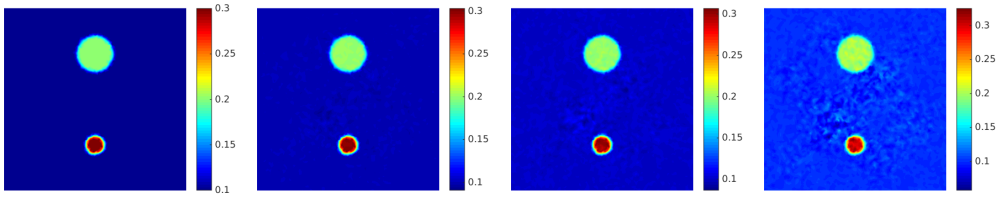


Figure 2.2: The absorption coefficient $\mu$ reconstructed using synthetic data containing different levels ($\epsilon = 0, 1, 2, 5$ from left to right) of noises. The *Direct Algorithm* is used in the reconstructions.

different sources $\{g_j\}_{j=1}^4$, $\{H_j\}_{j=1}^4$. We perform reconstructions using the *Direct Algorithm*. In Fig. 2.2 we show the reconstruction results from noisy synthetic data with noise levels $\epsilon = 0$, $\epsilon = 1$, $\epsilon = 2$, and $\epsilon = 5$. The true coefficients used to generate the data are shown in Fig. 2.1.

To measure the quality of the reconstruction, we use the relative $L^2$ error. This error is defined as the ratio between (i) the $L^2$ norm of the difference between the reconstructed coefficient and the true coefficient and (ii) the $L^2$ norm of the true coefficient, expressed in percentage. The relative $L^2$ errors in the reconstructions of $\mu$ in Fig 2.2 are 0.00%, 2.45%,4.98%, and 12.23% for $\epsilon = 0$, $\epsilon = 1$, $\epsilon = 2$ and $\epsilon = 5$ respectively.

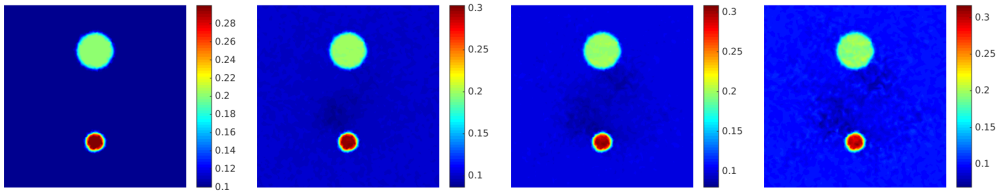


Figure 2.3: Same as in Fig. 2.2 except that the reconstructions are performed with the *Least-Square Algorithm*.

**Experiment II.** One of the main limitations on the *Direct Algorithm* is that it requires the use of illumination sources that are positive everywhere on the boundary. This is difficult to implement in practical applications. The *Least-Square Algorithm*, however, does not have such requirement on the optical sources (but it is computationally more expensive). Here we repeat the simulations in Experiment I with the *Least-Square Algorithm*. The reconstruction

results are shown in Fig 2.3. We observe that, with the same (not exactly the same since the realizations of the noise are different) data sets, the reconstructions from the two different algorithms are of very similar quality. The relative $L^2$ errors for the reconstructions in Fig 2.3 are 0.00%, 2.44%,4.62%, and 9.36% respectively for the four cases.

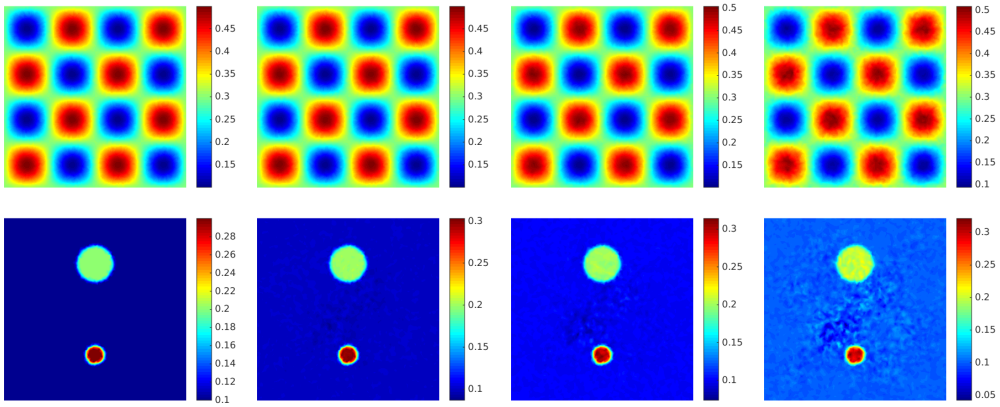

Figure 2.4: The absorption coefficient pair $\sigma$ (top row) and $\mu$ (bottom row) reconstructed using the *Direct Algorithm* with data at different noise levels ($\epsilon = 0, 1, 2, 5$ from left to right).

**Experiment III.** In the third set of numerical experiments, we study the simultaneous reconstructions of the single-photon and two-photon absorption coefficients, $\sigma$ and $\mu$. We again use data collected from four different sources. In Fig. 2.4, we show the reconstructions from data containing different noise levels using the *Direct Algorithm*. The relative $L^2$ error in the reconstructions of $(\sigma, \mu)$ are $(0.00\%, 0.00\%)$, $(0.79\%, 2.76\%)$,$(1.56\%, 5.55\%)$, and $(3.91\%, 13.71\%)$ respectively for data with noise levels $\epsilon = 0$, $\epsilon = 1$, $\epsilon = 2$

and $\epsilon = 5$.

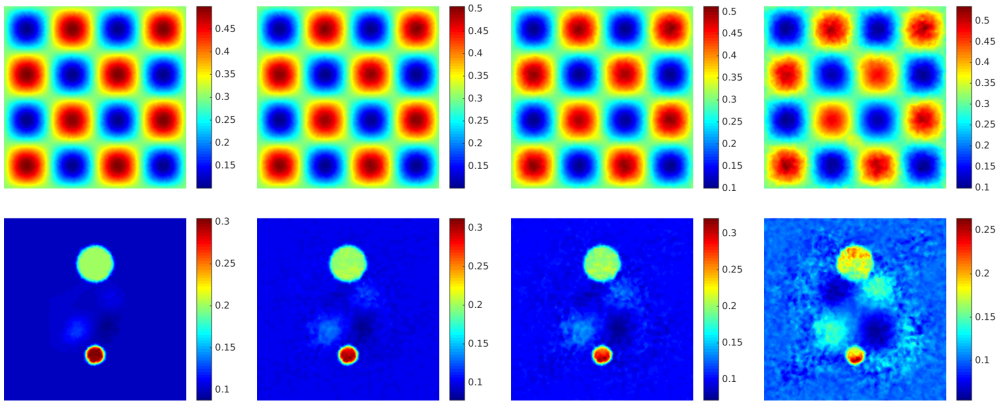

Figure 2.5: The same as in Fig. 2.4 except that the reconstructions are performed using the *Least-Square Algorithm*.

**Experiment IV.** We now repeat the simulations in Experiment III with the *Least-Square Algorithm*. The results are shown in Fig. 2.5. The relative $L^2$ errors in the reconstructions are now $(0.22\%, 2.38\%)$, $(1.21\%, 6.43\%)$,$(2.34\%, 10.98\%)$, $(5.64\%, 22.06\%)$ respectively for data with noise levels $\epsilon = 0$, $\epsilon = 1$, $\epsilon = 2$, and $\epsilon = 5$. The quality of the reconstructions is slightly lower than, but still comparable to, that in the reconstructions in Experiment III.

We observe from the above simulation results that, in general, the quality of the reconstructions is very high. When we have the illumination sources that satisfy the positivity requirement on the whole boundary of the domain, the *Direct Algorithm* provides an efficient and robust reconstruction method. The *Least-Square Algorithm* is less efficient but is as robust in terms of the quality of the reconstructions. The reconstructions with the *Least-Square Al-*

*gorithm* are done for a fixed regularization parameter that we selected by a couple of trial-error test. It is by no means the optimal regularization parameter that can be selected through more sophisticated algorithms [38]. However, this is an issue that we think is not important at the current stage of this project. Therefore, we did not pursue further in this direction.

## 2.6 Concluding Remarks

We studied in this chapter inverse problems in quantitative photoacoustic tomography with two-photon absorption. We derived uniqueness and stability results in the reconstruction of single-photon and two-photon absorption coefficients, and proposed explicit reconstruction methods in this case with well-selected illumination sources. We also studied the inverse problem of reconstructing the diffusion coefficient in addition to the absorption coefficients and obtained partial results on the uniqueness and stability of the reconstructions for the linearized problem. We presented some numerical studies based on the explicit reconstruction procedures as well as numerical optimization techniques to demonstrate the type of quality that can be achieved in reasonably controlled environments (where noise strength in the data is moderate).

Our focus in this chapter is to study the mathematical properties of the inverse problems. There are many issues that have to be address in the future. Mathematically, it would be nice to generalize the uniqueness and stability results in Section 2.4, on multiple coefficient reconstructions in linearized settings, to the full nonlinear problem. Computationally, detailed numerical

analysis, in three-dimensional setting, need to be performed to quantify the errors in the reconstructions in practically relevant scenarios. It is especially important to perform reconstructions starting from acoustic data directly to see how sensitive the reconstruction of the two-photon absorption coefficient is with respect to noise in the acoustic data. On the modeling side, it is very interesting to see if the current study can be generalized to radiative transport type models for photon propagation.

## Appendix A: Terminologies in overdetermined elliptic systems

We recall here, very briefly, some terminologies and notations related to overdetermined linear elliptic systems, following the presentation in [17, 114]. Let $M, \widetilde{M}, N$ be three positive integers such that $M > N$. we consider the following system of $M$ differential equations for $N$ variables $\{v_1, \cdots, v_N\}$ with $\widetilde{M}$ boundary conditions:

$$\mathcal{A}(\mathbf{x}, D)v = \mathcal{S}, \quad \text{in } \Omega \tag{2.53}$$

$$\mathcal{B}(\mathbf{x}, D)v = \phi, \quad \text{on } \partial\Omega \tag{2.54}$$

Here $\mathcal{A}(\mathbf{x}, D)$ is a matrix differential operator whose $(i, j)$ element, denoted by $\mathcal{A}_{ij}(\mathbf{x}, D)$ $(1 \leq i \leq M,\ 1 \leq j \leq N)$, is a polynomial in $D$ for any $\mathbf{x} \in \Omega$. $\mathcal{B}(\mathbf{x}, D)$ is a matrix differential operator whose $(k, \ell)$ element, denoted by $\mathcal{B}_{k\ell}(\mathbf{x}, D)$ $(1 \leq k \leq \widetilde{M},\ 1 \leq \ell \leq N)$, is a polynomial in $D$ for any $\mathbf{x} \in \partial\Omega$.

We associate an integer $s_i$ $(1 \leq i \leq M)$ to row $i$ of $\mathcal{A}$ and an integer $t_j$

to column $j$ $(1 \le j \le N)$ of $\mathcal{A}$.

**Definition 2.6.1.** *We call the integers* $\{s_i\}_{i=1}^M$ *and* $\{t_j\}_{j=1}^N$ *the Douglis-Nirenberg numbers associated to* $\mathcal{A}$ *if: (a)* $s_i \le 0$, $1 \le i \le M$; *(b) when* $s_i + t_j \ge 0$, *the order of* $\mathcal{A}_{ij}(\mathbf{x}, D)$ *is not greater than* $s_i + t_j$; *and (c) when* $s_i + t_j < 0$, $\mathcal{A}_{ij}(\mathbf{x}, D) = 0$.

**Definition 2.6.2.** *The principal part of* $\mathcal{A}$, *denoted by* $\mathcal{A}_0$, *is defined as the part of* $\mathcal{A}$ *such that the degree of* $\mathcal{A}_{0,ij}(\mathbf{x}, D)$ *is exactly* $s_i + t_j$.

We say that $\mathcal{A}$ is elliptic, in the sense of Douglis-Nirenberg, if the matrix $\mathcal{A}_0(\mathbf{x}, \boldsymbol{\xi})$ is of rank $N$ for all $\boldsymbol{\xi} \in \mathbb{S}^{n-1}$ and all $\mathbf{x} \in \Omega$.

Let $b_{k\ell}$ be the order of $\mathcal{B}_{k\ell}$ and define

$$\eta_k = \max_{1 \le \ell \le N} (b_{k\ell} - t_\ell), \quad 1 \le k \le \widetilde{M}. \tag{2.55}$$

**Definition 2.6.3.** *The principal part of* $\mathcal{B}$, *denoted by* $\mathcal{B}_0$, *is defined as the part of* $\mathcal{B}$ *such that the order of* $\mathcal{B}_{0,k\ell}$ *is exactly* $\eta_k + t_\ell$.

Let $\mathcal{B}_0(\mathbf{x}, D)$ be the principal part of $\mathcal{B}$. Fix $\mathbf{y} \in \partial\Omega$, and let $\boldsymbol{\nu}$ be the *inward* unit normal vector at $\mathbf{y}$. Let $\boldsymbol{\zeta} \in \mathbb{S}^{n-1}$ be a vector such that $\boldsymbol{\zeta} \cdot \boldsymbol{\nu} = 0$ and $|\boldsymbol{\zeta}| \ne 0$. We consider on the half line $\mathbf{y} + z\boldsymbol{\nu}, z > 0$ the system of ordinary equations

$$\mathcal{A}_0(\mathbf{y}, \mathrm{i}\boldsymbol{\zeta} + \boldsymbol{\nu}\frac{d}{dz})\widetilde{u}(z) \quad = 0, \quad z > 0, \tag{2.56}$$

$$\mathcal{B}_0(\mathbf{y}, \mathrm{i}\boldsymbol{\zeta} + \boldsymbol{\nu}\frac{d}{dz})\widetilde{u}(z) \quad = 0, \quad z = 0. \tag{2.57}$$

**Definition 2.6.4.** *If for any* $\mathbf{y} \in \partial\Omega$*, the only solution to the system* (2.56)-(2.57) *such that* $\widetilde{u}(z) \to 0$ *as* $z \to \infty$ *is* $\widetilde{u} \equiv 0$*, then we say that* $(\mathcal{A}, \mathcal{B})$ *satisfies the Lopatinskii criterion.*

It is well-established that [17, 95, 114] when $(\mathcal{A}, \mathcal{B})$ satisfies the Lopatinskii criterion, the system (2.53)-(2.54) can be solved up to possibly a finite dimensional subspace. Moreover, a general *a priori* stability estimate can be established for the system. Define the function space

$$\mathcal{W}_\ell = W^{\ell-s_1,2}(\Omega) \times \ldots \times W^{\ell-s_M,2}(\Omega) \times W^{\ell-\eta_1-\frac{1}{2},2}(\partial\Omega) \times \ldots W^{\ell-\sigma_{\widetilde{M}}-\frac{1}{2},2}(\partial\Omega),$$

for some $\ell > n + \frac{1}{2}$. Then it can be shown that, if $(\mathcal{S}, \phi) \in \mathcal{W}_\ell$,

$$\begin{aligned} & \textstyle\sum_{j=1}^{N} \|v_j\|_{W^{\ell+t_j,2}(\Omega)} \\ \leq\ & C\Big(\textstyle\sum_{i=1}^{M} \|\mathcal{S}_i\|_{W^{\ell-s_i,2}(\Omega)} + \sum_{i=1}^{\widetilde{M}} \|\phi_i\|_{W^{\ell-\eta_i-\frac{1}{2},2}(\partial\Omega)}\Big) + \widetilde{C} \textstyle\sum_{t_j>0} \|v_j\|_{L^2(\Omega)}, \end{aligned} \tag{2.58}$$

provided that all the quantities involved are regular enough. The last term in the estimate can be dropped when uniqueness of the solution can be proven. More details on this theory can be found in [17] and references therein.

## Appendix B: CGO solutions to equation (2.1)

This appendix is devoted to the construction of complex geometric optics (CGO) solutions [101, 107] to our model equation (2.1). We restrict the construction to the three-dimensional setting ($n = 3$). We start by revisiting CGO solutions to the classical diffusion problem that was first developed in [101]:

$$-\nabla \cdot (\gamma \nabla u) + \sigma u = 0, \quad \text{in } \Omega \tag{2.59}$$

with the assumption that $\gamma \in \mathcal{C}^2(\Omega)$ and $\sigma \in \mathcal{C}^1(\Omega)$. Let $u_*$ be a solution to this equation, then the Liouville transform defined in (2.26) shows that $\tilde{u}_* = \sqrt{\gamma} u_*$ solves

$$\Delta \tilde{u}_* - \Big( \frac{\Delta \sqrt{\gamma}}{\sqrt{\gamma}} + \frac{\sigma}{\gamma} \Big) \tilde{u}_* = 0, \quad \text{in } \Omega. \tag{2.60}$$

The following result is well-known.

**Theorem 2.6.5** ([16, 101, 107]). *Let $\gamma \in \mathcal{C}^4(\Omega)$ and $\sigma \in \mathcal{C}^2(\Omega)$. For any $\boldsymbol{\rho} \in \mathbb{C}^n$ such that $\boldsymbol{\rho} \cdot \boldsymbol{\rho} = 0$ and $|\boldsymbol{\rho}|$ sufficiently large, there is a function $g$ such that the solution to (2.60), with the boundary condition $\tilde{u}_*|_{\partial\Omega} = g$, takes the form*

$$\tilde{u}_* = e^{\boldsymbol{\rho} \cdot \mathbf{x}} (1 + \varphi(\mathbf{x})), \tag{2.61}$$

*with $\varphi(\mathbf{x})$ satisfying the estimate*

$$|\boldsymbol{\rho}| \|\varphi\|_{W^{2,2}(\Omega)} + \|\varphi\|_{W^{3,2}(\Omega)} \leq C \left\| \frac{\Delta \sqrt{\gamma}}{\sqrt{\gamma}} + \frac{\sigma}{\gamma} \right\|_{W^{2,2}(\Omega)}. \tag{2.62}$$

The function $\tilde{u}_*$ is called a complex geometric optics solution to (2.60) and

$$u_* = \gamma^{-1/2} e^{\boldsymbol{\rho} \cdot \mathbf{x}} (1 + \varphi(\mathbf{x})) \tag{2.63}$$

is a complex geometric optics solution to (2.59). With the regularity assumption on $\gamma$ and (2.62), it is easy to verify that

$$\nabla u_* \sim u_* (\boldsymbol{\rho} + O(1)). \tag{2.64}$$

We now show, using the Newton-Kantorovich method [75], that we can construct a CGO solution to our semilinear diffusion model that is very close, in $W^{3,2}(\Omega)$, to $u_*$ for some $\boldsymbol{\rho}$.

**Theorem 2.6.6.** *Let $\gamma \in \mathcal{C}^4(\Omega)$, $\sigma \in \mathcal{C}^2(\Omega)$ and $\mu \in \mathcal{C}^1(\Omega)$. Let $\boldsymbol{\rho} \in \mathbb{C}^n$ be such that $\boldsymbol{\rho} \cdot \boldsymbol{\rho} = 0$ and $|\boldsymbol{\rho}|$ sufficiently large. Assume further that $\boldsymbol{\rho}$ and $\Omega$ satisfy*

$$-\widetilde{\kappa}|\boldsymbol{\rho}| \leq \Re(\boldsymbol{\rho} \cdot \mathbf{x}) \leq -\kappa|\boldsymbol{\rho}|, \quad \forall \mathbf{x} \in \bar{\Omega}, \tag{2.65}$$

*for some $0 < \kappa < \widetilde{\kappa} < \infty$. Then, there exists a function $g$ such that the solution to (2.1) takes the form*

$$u(\mathbf{x}) = u_*(\mathbf{x}) + v(\mathbf{x}), \tag{2.66}$$

*with $v$ such that*

$$\|v\|_{W^{3,2}(\Omega)} \leq ce^{-\kappa'\kappa|\boldsymbol{\rho}|}, \tag{2.67}$$

*for some constant $c$ and some $\kappa' \in (1, 2)$.*

*Proof.* Let us first remark that since $\Omega$ is a bounded domain, the assumption in (2.65) is nothing more than the constraint that $\Re(\boldsymbol{\rho}) \leq \mathfrak{c}_0 < 0$ for some $\mathfrak{c}_0$. Moreover, the assumption in (2.65) allows us to bound the CGO solution $u_*$ and its gradient as

$$\|u_*\|_{L^\infty(\Omega)} \leq ce^{-\kappa|\boldsymbol{\rho}|}, \tag{2.68}$$

$$\|\nabla u_*\|_{L^\infty(\Omega)} \leq ce^{-\kappa|\boldsymbol{\rho}|}(|\boldsymbol{\rho}| + 1). \tag{2.69}$$

Let $\mathcal{P}(\mathbf{x}, D)$ be the differential operator defined in (2.1). We verify that, with the assumptions on the coefficients involved, $\mathcal{P}'_{u_*}$, the linearization of $\mathcal{P}$ at $u_*$, $\mathcal{P}'_{u_*} := -\nabla \cdot \gamma \nabla + \sigma + 2\mu|u_*|$, admits a bounded inverse as a linear map from $W^{3,2}(\Omega)$ to $W^{1,2}(\Omega)$.

We observe from the construction that $u_*$ is away from 0. Therefore, there exists a constant $r > 0$ such that the ball $B_r(u_*)$ (in the $W^{3,2}(\Omega)$ metric) contains functions that are away from 0. Let $u_1 \in B_r(u_*)$, $u_2 \in B_r(u_*)$ and $v \in W^{3,2}(\Omega)$ be given, we check that

$$\mathcal{P}'_{u_1} v - \mathcal{P}'_{u_2} v = 2\mu(|u_1| - |u_2|)v. \tag{2.70}$$

This leads to

$$\|\mathcal{P}'_{u_1} v - \mathcal{P}'_{u_2} v\|_{L^2(\Omega)} = \|2\mu(|u_1| - |u_2|)v\|_{L^2(\Omega)} \leq c\|u_1 - u_2\|_{W^{3,2}(\Omega)}\|v\|_{W^{3,2}(\Omega)}. \tag{2.71}$$

We can also bound $\|\nabla(\mathcal{P}'_{u_1} v - \mathcal{P}'_{u_2} v)\|_{L^2(\Omega)}$ as follows. We first verify that

$$\begin{aligned}
\|\nabla(\mathcal{P}'_{u_1} v - \mathcal{P}'_{u_2} v)\|_{L^2(\Omega)} &= 2\|\nabla\big(\mu(|u_1| - |u_2|)v\big)\|_{L^2(\Omega)} \\
&\leq 2\|\mu(|u_1| - |u_2|)\nabla v\|_{L^2(\Omega)} + 2\|\nabla\big(\mu(|u_1| - |u_2|)\big)v\|_{L^2(\Omega)} \\
&\leq 2\|\mu(|u_1| - |u_2|)\|_{L^\infty(\Omega)}\|\nabla v\|_{L^2(\Omega)} + 2\|\nabla\big(\mu(|u_1| - |u_2|)\big)\|_{L^\infty(\Omega)}\|v\|_{L^2(\Omega)} \\
&\leq C\|v\|_{W^{3,2}(\Omega)}\Big(\|u_1 - u_2\|_{L^\infty(\Omega)} + \|\nabla\big(\mu(|u_1| - |u_2|)\big)\|_{L^\infty(\Omega)}\Big).
\end{aligned} \tag{2.72}$$

We then perform the expansion, using the fact that $|u_j| > 0$ $(j = 1, 2)$,

$$\nabla\big(\mu(|u_1| - |u_2|)\big) = (|u_1| - |u_2|)\nabla\mu + \mu\Re\Big(\frac{u_1}{|u_1|}\nabla(\bar{u}_1 - \bar{u}_2) + (\frac{u_1}{|u_1|} - \frac{u_2}{|u_2|})\nabla\bar{u}_2\Big).$$

This gives us the bound

$$\|\nabla\big(\mu(|u_1| - |u_2|)\big)\|_{L^\infty(\Omega)} \leq c_1\|u_1 - u_2\|_{L^\infty(\Omega)} + c_2\|\nabla(u_1 - u_2)\|_{L^\infty(\Omega)}. \tag{2.73}$$

We can then combine (2.72) with (2.73) and use Sobolev embedding, for instance [46, Corollary 7.11], to conclude that

$$\|\nabla(\mathcal{P}'_{u_1} v - \mathcal{P}'_{u_2} v)\|_{L^2(\Omega)} \leq C\|u_1 - u_2\|_{W^{3,2}(\Omega)}\|v\|_{W^{3,2}(\Omega)}. \tag{2.74}$$

We then have, from the bounds in (2.71) and (2.74), the following bound on the operator norm of $\mathcal{P}'_{u_1} - \mathcal{P}'_{u_2}$ by

$$\|\mathcal{P}'_{u_1} - \mathcal{P}'_{u_2}\|_{\mathcal{L}\left(W^{3,2}(\Omega), W^{1,2}(\Omega)\right)} \leq c\|u_1 - u_2\|_{W^{3,2}(\Omega)}. \tag{2.75}$$

Let $w$ be the solution to $\mathcal{P}'_{u_*}(\mathbf{x}, D)w = \mathcal{P}(\mathbf{x}, D)u_*$ , that is,

$$-\nabla \cdot \gamma \nabla w + (\sigma + 2\mu|u_*|)w = \mu|u_*|u_*, \quad \text{in } \Omega, \qquad w = 0, \quad \text{on } \partial\Omega. \tag{2.76}$$

It then follows from classical elliptic theory that

$$\|(\mathcal{P}'_{u_*})^{-1}\mathcal{P}(\mathbf{x}, D)u_*\|_{W^{3,2}(\Omega)} \leq c\||u_*|u_*\|_{W^{1,2}(\Omega)} \leq \tilde{c}e^{-2\kappa|\boldsymbol{\rho}|}(|\boldsymbol{\rho}| + 1) \leq \tilde{\tilde{c}}e^{-\kappa'\kappa|\boldsymbol{\rho}|}, \tag{2.77}$$

for some $\kappa' \in (1, 2)$, where the last step comes from the bounds in (2.68) and (2.69).

It then follows from the Newton-Kantorovich theorem [75] that, when $|\boldsymbol{\rho}|$ is sufficiently large, there exists a solution to (2.1) in the ball of radius $r' = \tilde{\tilde{c}}e^{-\kappa'\kappa|\boldsymbol{\rho}|}$ centered at $u_*$, in $W^{3,2}(\Omega)$. The solution is of the form (2.66). □

# Chapter 3

# Hybrid Inverse Problems in Fluorescence PAT

## 3.1 Introduction

Fluorescence PAT (fPAT) is another variant of PAT that is used as a tool of optical molecular imaging [26, 82, 83, 109, 112, 111, 116]. The main objective here is to visualize particular cellular functions and molecular processes inside biological tissues by using target-specific exogenous contrasts. In a typical fPAT imaging process, we first inject fluorescent markers into the medium to be probed. The markers will travel inside the medium and accumulate on their targets, for instance cancerous tissues inside the normal tissue. We then send a short pulse of NIR photons at wavelength $\lambda_x$ to the medium to excite the fluorescent markers who then emit NIR photons at a different wavelength $\lambda_m$. The absorption of both the excitation and the emission photons by the medium will then generate ultrasound waves inside the medium following the photoacoustic effect just as in a regular PAT process, assuming that fluorescence takes place instantaneously as excitation light pulse is absorbed [92]. We then measure the ultrasound signals on the surface of the medium and

This chapter is based on K. Ren, R. Zhang, and Y. Zhong. Inverse transport problems in quantitative PAT for molecular imaging. *Inverse Problems*, 31, 2015. 125012. The author of this dissertation is the main contributor.

attempt to recover information associated with the biochemical markers.

The density distributions for the external light source and the fluorescent light in the tissues are both described by the radiative transport equation. Let $\Omega \subset \mathbb{R}^d$ ($d \geq 2$) be the domain of interests and $\mathbb{S}^{d-1}$ be the unit sphere in $\mathbb{R}^d$. We denote by $X = \Omega \times \mathbb{S}^{d-1}$ the phase space and $\Gamma_\pm = \{(\mathbf{x}, \mathbf{v}) \in \partial\Omega \times \mathbb{S}^{d-1} | \pm \mathbf{n}(\mathbf{x}) \cdot \mathbf{v} > 0\}$ its boundary sets. We denote by $u_x(\mathbf{x}, \mathbf{v})$ and $u_m(\mathbf{x}, \mathbf{v})$ the density of photons at the excitation and emission wavelengths respectively, at location $\mathbf{x}$, traveling in direction $\mathbf{v} \in \mathbb{S}^{d-1}$. Then $u_x(\mathbf{x}, \mathbf{v})$ and $u_m(\mathbf{x}, \mathbf{v})$ solve the following coupled system of radiative transport equations

$$\begin{array}{rcll} \mathbf{v} \cdot \nabla u_x + (\sigma_{a,x} + \sigma_{s,x}) u_x & = & \sigma_{s,x} K_\Theta(u_x), & \text{in } X \\ \mathbf{v} \cdot \nabla u_m + (\sigma_{a,m} + \sigma_{s,m}) u_m & = & \sigma_{s,m} K_\Theta(u_m) + \eta \sigma_{a,xf}(\mathbf{x}) K_I(u_x)(\mathbf{x}), & \text{in } X \\ u_x(\mathbf{x}, \mathbf{v}) = g_x(\mathbf{x}, \mathbf{v}), & & u_m(\mathbf{x}, \mathbf{v}) = 0, & \text{on } \Gamma_- \end{array} \tag{3.1}$$

where the subscripts $x$ and $m$ denote the quantities at the excitation and the emission wavelengths, respectively. The coefficients $\sigma_{a,x}$ and $\sigma_{s,x}$ (resp. $\sigma_{a,m}$ and $\sigma_{s,m}$) are respectively the absorption and scattering coefficients at wavelength $\lambda_x$ (resp. $\lambda_m$). The scattering operator $K_\Theta$ and the averaging operator $K_I$ are defined respectively as

$$\begin{array}{rcl} K_\Theta(u_x)(\mathbf{x}, \mathbf{v}) & = & \int_{\mathbb{S}^{d-1}} \Theta(\mathbf{v}, \mathbf{v}') u_x(\mathbf{x}, \mathbf{v}') d\mathbf{v}' \\ K_I(u_x)(\mathbf{x}, \mathbf{v}) & = & \int_{\mathbb{S}^{d-1}} u_x(\mathbf{x}, \mathbf{v}') d\mathbf{v}', \end{array} \tag{3.2}$$

with the scattering kernel $\Theta(\mathbf{v}, \mathbf{v}')$ describing the probability that a photon traveling in direction $\mathbf{v}'$ gets scattered into direction $\mathbf{v}$.

The total absorption coefficient $\sigma_{a,x}$ consists of a contribution $\sigma_{a,xi}$ from the intrinsic tissue chromophores and a contribution $\sigma_{a,xf}$ from the flu-

orophores of the biochemical markers: $\sigma_{a,x} = \sigma_{a,xi} + \sigma_{a,xf}$. The absorption coefficient due to fluorophores, $\sigma_{a,xf}$ is proportional to the concentration $\rho(\mathbf{x})$ and the extinction coefficient $\varepsilon(\mathbf{x})$ of the fluorophores, i.e. $\sigma_{a,xf} = \varepsilon(\mathbf{x})\rho(\mathbf{x})$. The coefficient $\eta(\mathbf{x})$ is the quantum efficiency of the fluorophores. The coefficients $\eta$ and $\sigma_{a,xf}$ are the main quantities associated with the biochemical markers.

The energy absorbed by the medium and the markers consists of two parts. The first part is from the excitation photons. This part can be written as $\sigma_{a,x}K_I(u_x)$. The second part of absorbed energy comes from emission photons. This part can be written as $\sigma_{a,m}K_I(u_m)$. Therefore, the pressure field generated by the photoacoustic effect can therefore be written as:

$$\begin{aligned} H(\mathbf{x}) &= \Xi(\mathbf{x})\Big[\big(\sigma_{a,x}(\mathbf{x}) - \eta(\mathbf{x})\sigma_{a,xf}(\mathbf{x})\big)K_I(u_x)(\mathbf{x}) + \sigma_{a,m}(\mathbf{x})K_I(u_m)(\mathbf{x})\Big], \\ &\equiv \Xi(\mathbf{x})\Big(\sigma^{\eta}_{a,x}K_I(u_x)(\mathbf{x}) + \sigma_{a,m}(\mathbf{x})K_I(u_m)(\mathbf{x})\Big), \end{aligned} \tag{3.3}$$

where $\Xi$ is the (*nondimensional*) Grüneisen coefficient that measures the photoacoustic efficiency of the underlying medium, and $\sigma^{\eta}_{a,x}$ is the short notation for $\sigma_{a,xi} + (1-\eta)\sigma_{a,xf}$. We want to emphasize that when calculating the initial pressure field generated, we have subtract a portion of the energy, $\eta\sigma_{a,xf}K_I(u_x)$, from the total energy absorbed by the medium and the markers. This is because that portion of energy is used to generate fluorescence, not the heating in the photoacoustic process.

The initial pressure field generated from the photoacoustic effect, $H$, evolves in space and time following the acoustic wave equation (1.3) as in a

regular PAT process. The data that we measure are the solutions to the wave equation (1.3) on the surface of the medium, $p_{|(0,t_{\max})\times\partial\Omega}$, $t_{\max}$ being large enough, for various excitation light sources.

Following [92], we call the process of reconstructing information on $\eta$ and $\sigma_{a,xf}$ from datum $p_{|(0,t_{max})\times\partial\Omega}$ fluorescence PAT (fPAT). This is a molecular imaging modality that combines PAT with fluorescence optical imaging. We refer interested readers to [92] for more discussions on the mathematical modeling of fPAT, including detailed derivation and justification the models (3.1) (in diffusive regime) and (1.3), and to [26, 82, 83, 109, 112] for some experimental and computational results on fPAT. Recent progress on fluorescence optical imaging itself can be found in [6, 11, 47, 66, 79, 96] and references therein.

Image reconstruction in fPAT is a two-step process as in regular PAT. In the first step, we reconstruct $H$ from measured acoustic data. We assume here that this step has been finished with methods such as those in [4, 10, 27, 29, 40, 50, 52, 57, 61, 63, 81, 98] and we are given the internal datum (3.3). Moreover, we assume that: (**A-i**) the Grüneisen coefficient $\Xi$ as well as the absorption and scattering coefficients of the medium at the excitation wavelength, $\sigma_{a,xi}$ and $\sigma_{s,x}$, have been known from other imaging technologies (for instance a multi-spectral quantitative PAT step [21, 72]) before the fluorescent biochemical markers are injected into the medium; and (**A-ii**) the absorption and scattering coefficients at the emission wavelength, $\sigma_{a,m}$ and $\sigma_{s,m}$, are also reconstructed by other imaging methods (for instance a regular quantitative

PAT technique [8, 18, 19, 21, 22, 31, 33, 44, 72, 80, 88, 94, 123] after the Grüneisen coefficient is known). Therefore, our main objective is only to reconstruct the quantum efficiency $\eta$ and the fluorescence absorption coefficient $\sigma_{a,xf}(\mathbf{x})$ in the system (3.1) from the datum $H$ in (3.3). This is the quantitative fPAT (QfPAT) problem.

Let us now remark on a couple of issues regarding the practical relevance of the current work. First of all, in many practical applications, it is preferable to use contrast agents that do not emit photons after absorbing incoming excitation photons. In other words, the biochemical markers have quantum efficiency $\eta = 0$. In this case, the second equation in (3.1) drops out of the transport system, and the terms involve $\eta$ and $u_m$ all drop out from the datum (3.3). We are therefore back to the same mathematical problem as in a regular quantitative PAT process. The theory of the reconstruction in this case is covered in Theorem 3.3.3 of our results. Our results in this chapter are in fact more general in the sense that we can deal with the general case of non-negligible quantum efficiency, that is $\eta \gg 0$. When $\eta \gg 0$, we have to take into account the impact of the emitted fluorescence photons in the reconstruction process. Neglecting this impact in the model would certainly introduce errors in the images reconstructed. The second issue we need to address is the difference between the work we have here and the theory on the same problem that have been developed in the diffusive regime [92]. It is generally believed that the radiative transport equation is a more accurate model than the diffusion equation to describe the propagation of NIR photons in

biological tissues [12, 87], even though it is more complicated to theoretically analyze and numerically solve. Our analysis in this chapter is useful when the diffusion approximation to the radiative transport equation breaks down, for instance in media of small volumes but large mean free paths. Optical imaging of small animals [56], for instance, is one of such biomedical applications for our work here.

The rest of the chapter is organized as follows. We first present in Section 3.2 some general properties of the inverse problem, especially the continuous dependence of the datum $H$ on the unknown coefficients. We then consider in Section 3.3 the reconstruction of a single coefficient from a single internal data set. We derive some uniqueness and stability results on the reconstruction. In Section 3.4 we study the problem of reconstructing two coefficients simultaneously, mainly in linearized settings. We then present some numerical simulations based on synthetic data in Section 3.5 to validate the theory and the reconstruction algorithms we developed. Concluding remarks are offered in Section 3.6.

## 3.2 General Properties of the Inverse Problems

We review in this section some general properties of the inverse problem of reconstructing $\eta(\mathbf{x})$ and/or $\sigma_{a,xf}(\mathbf{x})$ in the transport system (3.1) from the datum $H$ in (3.3). We denote by $L^p(X)$ (resp. $L^p(\Omega)$) the Lebesgue space of real-valued functions whose $p$-th power are Lebesgue integrable on $X$ (resp. $\Omega$), and $\mathcal{H}_p^1(X)$ the space of $L^p(X)$ functions whose derivative in direction $\mathbf{v}$

is in $L^p(X)$, i.e. $\mathcal{H}_p^1(X) = \{f(\mathbf{x},\mathbf{v}) : f \in L^p(X) \text{ and } \mathbf{v}\cdot\nabla f \in L^p(X)\}$. We denote by $L^p(\Gamma_-)$ the space of functions that are traces of $\mathcal{H}_p^1(X)$ functions on $\Gamma_-$ under the norm $\|f\|_{L^p(\Gamma_-)} = (\int_{\partial\Omega}\int_{\mathbb{S}^{d-1}_{\mathbf{x}-}} |\mathbf{n}(\mathbf{x})\cdot\mathbf{v}||f|^p d\mathbf{v}d\gamma)^{1/p}$, $d\gamma$ being the surface measure on $\partial\Omega$ and $\mathbb{S}^{d-1}_{\mathbf{x}-} = \{\mathbf{v} : \mathbf{v}\in\mathbb{S}^{d-1} \text{ s.t. } -\mathbf{n}(\mathbf{x})\cdot\mathbf{v} > 0\}$. It is well-known [2, 34] that both $\mathcal{H}_p^1(X)$ and $L^p(\Gamma_-)$ are well-defined. To avoid confusion with $\mathcal{H}_p^1(X)$, we use $W_2^k(\Omega)$ to denote the usual Hilbert space of $L^2(\Omega)$ functions whose partial derivatives up to order $k$ are all in $L^2(\Omega)$. Besides the assumptions in (**A-i**)-(**A-ii**), we assume further that:

(**A-iii**) The domain $\Omega$ is simply-connected with $C^2$ boundary $\partial\Omega$. The known optical coefficients satisfy $0 < c_1 \le \sigma_{a,xi}, \sigma_{s,x}, \sigma_{a,m}, \sigma_{s,m}, \Xi \le c_2 < +\infty$ for some positive constants $c_1$ and $c_2$. The unknown coefficients, $(\eta, \sigma_{a,xf})$ belongs to the class

$$\mathcal{A} = \{(\eta,\sigma_{a,xf}) : 0 < c_3 \le \eta \le c_4 < 1,\ 0 < c_5 \le \sigma_{a,xf} \le c_6 < +\infty\} \tag{3.4}$$

for some positive constants $c_3$, $c_4$, $c_5$ and $c_6$. The scattering kernel $\Theta$ is symmetric, bounded and normalized in the sense that

$$\begin{aligned} &\Theta(\mathbf{v},\mathbf{v}') = \Theta(\mathbf{v}',\mathbf{v}), \quad 0 < c_7 \le \Theta(\mathbf{v},\mathbf{v}') \le c_8 < +\infty, \quad \forall \mathbf{v},\mathbf{v}' \in \mathbb{S}^{d-1}, \\ &\int_{\mathbb{S}^{d-1}} \Theta(\mathbf{v},\mathbf{v}')d\mathbf{v}' = \int_{\mathbb{S}^{d-1}} \Theta(\mathbf{v}',\mathbf{v})d\mathbf{v}' = 1, \quad \forall \mathbf{v}\in\mathbb{S}^{d-1}, \end{aligned} \tag{3.5}$$

for some positive constants $c_7$ and $c_8$. The illumination $g_x(\mathbf{x},\mathbf{v})$ is strictly positive such that $0 < c_9 \le g_x(\mathbf{x},\mathbf{v})$ for some $c_9$.

With the above settings, it is easy to see, following standard results in [2, 34], that the system (3.1) admits a unique solution in the following sense.

**Lemma 3.2.1.** *Let $p \in [1, \infty]$ and assume that (**A-iii**) holds. Then for any given function $g_x(\mathbf{x}, \mathbf{v}) \in L^p(\Gamma_-)$, there exists a unique solution $(u_x, u_m) \in \mathcal{H}^1_p(X) \times \mathcal{H}^1_p(X)$ to the couple transport system (3.1). Moreover, the following bound holds:*

$$\|u_x\|_{L^p(X)} + \|u_m\|_{L^p(X)} \leq c\|g_x\|_{L^p(\Gamma_-)} \tag{3.6}$$

*with the constant $c$ depending only on $\Omega$ and the bounds for the coefficients in assumption (**A-iii**).*

*Proof.* When the assumptions are satisfied, it follows directly from standard transport theory in [2, 34] that the first transport equation admits a unique solution $u_x \in \mathcal{H}^1_p(X)$ such that $\|u_x\|_{L^p(X)} \leq \tilde{c}\|g_x\|_{L^p(\Gamma_-)}$. We then deduce, with the same argument that the second equation admit a unique solution $u_m \in \mathcal{H}^1_p(X)$ such that $\|u_m\|_{L^p(X)} \leq \hat{c}\|\eta\sigma_{a,xf}K_I(u_x)\|_{L^p(\Omega)} \leq \hat{\hat{c}}\|u_x\|_{L^p(X)}$. The bound in (3.6) then follows from selecting $c = \tilde{c}(1 + \hat{\hat{c}})$. □

The above lemma ensures that the datum $H$ in (3.3) is well-defined for any $g_x(\mathbf{x}, \mathbf{v}) \in L^p(\Gamma_-)$ ($p \in [1, \infty]$) that satisfies the assumptions in (**A-iii**). Moreover $H \in L^p(\Omega)$ following standard results in [34]. The next result shows that the datum $H$ depends continuously on the unknown coefficients and is differentiable with respect to the coefficients in appropriate sense.

**Proposition 3.2.2.** *Let $p \in [1, \infty]$ and assume that (**A-iii**) holds. Then for any given function $g_x(\mathbf{x}, \mathbf{v}) \in L^p(\Gamma_-)$, the datum $H$ defined in (3.3), viewed*

*as the map*

$$H[\eta,\sigma_{a,xf}]:\begin{array}{ccc}(\eta,\sigma_{a,xf}) & \mapsto & \Xi\big(\sigma^{\eta}_{a,x}K_I(u_x)+\sigma_{a,m}K_I(u_m)\big)\\ L^\infty(\Omega)\times L^\infty(\Omega) & \mapsto & L^p(\Omega)\end{array} \tag{3.7}$$

*is Fréchet differentiable at any* $(\eta,\sigma_{a,xf})\in L^\infty(\Omega)\times L^\infty(\Omega)$ *in the direction* $(\delta\eta,\delta\sigma_{a,xf})\in L^\infty(\Omega)\times L^\infty(\Omega)$ *that satisfy* $(\eta,\sigma_{a,xf})\in\mathcal{A}$ *and* $(\eta+\delta\eta,\sigma_{a,xf}+\delta\sigma_{a,xf})\in\mathcal{A}$. *The derivative is given by*

$$\begin{aligned}&H'[\eta,\sigma_{a,xf}](\delta\eta,\delta\sigma_{a,xf})\\ &=\Xi\Big((-\delta\eta\sigma_{a,xf}+(1-\eta)\delta\sigma_{a,xf})K_I(u_x)+\sigma^{\eta}_{a,x}K_I(v_x)+\sigma_{a,m}K_I(v_m)\Big)\end{aligned} \tag{3.8}$$

*where* $(v_x,v_m)\in\mathcal{H}^1_p(X)\times\mathcal{H}^1_p(X)$ *is the unique solution to*

$$\begin{array}{rcll}\mathbf{v}\cdot\nabla v_x+\sigma_{t,x}v_x &=& \sigma_{s,x}K_\Theta(v_x)-\delta\sigma_{a,xf}u_x, & \text{in } X\\ \mathbf{v}\cdot\nabla v_m+\sigma_{t,m}v_m &=& \sigma_{s,m}K_\Theta(v_m)+\eta\sigma_{a,xf}K_I(v_x) & \\ & & +(\eta\delta\sigma_{a,xf}+\delta\eta\sigma_{a,xf})K_I(u_x), & \text{in } X\\ v_x(\mathbf{x},\mathbf{v})=0, & & v_m(\mathbf{x},\mathbf{v})=0 & \text{on } \Gamma_-\end{array} \tag{3.9}$$

*where* $\sigma_{t,x}=\sigma_{a,x}+\sigma_{s,x}$ *and* $\sigma_{t,m}=\sigma_{a,m}+\sigma_{s,m}$.

*Proof.* Let $\tilde\eta=\eta+\delta\eta$, $\tilde\sigma_{a,xf}=\sigma_{a,xf}+\delta\sigma_{a,xf}$, and define $\Delta(\eta\sigma_{a,xf})=\tilde\eta\tilde\sigma_{a,xf}-\eta\sigma_{a,xf}$. We denote by $(\tilde u_x,\tilde u_m)$ the solution to (3.1) with the coefficients $(\tilde\eta,\tilde\sigma_{a,xf})$, and $\tilde H$ the corresponding datum. It is straightforward to verify that $(u'_x,u'_m)\equiv(\tilde u_x-u_x,\tilde u_m-u_m)$ solves the following system of transport equations

$$\begin{array}{rcll}\mathbf{v}\cdot\nabla u'_x+\sigma_{t,x}u'_x &=& \sigma_{s,x}K_\Theta(u'_x)-\delta\sigma_{a,xf}\tilde u_x, & \text{in } X\\ \mathbf{v}\cdot\nabla u'_m+\sigma_{t,m}u'_m &=& \sigma_{s,m}K_\Theta(u'_m)+\eta\sigma_{a,xf}K_I(u'_x)+F(\mathbf{x}), & \text{in } X\\ u'_x(\mathbf{x},\mathbf{v})=0, & & u'_m(\mathbf{x},\mathbf{v})=0 & \text{on } \Gamma_-\end{array} \tag{3.10}$$

with $F(\mathbf{x}) = \Delta(\eta\sigma_{a,x})K_I(\tilde{u}_x)$, and $(u''_x, u''_m) \equiv (u'_x - v_x, u'_m - v_m)$ solves the following system

$$\begin{array}{rcll} \mathbf{v}\cdot\nabla u''_x + \sigma_{t,x}u''_x &=& \sigma_{s,x}K_\Theta(u''_x) - \delta\sigma_{a,xf}u'_x, & \text{in } X \\ \mathbf{v}\cdot\nabla u''_m + \sigma_{t,m}u''_m &=& \sigma_{s,m}K_\Theta(u''_m) + \eta\sigma_{a,xf}K_I(u''_x) + G(\mathbf{x}), & \text{in } X \\ u''_x(\mathbf{x},\mathbf{v}) = 0, && u''_m(\mathbf{x},\mathbf{v}) = 0 & \text{on } \Gamma_-, \end{array} \tag{3.11}$$

with $G(\mathbf{x}) = \Delta(\eta\sigma_{a,xf})K_I(u'_x) + \delta\eta\delta\sigma_{a,xf}K_I(u_x)$.

With the assumptions on the coefficients and the illumination source $g_x$, we conclude that $(u_x, u_m) \in \mathcal{H}^1_p(X) \times \mathcal{H}^1_p(X)$ and $(\tilde{u}_x, \tilde{u}_m) \in \mathcal{H}^1_p(X) \times \mathcal{H}^1_p(X)$ [2, 34]. This implies that $F \in L^p(\Omega)$ and

$$\begin{aligned} &\|F\|_{L^p(\Omega)} = \|(\eta\delta\sigma_{a,x} + \delta\eta\sigma_{a,xf} + \delta\eta\delta\sigma_{a,xf})K_I(\tilde{u}_x)\|_{L^p(\Omega)} \\ &\leq (\tilde{c}_1\|\delta\eta\|_{L^\infty(\Omega)} + \tilde{c}_2\|\delta\sigma_{a,xf}\|_{L^\infty(\Omega)} + \tilde{c}_3\|\delta\eta\|_{L^\infty(\Omega)}\|\delta\sigma_{a,xf}\|_{L^\infty(\Omega)})\|\tilde{u}_x\|_{L^p(X)} \\ &\leq (\tilde{\tilde{c}}_1\|\delta\eta\|_{L^\infty(\Omega)} + \tilde{\tilde{c}}_2\|\delta\sigma_{a,xf}\|_{L^\infty(\Omega)} + \tilde{\tilde{c}}_3\|\delta\eta\|_{L^\infty(\Omega)}\|\delta\sigma_{a,xf}\|_{L^\infty(\Omega)})\|g_x\|_{L^p(\Gamma_-)}, \end{aligned} \tag{3.12}$$

Following the same argument as in Lemma 3.2.1 we conclude that (3.10) admits a unique solution $(u'_x, u'_m) \in \mathcal{H}^1_p(X) \times \mathcal{H}^1_p(X)$ that satisfies

$$\begin{aligned} &\|u'_x\|_{L^p(X)} \leq \hat{c}\|\delta\sigma_{a,xf}\tilde{u}_x\|_{L^p(X)} \leq \hat{c}\|\delta\sigma_{a,xf}\|_{L^\infty(\Omega)}\|\tilde{u}_x\|_{L^p(X)} \\ &\leq \hat{\hat{c}}\|\delta\sigma_{a,xf}\|_{L^\infty(\Omega)}\|g_x\|_{L^p(\Gamma_-)}, \end{aligned} \tag{3.13}$$

and

$$\begin{aligned} &\|u'_m\|_{L^p(X)} \leq \bar{c}\big(\|\eta\sigma_{a,xf}K_I(u'_x)\|_{L^p(\Omega)} + \|F\|_{L^p(\Omega)}\big) \leq \bar{\bar{c}}\big(\|u'_x\|_{L^p(X)} + \|F\|_{L^p(\Omega)}\big) \\ &\leq (\bar{c}_1\|\delta\eta\|_{L^\infty(\Omega)} + \bar{c}_2\|\delta\sigma_{a,xf}\|_{L^\infty(\Omega)} + \bar{c}_3\|\delta\eta\|_{L^\infty(\Omega)}\|\delta\sigma_{a,xf}\|_{L^\infty(\Omega)})\|g_x\|_{L^p(\Gamma_-)}. \end{aligned} \tag{3.14}$$

Therefore we have $G \in L^p(\Omega)$ and the bound

$$\begin{aligned}\|G\|_{L^p(\Omega)} &\leq \|(\eta\delta\sigma_{a,x}+\delta\eta\sigma_{a,xf}+\delta\eta\delta\sigma_{a,xf})K_I(u'_x)\|_{L^p(\Omega)}+\|\delta\eta\delta\sigma_{a,xf}K_I(u_x)\|_{L^p(\Omega)}\\ &\leq (c'_1\|\delta\eta\|_{L^\infty(\Omega)} + c'_2\|\delta\sigma_{a,xf}\|_{L^\infty(\Omega)} + c'_3\|\delta\eta\|_{L^\infty(\Omega)}\|\delta\sigma_{a,xf}\|_{L^\infty(\Omega)})\|u'_x\|_{L^p(X)}\\ &\qquad + \|\delta\eta\|_{L^\infty(\Omega)}\|\delta\sigma_{a,xf}\|_{L^\infty(\Omega)})\|u_x\|_{L^p(X)}\\ &\leq (c''_1\|\delta\eta\|_{L^\infty(\Omega)} + c'_2\|\delta\sigma_{a,xf}\|_{L^\infty(\Omega)} + c'_3\|\delta\eta\|_{L^\infty(\Omega)}\|\delta\sigma_{a,xf}\|_{L^\infty(\Omega)})\\ &\qquad \times \|\delta\sigma_{a,xf}\|_{L^\infty(\Omega)}\|g_x\|_{L^p(\Gamma_-)}. \quad (3.15)\end{aligned}$$

We then deduce, in the same manner as above, that (3.11) admits a unique solution $(u''_x, u''_m)$ that satisfies

$$\begin{aligned}\|u''_x\|_{L^p(X)} &\leq \hat{c}\|\delta\sigma_{a,xf}u'_x\|_{L^p(\Omega)} \leq \hat{c}\|\delta\sigma_{a,xf}\|_{L^\infty(\Omega)}\|u'_x\|_{L^p(X)}\\ &\leq \hat{c}\hat{\hat{c}}\|\delta\sigma_{a,xf}\|^2_{L^\infty(\Omega)}\|g_x\|_{L^p(\Gamma_-)}, \quad (3.16)\end{aligned}$$

and

$$\begin{aligned}\|u'_m\|_{L^p(X)} &\leq \bar{c}\big(\|\eta\sigma_{a,xf}K_I(u'_x)\|_{L^p(\Omega)} + \|F\|_{L^p(\Omega)}\big) \leq \bar{\bar{c}}\big(\|u'_x\|_{L^p(X)} + \|F\|_{L^p(\Omega)}\big)\\ &\leq (\bar{c}_1\|\delta\eta\|_{L^\infty(\Omega)} + \bar{c}_2\|\delta\sigma_{a,xf}\|_{L^\infty(\Omega)} + \bar{c}_3\|\delta\eta\|_{L^\infty(\Omega)}\|\delta\sigma_{a,xf}\|_{L^\infty(\Omega)})\|g_x\|_{L^p(\Gamma_-)}. \quad (3.17)\end{aligned}$$

The estimates (3.16) and (3.17) show that $(u_x, u_m)$ is Fréchet differentiable with respect to $\eta$ and $\sigma_{a,xf}$ as a map: $L^\infty(\Omega) \times L^\infty(\Omega) \mapsto L^p(\Omega) \times L^p(\Omega)$ ($p \in [1, \infty]$). Note that $u_x$ is independent of $\eta$, so its derivative with respect to $\eta$ is zero, as can be seen from (3.16).

The differentiability of $H$ with respect to $(\eta, \sigma_{a,xf})$ then follows from the chain rule and the fact that $\sigma^\eta_{a,x}$ is differentiable with respect to $(\eta, \sigma_{a,xf})$.

Alternatively, it can also be seen easily from the bounds (3.13), (3.16), (3.17) and the following algebraic calculation:

$$\begin{aligned} &H[\tilde{\eta},\tilde{\sigma}_{a,xf}]-H[\eta,\sigma_{a,xf}]-H'[\eta,\sigma_{a,xf}](\delta\eta,\delta\sigma_{a,xf}) \\ &=\Xi\Big[\sigma^{\eta}_{a,x}K_I(u''_x)+\sigma_{a,m}K_I(u''_m)+(\delta\sigma_{a,xf}-\Delta(\eta\sigma_{a,x})K_I(u'_x)-\delta\eta\delta\sigma_{a,xf}K_I(u_x)\Big]. \end{aligned} \tag{3.18}$$

This completes the proof. □

We will study Born approximation, i.e. linearization, of the inverse problem of QfPAT in Section 3.4. The above result justifies the linearization process. To compute the partial derivative with respect to $\eta$ (resp. $\sigma_{a,xf}$), denoted by $H'_\eta[\eta,\sigma_{a,xf}]$ (resp. $H'_\sigma[\eta,\sigma_{a,xf}]$), we simply set $\delta\sigma_{a,xf}=0$ (resp. $\delta\eta=0$) in (3.8) and (3.9). It is straightforward to check that

$$\frac{H'_\eta[\eta,\sigma_{a,xf}](\delta\eta)}{\Xi\sigma_{a,xf}K_I(u_x)}=-\delta\eta+\frac{\sigma_{a,m}}{\sigma_{a,xf}K_I(u_x)}K_I(v_m), \tag{3.19}$$

with $v_m\in\mathcal{H}^1_p(X)$ the unique solution to

$$\begin{aligned} \mathbf{v}\cdot\nabla v_m+\sigma_{t,m}v_m &= \sigma_{s,m}K_\Theta(v_m)+\delta\eta\sigma_{a,xf}K_I(u_x), && \text{in } X \\ v_m(\mathbf{x},\mathbf{v}) &= 0, && \text{on } \Gamma_-, \end{aligned} \tag{3.20}$$

and

$$\frac{H'_\sigma[\eta,\sigma_{a,xf}](\delta\sigma_{a,xf})}{\Xi(1-\eta)K_I(u_x)}=\delta\sigma_{a,xf}+\frac{\sigma^{\eta}_{a,x}}{(1-\eta)K_I(u_x)}K_I(v_x)+\frac{\sigma_{a,m}}{(1-\eta)K_I(u_x)}K_I(v_m), \tag{3.21}$$

with $(v_x,v_m)\in\mathcal{H}^1_p(X)\times\mathcal{H}^1_p(X)$ the unique solution to

$$\begin{aligned} \mathbf{v}\cdot\nabla v_x+\sigma_{t,x}v_x &= \sigma_{s,x}K_\Theta(v_x)-\delta\sigma_{a,xf}u_x, && \text{in } X \\ \mathbf{v}\cdot\nabla v_m+\sigma_{t,m}v_m &= \sigma_{s,m}K_\Theta(v_m)+\eta\sigma_{a,xf}K_I(v_x)+\eta\delta\sigma_{a,xf}K_I(u_x), && \text{in } X \\ v_x(\mathbf{x},\mathbf{v})=0, \quad & v_m(\mathbf{x},\mathbf{v})=0 && \text{on } \Gamma_-. \end{aligned} \tag{3.22}$$

The following result is a standard application of the averaging lemma [34, 48, 73]. It will be useful in Section 3.4.

**Lemma 3.2.3.** *Assume that (**A-iii**) holds. Let $g_x(\mathbf{x},\mathbf{v}) \in L^\infty(\Gamma_-)$ be such that $K_I(u_x) \geq c > 0$ for some constant $c$. Then the rescaled linearized data $\frac{H'_\sigma[\eta,\sigma_{a,xf}](\delta\sigma_{a,xf})}{\Xi(1-\eta)K_I(u_x)}$, viewed as the linear operator*

$$\frac{H'_\sigma[\eta,\sigma_{a,xf}](\delta\sigma_{a,xf})}{\Xi K_I(u_x)} : \begin{array}{ccc} \delta\sigma_{a,xf} & \mapsto & (1-\eta)\delta\sigma_{a,xf} + \frac{\sigma^\eta_{a,x}}{K_I(u_x)}K_I(v_x) + \frac{\sigma_{a,m}}{K_I(u_x)}K_I(v_m) \\ L^2(\Omega) & \mapsto & L^2(\Omega) \end{array} \tag{3.23}$$

*is Fredholm. The same is true for $\frac{H'_\eta[\eta,\sigma_{a,xf}](\delta\eta)}{\Xi K_I(u_x)}$ if the background coefficient $\sigma_{a,xf} \geq \tilde{c} > 0$ for some $\tilde{c}$.*

*Proof.* Let us denote by $S_z$ ($z \in \{x,m\}$) the solution operator of the transport equation with coefficients $\sigma_{a,z}$, $\sigma_{s,z}$ and vacuum boundary condition, i.e. $w_z = S_z(f)$ with $w_z$ the solution to:

$$\mathbf{v}\cdot\nabla w_z + \sigma_{t,z}w_x - \sigma_{s,z}K_\Theta(w_z) = f, \quad \text{in } X, \qquad w_z = 0 \quad \text{on } \Gamma_-.$$

We can then write $K_I(v_x)$ and $K_I(v_m)$ in (3.23) respectively as

$$K_I(v_x) = -\Lambda_x(\delta\sigma_{a,xf}), \quad \text{and,} \quad K_I(v_m) = -\Lambda_{mx}(\delta\sigma_{a,xf}) + \Lambda_m(\eta\delta\sigma_{a,xf}) \tag{3.24}$$

where the operators $\Lambda_x$, $\Lambda_m$ and $\Lambda_{mx}$ are defined as

$$\Lambda_x(\delta\sigma_{a,xf}) \equiv K_I\big(S_x(u_x\delta\sigma_{a,xf})\big), \ \Lambda_m(\delta\sigma_{a,xf}) = K_I\big(S_m(K_I(u_x)\delta\sigma_{a,xf})\big), \tag{3.25}$$

$$\Lambda_{mx}(\delta\sigma_{a,xf}) \equiv K_I\big(S_m(\eta\sigma_{a,xf}K_I(S_x(u_x\delta\sigma_{a,xf}))\big). \tag{3.26}$$

Following the averaging lemma [34, 48, 73] and the compact embedding of $W_2^{1/2}(\Omega)$ to $L^2(\Omega)$, we conclude $K_I : L^2(X) \to L^2(\Omega)$ is compact. Due to boundedness of $u_x$ (and therefore $K_I(u_x)$), $\eta$ and $\sigma_{a,xf}$, both $S_x$ and $S_m$ are compact as operators from $L^2(\Omega)$ to $L^2(X)$ with the assumptions on the coefficients in (**A-i**) [34, 73]. Hence, $\Lambda_x$, $\Lambda_m$, and $\Lambda_{mx}$ are all compact operators on $L^2(\Omega)$. Therefore $\frac{H'_\sigma[\eta,\sigma_{a,xf}](\delta\sigma_{a,xf})}{\Xi K_I(u_x)}$ as an operator can be represented as $(1-\eta)\mathcal{I}+\mathcal{K}$ with $\mathcal{K}$ compact. Therefore it is Fredholm. The same argument works for $\frac{H'_\eta[\eta,\sigma_{a,xf}](\delta\eta)}{\Xi K_I(u_x)}$. □

## 3.3 Reconstructing of a Single Coefficient

In this section, we consider the reconstruction of one of the two coefficients of interests, assuming the other is known. We start with the reconstruction of the quantum efficiency.

### 3.3.1 The reconstruction of $\eta$

Assume now that the fluorescence absorption coefficient $\sigma_{a,xf}$ is *known* and we are interested in reconstructing only $\eta$. This is a linear inverse source problem. We can derive the following stability result on the reconstruction.

**Theorem 3.3.1.** *Let $p \in [1,\infty]$ and the source $g_x \in L^p(\Gamma_-)$ be such that the transport solution $u_x$ to (3.1) satisfies $K_I(u_x) \geq \tilde{c} > 0$ for any $(\eta, \sigma_{a,xf}) \in \mathcal{A}$. Let $H$ and $\tilde{H}$ be two data sets generated with coefficients $(\eta, \sigma_{a,xf})$ and $(\tilde{\eta}, \sigma_{a,xf})$ respectively. Then $H = \tilde{H}$ a.e. implies $\eta = \tilde{\eta}$ a.e.. Moreover, the following*

*stability estimate holds,*

$$c\|H-\tilde{H}\|_{L^p(\Omega)} \leq \|(\eta-\tilde{\eta})\sigma_{a,xf}K_I(u_x)\|_{L^p(\Omega)} \leq C\|H-\tilde{H}\|_{L^p(\Omega)} \tag{3.27}$$

*where the constants $c$ and $C$ depend on $\Omega$ and the coefficients $\sigma_{a,xi}$, $\sigma_{a,m}$, $\sigma_{s,x}$, $\sigma_{s,m}$, and $\Xi$.*

*Proof.* Let $(u_x, u_m)$ and $(\tilde{u}_x, \tilde{u}_m)$ be solutions to the coupled transport system (3.1) with coefficients $(\eta, \sigma_{a,xf})$ and $(\tilde{\eta}, \sigma_{a,xf})$ respectively. We notice immediately that $u_x = \tilde{u}_x$. Define $w_m = u_m - \tilde{u}_m$. We then verify that

$$(H-\tilde{H})/\Xi = -(\eta-\tilde{\eta})\sigma_{a,xf}K_I(u_x) + \sigma_{a,m}K_I(w_m) \tag{3.28}$$

This leads to the bound

$$\|H-\tilde{H}\|_{L^p(\Omega)} \leq c_1\|(\eta-\tilde{\eta})\sigma_{a,xf}K_I(u_x)\|_{L^p(\Omega)} + c_2(\sigma_{a,m})\|K_I(w_m)\|_{L^p(\Omega)}. \tag{3.29}$$

and the bound

$$\|(\eta-\tilde{\eta})\sigma_{a,xf}K_I(u_x)\|_{L^p(\Omega)} \leq \tilde{c}_1(\Xi)\|H-\tilde{H}\|_{L^p(\Omega)} + \tilde{c}_2(\sigma_{a,m})\|K_I(w_m)\|_{L^p(\Omega)}, \tag{3.30}$$

We check also that $w_m$ solves the transport equation

$$\begin{array}{rcll} \mathbf{v}\cdot\nabla w_m + (\sigma_{a,m}+\sigma_{s,m})w_m &=& \sigma_{s,m}K_\Theta(w_m) + (\eta-\tilde{\eta})\sigma_{a,xf}K_I(u_x), & \text{in } X \\ w_m(\mathbf{x},\mathbf{v}) &=& 0, & \text{on } \Gamma_-. \end{array} \tag{3.31}$$

It then follows from classical results in transport theory [2, 34] that this equation admits a unique solution $w_m \in \mathcal{H}^1_p(X)$ that satisfies the following stability estimate

$$\|w_m\|_{L^p(X)} \leq c_3(\Omega, \sigma_{a,m}, \sigma_{s,m}, \Xi)\|(\eta-\tilde{\eta})\sigma_{a,xf}K_I(u_x)\|_{L^p(\Omega)}. \tag{3.32}$$

The left bound in (3.27) then follows from (3.29) and (3.32).

To derive the right bound in (3.27), we replace the last term in the transport equation (3.31) with $\sigma_{a,m}K_I(w_m) - (H - \tilde{H})/\Xi$ to get

$$\begin{array}{rcll} \mathbf{v}\cdot\nabla w_m + (\sigma_{a,m}+\sigma_{s,m})w_m & = & \sigma_{a,m}K_I(w_m) + \sigma_{s,m}K_\Theta(w_m) - \frac{H-\tilde{H}}{\Xi}, & \text{in } X \\ w_m(\mathbf{x},\mathbf{v}) & = & 0, & \text{on } \Gamma_-. \end{array} \tag{3.33}$$

We define $\widetilde{\Theta}(\mathbf{x},\mathbf{v},\mathbf{v}') = \frac{\sigma_{a,m}}{\sigma_{a,m}+\sigma_{s,m}} + \frac{\sigma_{s,m}}{\sigma_{a,m}+\sigma_{s,m}}\Theta$. It is straightforward to verify that $\widetilde{\Theta}$ is symmetric and normalized in the sense of (3.5). We can then rewrite the above transport equation as

$$\begin{array}{rcll} \mathbf{v}\cdot\nabla w_m + (\sigma_{a,m}+\sigma_{s,m})w_m & = & (\sigma_{a,m}+\sigma_{s,m})K_{\widetilde{\Theta}}(w_m) - \frac{H-\tilde{H}}{\Xi}, & \text{in } X \\ w_m(\mathbf{x},\mathbf{v}) & = & 0, & \text{on } \Gamma_-. \end{array} \tag{3.34}$$

This is a transport equation for a conservative medium. Due to the fact that $\Omega$ is bounded, classical results in transport theory (see for instance [34, Theorem 1 on page 337]) then concludes that the equation admits a unique solution $w_m \in \mathcal{H}^1_p(X)$. Moreover, we have the stability estimate

$$\|w_m\|_{L^p(X)} \leq c_4(\Omega,\sigma_{a,m},\sigma_{s,m},\Xi)\|H-\tilde{H}\|_{L^p(\Omega)} \tag{3.35}$$

The right bound in (3.27) then follows from (3.30) and (3.35). The uniqueness of the reconstruction then follows from the fact that $H = \tilde{H}$ implies $w_m = 0$ from (3.34), which then implies $\eta = \tilde{\eta}$ from (3.28). □

Note that the bound in (3.27) is weighted in the sense that it is on $(\eta - \tilde{\eta})K_I(u_x)$ not directly on $(\eta - \tilde{\eta})$. This means that if $K_I(u_x)$ is too small, it is very hard to reconstruct accurately $\eta$.

The proof of the above stability result is constructive in the sense that it provides an explicit reconstruction procedure for the recovery of $\eta$. We now summarize the procedure in the following algorithm.

**Reconstruction Algorithm I.**

S1. Given $\sigma_{a,xf}$, solve the first transport equation in (3.1) with the boundary condition $g_x$ for $u_x$;

S2. Evaluate the function $q(\mathbf{x}) = \sigma_{a,x} K_I(u_x) - \frac{H}{\Xi}$;

S3. Solve the following transport equation for $u_m$:

$$\begin{aligned} \mathbf{v}\cdot\nabla u_m + (\sigma_{a,m}+\sigma_{s,m})u_m &= (\sigma_{a,m}+\sigma_{s,m})K_{\widetilde{\Theta}}(u_m) + q(\mathbf{x}), \quad \text{in } X \\ u_m(\mathbf{x},\mathbf{v}) &= 0, \qquad\qquad\qquad\qquad\qquad\quad \text{on } \Gamma_-. \end{aligned} \tag{3.36}$$

S4. Reconstruct $\eta$ as $-\big(\frac{H}{\Xi} - \sigma_{a,x}K_I(u_x) - \sigma_{a,m}K_I(u_m)\big)/(\sigma_{a,xf}K_I(u_x))$.

This is a direct reconstruction algorithm in the sense that it does not involve any iteration on the the unknown coefficient. The algorithm is very efficient since it requires solving the transport equation (3.36) only once.

**Remark 3.3.2.** *Thanks to the fact that the problem of reconstructing $\eta$ given $\sigma_{a,xf}$ is linear, we can easily verify that the same type of uniqueness and stability results in Theorem 3.3.1 hold for the linearized problem of reconstructing $\eta$ defined in (3.20) and (3.19). Moreover, the above reconstruction algorithm works in exactly the same manner in the linearized setting.*

### 3.3.2 The reconstruction of $\sigma_{a,xf}$

We now assume that we know $\eta$ and aim at reconstructing $\sigma_{a,xf}$. In this case, we can show the following result.

**Theorem 3.3.3.** *Let $g_x \in L^p(\Gamma_-)$ ($p \in [1,\infty]$) be such that the solution $u_x$ to the transport system (3.1) satisfies $u_x = K_I(u_x) \geq \tilde{c} > 0$ for any coefficient pair $(\eta, \sigma_{a,xf}) \in \mathcal{A}$. Let $H$ and $\tilde{H}$ be data sets generated with coefficient pairs $(\eta, \sigma_{a,xf})$ and $(\eta, \tilde{\sigma}_{a,xf})$ respectively. Then $H = \tilde{H}$ a.e. implies $\sigma_{a,xf} = \tilde{\sigma}_{a,xf}$ a.e.. Moreover, the following bound holds,*

$$c\|H - \tilde{H}\|_{L^p(\Omega)} \leq \|(\sigma_{a,xf} - \tilde{\sigma}_{a,xf})K_I(u_x)\|_{L^p(\Omega)} \leq C\|H - \tilde{H}\|_{L^p(\Omega)}, \quad (3.37)$$

*with $c$ and $C$ depending on $\Omega$, $\sigma_{a,xi}$, $\sigma_{a,m}$, $\sigma_{s,x}$, $\sigma_{s,m}$, $\eta$ and $\Xi$.*

*Proof.* Let $(u_x, u_m)$ and $(\tilde{u}_x, \tilde{u}_m)$ be solutions to the coupled transport system (3.1) with coefficients $(\eta, \sigma_{a,xf})$ and $(\eta, \tilde{\sigma}_{a,xf})$ respectively. Define $w_x = u_x - \tilde{u}_x$ and $w_m = u_m - \tilde{u}_m$. Then we have

$$\frac{H - \tilde{H}}{\Xi} = \tilde{\sigma}_{a,x}^{\eta} K_I(w_x) + \sigma_{a,m} K_I(w_m) + (1-\eta)(\sigma_{a,xf} - \tilde{\sigma}_{a,xf})K_I(u_x). \quad (3.38)$$

This leads to the bound

$$\|H - \tilde{H}\|_{L^p(\Omega)} \leq c_1' \|K_I(w_x)\|_{L^p(\Omega)} + c_2' \|K_I(w_m)\|_{L^p(\Omega)} + c_3' \|(\sigma_{a,xf} - \tilde{\sigma}_{a,xf})K_I(u_x)\|_{L^p(\Omega)}, \quad (3.39)$$

and the bound

$$\|(\sigma_{a,xf} - \tilde{\sigma}_{a,xf})K_I(u_x)\|_{L^p(\Omega)} \leq c_1'' \|H - \tilde{H}\|_{L^p(\Omega)} + c_2'' \|K_I(w_x)\|_{L^p(\Omega)} + c_3'' \|K_I(w_m)\|_{L^p(\Omega)}. \quad (3.40)$$

We now verify that $(w_x, w_m)$ solves the following transport system:

$$\begin{array}{rcll} \mathbf{v}\cdot\nabla w_x + \tilde{\sigma}_{t,x} w_x &=& \sigma_{s,x} K_\Theta(w_x) - (\sigma_{a,xf} - \tilde{\sigma}_{a,xf}) u_x, & \text{in } X \\ \mathbf{v}\cdot\nabla w_m + \sigma_{t,m} w_m &=& \sigma_{s,m} K_\Theta(w_m) + \eta\tilde{\sigma}_{a,xf} K_I(w_x) & \\ & & +\eta(\sigma_{a,xf} - \tilde{\sigma}_{a,xf}) K_I(u_x), & \text{in } X \\ w_x(\mathbf{x},\mathbf{v}) = 0, & & w_m(\mathbf{x},\mathbf{v}) = 0, & \text{on } \Gamma_- \end{array} \tag{3.41}$$

where $\sigma_{t,x} = \sigma_{a,xi} + \tilde{\sigma}_{a,xf} + \sigma_{s,m}$. We then deduce, following similar procedure as in the proof of Proposition 3.2.2, that

$$\|w_x\|_{L^p(X)} + \|w_m\|_{L^p(X)} \leq c_4' \|(\sigma_{a,xf} - \tilde{\sigma}_{a,xf}) K_I(u_x)\|_{L^p(\Omega)}. \tag{3.42}$$

The left bound in (3.37) then follows from (3.39) and (3.42).

To derive the right bound in (3.37), we use (3.38) to eliminate the quantity $\sigma_{a,xf} - \tilde{\sigma}_{a,xf}$ in the transport system (3.41) to obtain:

$$\begin{array}{rcll} \mathbf{v}\cdot\nabla w_x + \tilde{\sigma}_{t,x} w_x &=& \sigma_{s,x} K_\Theta(w_x) + \sigma'_{s,x} K_I(w_x) + \sigma'_{s,xm} K_I(w_m) & \\ & & -\frac{(H-\tilde{H})u_x}{\Xi(1-\eta)K_I(u_x)}, & \text{in } X \\ \mathbf{v}\cdot\nabla w_m + \sigma_{t,m} w_m &=& \sigma_{s,m} K_\Theta(w_m) - \sigma'_{s,m} K_I(w_m) - \sigma'_{s,mx} K_I(w_x) & \\ & & +\frac{(H-\tilde{H})\eta}{\Xi(1-\eta)}, & \text{in } X \\ w_x(\mathbf{x},\mathbf{v}) = 0, & & w_m(\mathbf{x},\mathbf{v}) = 0, & \text{on } \Gamma_- \end{array} \tag{3.43}$$

where $\sigma'_{s,x} = \frac{\tilde{\sigma}^\eta_{a,x} u_x}{(1-\eta)K_I(u_x)}$, $\sigma'_{s,xm} = \frac{\sigma_{a,m} u_x}{(1-\eta)K_I(u_x)}$, $\sigma'_{s,m} = \frac{\eta\sigma_{a,m}}{1-\eta}$, and $\sigma'_{s,mx} = \frac{\eta\sigma_{a,xi}}{1-\eta}$. To write the system in standard form, we perform the change of variable $w_x \to -w_x$. We then have

$$\begin{array}{rcll} \mathbf{v}\cdot\nabla w_x + \tilde{\sigma}_{t,x} w_x + \sigma'_{s,xm} K_I(w_m) &=& \sigma_{s,x} K_\Theta(w_x) + \sigma'_{s,x} K_I(w_x) & \\ & & +\frac{(H-\tilde{H})u_x}{\Xi(1-\eta)K_I(u_x)}, & \text{in } X \\ \mathbf{v}\cdot\nabla w_m + \sigma_{t,m} w_m + \sigma'_{s,m} K_I(w_m) &=& \sigma_{s,m} K_\Theta(w_m) + \sigma'_{s,mx} K_I(w_x) & \\ & & +\frac{(H-\tilde{H})\eta}{\Xi(1-\eta)}, & \text{in } X \\ w_x(\mathbf{x},\mathbf{v}) = 0, & & w_m(\mathbf{x},\mathbf{v}) = 0, & \text{on } \Gamma_- \end{array} \tag{3.44}$$

With the assumption on $g_x$, the coefficients $\sigma'_{s,x}$, $\sigma'_{s,xm}$, $\sigma'_{s,m}$, and $\sigma'_{s,mx}$ are all positive. We check also, after using the assumption $u_x = K_I(u_x)$, that $\Delta_1 \equiv \tilde{\sigma}_{t,x} + \sigma'_{s,xm} - \sigma_{s,x} - \sigma'_{s,x} = \tilde{\sigma}_{a,x} + (\sigma_{a,m} - \tilde{\sigma}^{\eta}_{a,x})/[(1-\eta)]$ and $\Delta_2 \equiv \sigma_{t,m} + \sigma'_{s,m} - \sigma_{s,m} - \sigma'_{s,mx} = (\sigma_{a,m} - \eta\sigma_{a,xi})/(1-\eta)$. The conditions in Theorem 3.3.3 ensure that $\Delta_1, \Delta_2 \geq c' > 0$ for some $c'$. We can therefore combine the techniques in [49, 102, 103, 115], see detailed analysis in [85], to show that system (3.44) admits a unique solution $(w_x, w_m)$ that satisfies

$$\|w_x\|_{L^p(X)} + \|w_m\|_{L^p(X)} \leq c''_4 \|H - \tilde{H}\|_{L^p(\Omega)}. \tag{3.45}$$

We can now combine (3.40) and (3.45) to obtain the right bound in (3.37). The uniqueness result follows from the fact that (3.44) admits only the trivial solution $(w_x, w_m) = (0, 0)$ when $H = \tilde{H}$. □

**Linearized Case.** Unlike in the case of reconstructing $\eta$, the above proof is not constructive since the unknown coefficient $\sigma_{a,xf}$ shows up in the transport system (3.44). Therefore, the proof does not provide directly a reconstruction algorithm. For numerical reconstructions in this nonlinear setting, we use the optimization-based algorithm in Section 3.4.4. If we consider the same problem in linearized setting, we can indeed derive an explicit reconstruction procedure. To do that, we replace the $\delta\sigma_{a,xf}$ in (3.22) with its expression given

in the linearized datum (3.21) to get the following system:

$$\begin{aligned}
\mathbf{v}\cdot\nabla v_x+\sigma_{t,x}v_x+\sigma'_{s,xm}K_I(v_m) &= \sigma_{s,x}K_\Theta(v_x)+\sigma'_{s,x}K_I(v_x) \\
&\quad -\tfrac{u_xH'_\sigma}{(1-\eta)\Xi K_I(u_x)}, && \text{in } X \\
\mathbf{v}\cdot\nabla v_m+\sigma_{t,m}v_m+\sigma'_{s,m}K_I(v_m) &= \sigma_{s,m}K_\Theta(v_m)+\sigma'_{s,mx}K_I(v_x) \\
&\quad +\tfrac{\eta H'_\sigma}{(1-\eta)\Xi}, && \text{in } X \\
v_x(\mathbf{x},\mathbf{v})=0, \qquad & v_m(\mathbf{x},\mathbf{v})=0, && \text{on } \Gamma_-
\end{aligned} \tag{3.46}$$

where we have performed the change of variable $v_x \to -v_x$, and the coefficient $\sigma'_{s,x} = \frac{\sigma^\eta_{a,x}u_x}{(1-\eta)K_I(u_x)}$, while the coefficients $\sigma'_{s,xm}$, $\sigma'_{s,m}$, and $\sigma'_{s,mx}$ are defined as in (3.43). This system does not contain the unknown coefficient $\delta\sigma_{a,xf}$. It can be solved for $(v_x, v_m)$. We can then reconstruct $\delta\sigma_{a,xf}$ following (3.21). The reconstruction procedure can be summarized into the following reconstruction algorithm.

**Reconstruction Algorithm II.**

S1. Given the background coefficient $\sigma_{a,xf}$, solve the first transport equation in (3.1) with the boundary condition $g_x$ for $u_x$ (and therefore $K_I(u_x)$);

S2. Evaluate the coefficients $\sigma'_{s,x}$, $\sigma'_{s,xm}$, $\sigma'_{s,m}$ and $\sigma'_{s,mx}$;

S3. Solve the transport system (3.46) for $(v_x, v_m)$ and perform the transform $(-v_x, v_m) \to (v_x, v_m)$;

S4. Reconstruct $\delta\sigma_{a,xf}$ as $\big[\frac{H'_\sigma}{\Xi} - \sigma^\eta_{a,x}K_I(v_x) - \sigma_{a,m}K_I(v_m)\big]\big/\big[(1-\eta)K_I(u_x)\big]$.

Following the control theory for transport equations developed in [1, 3, 62], we can show, under reasonable assumptions, the existence of sources $g_x$ such that

$u_x = K_I(u_x)$ holds for each pair $(\eta, \sigma_{a,xf}) \in \mathcal{A}$. Such sources, however, might be complicated, for instance we might need to solve a control problem, to construct in practical applications. The usefulness of Reconstruction Algorithm II is therefore limited by this fact. Note that in applications where the medium is scattering-free, see for instance discussions in [37, 72], this algorithm is indeed very useful since there are many ways to construct illuminations sources to have $u_x = K_I(u_x)$.

## 3.4 Simultaneous Reconstruction of Two Coefficients

We now consider the problem of simultaneous reconstruction of the quantum efficiency and the fluorescence absorption coefficient. We start with the linearized case.

### 3.4.1 Linearization around $(\eta, \sigma_{a,xf}) = (0, 0)$

We first consider the special case where both coefficients are small. In this case the product of the coefficient is small so that generation of fluorescence is very small and can be neglected. Therefore, the system involves only the light at the excitation wavelength. The QfPAT problem reduces to the usual quantitative PAT problem. To be precise, we linearize the problem around the background $(\eta, \sigma_{a,xf}) = (0, 0)$. Then the second transport equation in (3.9) has the solution $v_m = 0$. Therefore, the datum (3.8) simplifies to

$$\frac{1}{\Xi} H'[0,0](\delta\eta, \delta\sigma_{a,xf}) = \delta\sigma_{a,xf} K_I(u_x) + \sigma_{a,xi} K_I(v_x), \tag{3.47}$$

and the first transport equation in system (3.9) simplifies to

$$\begin{array}{rcll} \mathbf{v}\cdot\nabla v_x + (\sigma_{a,xi}+\sigma_{s,x})v_x &=& \sigma_{s,x}K_\Theta(v_x) - \delta\sigma_{a,xf}u_x, & \text{in } X \\ v_x(\mathbf{x},\mathbf{v}) &=& 0, & \text{on } \Gamma_-. \end{array} \tag{3.48}$$

We observe that $\delta\eta$ does not appear in the datum (3.47) or the equation (3.48). Therefore, it can *not* be reconstructed in this setting. We can show the following result.

**Proposition 3.4.1.** *Let $u_x$ be the solution to the first transport equation in (3.1) with $\sigma_{a,xf} = 0$. Let $g_x \in L^p(\Gamma_-)$ ($p \in [1,\infty]$) be such that $u_x = K_I(u_x) \geq \tilde{c} > 0$. Denote by $H'[0,0]$ and $\widetilde{H}'[0,0]$ the perturbed data sets in the form of (3.47), generated with perturbed coefficients ($\delta\eta$, $\delta\sigma_{a,xf}$) and ($\widetilde{\delta\eta}$, $\widetilde{\delta\sigma}_{a,xf}$) respectively. Then $H'[0,0] = \widetilde{H}'[0,0]$ a.e. implies $\delta\sigma_{a,xf} = \widetilde{\delta\sigma}_{a,xf}$ a.e.. In addition, we have,*

$$\begin{aligned} c\|H'[0,0] - \widetilde{H}'[0,0]\|_{L^p(\Omega)} &\leq \|(\delta\sigma_{a,xf} - \widetilde{\delta\sigma}_{x,f})K_I(u_x)\|_{L^p(\Omega)} \\ &\leq C\|H'[0,0] - \widetilde{H}'[0,0]\|_{L^p(\Omega)}, \end{aligned} \tag{3.49}$$

*with $c$ and $C$ constants that depend on $\Omega$, $\Xi$, $\sigma_{a,xi}$ and $\sigma_{s,x}$.*

*Proof.* The datum (3.47) implies directly that

$$\|H'[0,0] - \widetilde{H}'[0,0]\|_{L^p(\Omega)} \leq c_1\|(\delta\sigma_{a,xf} - \widetilde{\delta\sigma}_{a,xf})K_I(u_x)\|_{L^p(\Omega)} + c_2\|v_x - \tilde{v}_x\|_{L^p(X)}, \tag{3.50}$$

and

$$\|(\delta\sigma_{a,xf} - \widetilde{\delta\sigma}_{a,xf})K_I(u_x)\|_{L^p(\Omega)} \leq c_1'\|H'[0,0] - \widetilde{H}'[0,0]\|_{L^p(\Omega)} + c_2'\|v_x - \tilde{v}_x\|_{L^p(X)}, \tag{3.51}$$

with the constants depend on $\Omega$, $\sigma_{a,xi}$ and $\Xi$.

With the assumptions in the theorem, we deduce from the transport equation (3.48) that

$$\|v_x - \tilde{v}_x\|_{L^p(\Omega)} \leq c_3 \|(\delta\sigma_{a,xf} - \widetilde{\delta\sigma}_{a,xf}) K_I(u_x)\|_{L^p(\Omega)}. \tag{3.52}$$

The left bound in (3.49) then follows from (3.50) and (3.52). To get the right bound in (3.49), we use the datum (3.47), and the assumption that $u_x = K_I(u_x)$, to rewrite (3.48) as

$$\begin{array}{rcll} \mathbf{v}\cdot\nabla v_x + (\sigma_{a,xi}+\sigma_{s,x})v_x & = & \sigma_{s,x}K_\Theta(v_x) + \sigma_{a,xi}K_I(v_x) - \frac{H'[0,0]}{\Xi}, & \text{in } X \\ v_x(\mathbf{x},\mathbf{v}) & = & 0, & \text{on } \Gamma_-. \end{array} \tag{3.53}$$

This is a conservative transport equation that admits a unique solution with the stability result:

$$\|v_x - \tilde{v}_x\|_{L^p(\Omega)} \leq c_3' \|H'[0,0] - \widetilde{H}'[0,0]\|_{L^p(\Omega)}, \tag{3.54}$$

where $c_3'$ depends on $\Omega$, $\sigma_{a,xi}$, $\sigma_{s,x}$ and $\Xi$. The right bound in (3.49) then follows from (3.51) and (3.54). □

The above proof is again constructive when a $g_x$ that satisfies the assumption in the theorem is available to us, in the sense that we only need to solve (3.53) for $v_x$ and then compute $\delta\sigma_{a,xf} = (H'[0,0]/\Xi - \sigma_{a,xi}K_I(v_x))/K_I(u_x)$.

### 3.4.2 Linearization around a general background

We now consider the linearization around a general background ($\eta \not\equiv 0, \sigma_{a,xf} \not\equiv 0$). We study the case where we have $J \geq 2$ data sets, $1 \leq j \leq J$:

$$\frac{H_j'[\eta, \sigma_{a,xf}](\delta\eta, \delta\sigma_{a,xf})}{\Xi K_I(u_x^j)} = (-\delta\eta\sigma_{a,xf} + (1-\eta)\delta\sigma_{a,xf}) + \frac{\sigma_{a,x}^{\eta}}{K_I(u_x^j)} K_I(v_x^j) + \frac{\sigma_{a,m}}{K_I(u_x^j)} K_I(v_m^j) \quad (3.55)$$

where $u_x^j$ is the solution to the first transport equation in (3.1) with background coefficient $\sigma_{a,xf}$ and illumination source $g_x^j$, while $(v_x^j, v_m^j)$ is the solution to the coupled system (3.9).

To study the linear inverse problem defined in (3.55), we introduce two new variables $\zeta = \delta\eta\sigma_{a,xf} + \eta\delta\sigma_{a,xf}$ and $\xi = \delta\sigma_{a,xf}$. It is straightforward to verify that $(\zeta, \xi)$ uniquely determines $(\delta\eta, \delta\sigma_{a,xf})$ when $\eta \not\equiv 0$ and $\sigma_{a,xf} \not\equiv 0$. We can then collect the $J$ data sets to have the following linear system for the unknown coefficient pair $(\zeta, \xi)$:

$$\mathbf{\Pi} \begin{pmatrix} \zeta \\ \xi \end{pmatrix} = \mathbf{z}, \text{ with, } \mathbf{\Pi} = \begin{pmatrix} -\mathcal{I} + \Pi_\zeta^1 & \mathcal{I} - \Pi_\xi^1 \\ \vdots & \vdots \\ -\mathcal{I} + \Pi_\zeta^J & \mathcal{I} - \Pi_\xi^J \end{pmatrix} \text{ and } \mathbf{z} = \begin{pmatrix} \frac{H_1'[\eta, \sigma_{a,xf}]}{\Xi K_I(u_x^1)} \\ \vdots \\ \frac{H_J'[\eta, \sigma_{a,xf}]}{\Xi K_I(u_x^J)} \end{pmatrix} \quad (3.56)$$

with $\Pi_\zeta^j = \frac{\sigma_{a,m}}{K_I(u_x^j)} \Lambda_m^j$ and $\Pi_\xi^j = \frac{\sigma_{a,x}^{\eta}}{K_I(u_x^j)} \Lambda_x^j + \frac{\sigma_{a,m}}{K_I(u_x^j)} \Lambda_{mx}^j$. Here $\Lambda_x^j$, $\Lambda_{mx}^j$ and $\Lambda_m^j$ are defined as in (3.25) and (3.26) with $u_x$ replaced by $u_x^j$. From Lemma 3.2.3 we know that $\Pi_\zeta^j$ and $\Pi_\xi^j$ $(1 \leq j \leq J)$ are compact operators on $L^2(\Omega)$.

From the discussion in the previous sections, we know that $\mathcal{I} - \Pi_\zeta^j$ and $\mathcal{I} - \Pi_\xi^j$ are all invertible for well-selected illumination sources $g_x^j$, $1 \leq j \leq J$.

However, that does not guarantee the invertibility of the linear system (3.56). For the case of $J = 2$, the invertibility of the system (3.56) is equivalent to the invertibility of $(\mathcal{I} - \Pi^2_\zeta)^{-1}(\mathcal{I} - \Pi^2_\xi) - (\mathcal{I} - \Pi^1_\zeta)^{-1}(\mathcal{I} - \Pi^1_\xi)$. Therefore, we need to choose illumination sources $g^1_x$ and $g^2_x$ such that $(\mathcal{I} - \Pi^2_\zeta)^{-1}(\mathcal{I} - \Pi^2_\xi) - (\mathcal{I} - \Pi^1_\zeta)^{-1}(\mathcal{I} - \Pi^1_\xi)$ is invertible; see next section for some discussions on the regularized version of this problem.

### 3.4.3 A partially linearized model

We now briefly discuss a very popular simplification of the mathematical model in the fluorescence optical tomography literature. This simplification assumes that the fluorescence absorption coefficient $\sigma_{a,xf}$ is small compared to the background tissue absorption coefficient $\sigma_{a,xi}$. Therefore, it can be dropped from the first equation in the model (3.1); see for instance [77]. In other words, the model, for source $g^j_x$ $(1 \le j \le J)$, now reads,

$$\begin{array}{rcll} \mathbf{v}\cdot\nabla u^j_x + (\sigma_{a,xi}+\sigma_{s,x})u^j_x &=& \sigma_{s,x}K_\Theta(u^j_x), & \text{in } X \\ \mathbf{v}\cdot\nabla u^j_m + (\sigma_{a,m}+\sigma_{s,m})u^j_m &=& \sigma_{s,m}K_\Theta(u^j_m) + \eta\sigma_{a,xf}K_I(u^j_x), & \text{in } X \\ u^j_x(\mathbf{x},\mathbf{v}) = g^j_x, && u^j_m(\mathbf{x},\mathbf{v}) = 0 & \text{on } \Gamma_-. \end{array} \tag{3.57}$$

The data, for source $g^j_x$ $(1 \le j \le J)$, now simplify to,

$$\widetilde{H}_j \equiv \frac{H_j}{\Xi K_I(u^j_x)} - \sigma_{a,xi} = (1-\eta)\sigma_{a,xf} + \frac{\sigma_{a,m}}{K_I(u^j_x)}K_I(u^j_m). \tag{3.58}$$

The inverse problem of reconstructing $\eta$ and $\sigma_{a,xf}$ from datum (3.58) is a nonlinear problem despite the fact that a partial linearization has been performed on the transport model. However, if we define $\zeta = (1-\eta)\sigma_{a,xf}$ and

$\xi = \sigma_{a,xf}$, then the inverse problem is bilinear with respect to $(\zeta, \xi)$. Precisely, we can write the datum as,

$$\widetilde{H}_j = \zeta - \Pi_\zeta^j(\zeta) + \Pi_\zeta^j(\xi), \qquad 1 \le j \le J \tag{3.59}$$

with $\Pi_\zeta^j = \frac{\sigma_{a,m}}{K_I(u_x^j)}\Lambda_m^j$ defined the same way as before and being compact on $L^2(\Omega)$. This can again be written into the form of linear system (3.56) with the coefficient matrix and source vector respectively

$$\mathbf{\Pi} = \begin{pmatrix} \mathcal{I} - \Pi_\zeta^1 & \Pi_\zeta^1 \\ \vdots & \vdots \\ \mathcal{I} - \Pi_\zeta^J & \Pi_\zeta^J \end{pmatrix}, \qquad \text{and,} \qquad \mathbf{z} = \begin{pmatrix} \widetilde{H}_1 \\ \vdots \\ \widetilde{H}_J \end{pmatrix}. \tag{3.60}$$

**Regularized Inversion with $J = 2$.** In the case that two data sets are available, we can solve the inverse problems in this section and Section. 3.4.2 in regularized form. To do that, we observe that if we define

$$\mathbf{\Pi}_\alpha = \mathbf{\Pi} + \begin{pmatrix} 0 & 0 \\ 0 & \alpha\mathcal{I} \end{pmatrix}, \qquad \alpha > 0 \tag{3.61}$$

then $\mathbf{\Pi}_\alpha$ is a Fredholm operator on $L^2(\Omega) \times L^2(\Omega)$ for the $\mathbf{\Pi}$ defined in both (3.56) and (3.60). To be precise, $\mathbf{\Pi}_\alpha$ are respectively,

$$\begin{aligned} \mathbf{\Pi}_\alpha = \begin{pmatrix} -\mathcal{I} + \Pi_\zeta^1 & \mathcal{I} - \Pi_\xi^1 \\ -\mathcal{I} + \Pi_\zeta^2 & \alpha\mathcal{I} + \mathcal{I} - \Pi_\xi^2 \end{pmatrix} &\sim \begin{pmatrix} -\mathcal{I} + \Pi_\zeta^1 & \mathcal{I} - \Pi_\xi^1 \\ \Pi_\zeta^2 - \Pi_\zeta^1 & \alpha\mathcal{I} + \Pi_\xi^1 - \Pi_\xi^2 \end{pmatrix} \\ &= \begin{pmatrix} -\mathcal{I} + \Pi_\zeta^1 & \mathcal{I} \\ 0 & \alpha\mathcal{I} + \Pi_\xi^1 \end{pmatrix} + \begin{pmatrix} 0 & -\Pi_\xi^1 \\ \Pi_\zeta^2 - \Pi_\zeta^1 & -\Pi_\xi^2 \end{pmatrix}, \end{aligned} \tag{3.62}$$

and

$$\mathbf{\Pi}_\alpha = \begin{pmatrix} \mathcal{I} - \Pi_\zeta^1 & \Pi_\zeta^1 \\ \mathcal{I} - \Pi_\zeta^2 & \alpha\mathcal{I} + \Pi_\zeta^2 \end{pmatrix} = \begin{pmatrix} \mathcal{I} - \Pi_\zeta^1 & 0 \\ \mathcal{I} & \alpha\mathcal{I} \end{pmatrix} + \begin{pmatrix} 0 & \Pi_\zeta^1 \\ -\Pi_\zeta^2 & \Pi_\zeta^2 \end{pmatrix} \tag{3.63}$$

where $\sim$ is used to denote the elementary operation of subtracting the first row from the second row. For any fixed $\alpha > 0$, let us denote by $\mathcal{N}(\mathbf{\Pi}_\alpha)$ the null space of matrix operator $\mathbf{\Pi}_\alpha$, then the following result follows immediately from classical stability theory of Fredholm operators [59].

**Proposition 3.4.2.** *Let* $\mathbf{z}$ *and* $\widetilde{\mathbf{z}}$ *be two perturbed data sets defined as in* (3.56) *or* (3.60). *Let* $(\zeta, \xi)^t$ *and* $(\widetilde{\zeta}, \widetilde{\xi})^t$ *be the solution to* $\mathbf{\Pi}_\alpha \begin{pmatrix} \zeta \\ \xi \end{pmatrix} = \mathbf{z}$ *and* $\mathbf{\Pi}_\alpha \begin{pmatrix} \widetilde{\zeta} \\ \widetilde{\xi} \end{pmatrix} = \widetilde{\mathbf{z}}$ *respectively for some* $\alpha > 0$. *Then we have*

$$\tilde{c}\|\mathbf{z} - \widetilde{\mathbf{z}}\|_{(L^2(\Omega))^2} \leq \|(\zeta, \xi) - (\widetilde{\zeta}, \widetilde{\xi})\|_{(L^2(\Omega))^2/\mathcal{N}(\mathbf{\Pi}_\alpha)} \leq \tilde{C}\|\mathbf{z} - \widetilde{\mathbf{z}}\|_{(L^2(\Omega))^2}. \quad (3.64)$$

*for some constants* $\tilde{c}$ *and* $\tilde{C}$.

In the numerical computation, to solve (3.56) or (3.60) directly, we have to construct the operator $\mathbf{\Pi}$ explicitly. This is hard to do in practice since it essentially requires the analytical form of the Green's function for the transport equation at the emission wavelength. We do not have access to this Green's function. Instead, solve the linear problem with a classical method of Landweber iteration [60] that we summarize in the following algorithm.

**Reconstruction Algorithm III.**

S1. Take initial guess $(\zeta_0, \xi_0)$;

S2. Iteratively update the unknown through the iteration:

$$\begin{pmatrix} \zeta_{k+1} \\ \xi_{k+1} \end{pmatrix} = (\mathbf{I} - \tau \mathbf{\Pi}^* \mathbf{\Pi}) \begin{pmatrix} \zeta_k \\ \xi_k \end{pmatrix} + \tau \mathbf{\Pi}^* \mathbf{z}, \quad k \geq 0. \quad (3.65)$$

Stop the iteration when desired convergence criteria are satisfied.

Here $\tau$ is a positive algorithmic parameter that we select by trial and error. The adjoint operator $\mathbf{\Pi}^*$ is formed by transposing $\mathbf{\Pi}$ and replacing $\Pi_\zeta^j$ and $\Pi_\xi^j$ with $\Pi_\zeta^{j*} = K_I(u_x^j) S_m^* \circ K_I \circ \frac{\sigma_{a,m}}{K_I(u_x^j)}$ and $\Pi_\xi^{j*} = u_x^j S_x^* \circ K_I \circ \frac{\sigma_{a,x}^\eta}{K_I(u_x^j)} + u_x^j S_x^* \circ K_I \circ \eta\sigma_{a,xf} S_m^* \circ K_I \circ \frac{\sigma_{a,m}}{K_I(u_x^j)}$ respectively. Here $S_z^*$ is the adjoint of $S_z$ ($z \in \{x, m\}$) that is defined as the solution operator of the adjoint transport equation with coefficients $\sigma_{a,z}$, $\sigma_{s,z}$ and vacuum boundary condition, i.e. $w_z = S_z^*(f)$ with $w_z$ the solution to:

$$-\mathbf{v} \cdot \nabla w_z + (\sigma_{a,z} + \sigma_{s,z}) w_x - \sigma_{s,z} K_\Theta(w_z) = f, \quad \text{in } X, \qquad w_z = 0 \quad \text{on } \Gamma_+.$$

Therefore, at iteration $k$ of the Landweber algorithm, we solve $J$ forward transport systems and then $J$ adjoint transport systems to apply the operator $\mathbf{\Pi}^*\mathbf{\Pi}$ to the vector $(\zeta_k, \xi_k)^t$.

### 3.4.4 Iterative reconstruction for the nonlinear case

For the simultaneous reconstruction of $\eta$ and $\sigma_{a,xf}$ in the general nonlinear case, we do not have any theoretical results on uniqueness and stability currently. Nor do we have more explicit reconstruction methods. We rely mostly on general computational optimization techniques to solve the inverse problem. More precisely, we search for solutions to the inverse problem by minimizing the objective functional:

$$\Phi(\eta, \sigma_{a,xf}) \equiv \frac{1}{2} \sum_{j=1}^{J} \int_\Omega \left\{ \Xi\left[\sigma_{a,x}^\eta K_I(u_x^j) + \sigma_{a,m} K_I(u_m^j)\right] - H_j \right\}^2 d\mathbf{x} + \beta R(\eta, \sigma_{a,xf}) \tag{3.66}$$

where the regularization functional is taken as $R(\eta, \sigma_{a,xf}) = \frac{1}{2}(\|\nabla\eta\|^2_{[L^2(\Omega)]^d} + \|\nabla\sigma_{a,xf}\|^2_{[L^2(\Omega)]^d})$.

Following the result in Proposition 3.2.2 and the chain rule, we can obtain the following result straightforwardly.

**Corollary 3.4.3.** *The functional $\Phi(\eta, \sigma_{a,xf})$, viewed as the map: $\Phi : W_2^1(\Omega) \times W_2^1(\Omega) \mapsto \mathbb{R}_+$ is Fréchet differentiable at any $(\eta, \sigma_{a,xf}) \in W_2^1(\Omega) \times W_2^1(\Omega) \cap \mathcal{A}$. The partial derivatives in the direction $\delta\eta$ (such that $(\eta + \delta\eta, \sigma_{a,xf}) \in \mathcal{A}$) and the direction $\delta\sigma_{a,xf}$ (such that $(\eta, \sigma_{a,xf} + \delta\sigma_{a,xf}) \in \mathcal{A}$) are given respectively as*

$$\begin{aligned}
&\Phi'_\eta[\eta, \sigma_{a,xf}](\delta\eta) \\
&= \int_\Omega \Big\{ \sum_{j=1}^{J} z_j \Xi\big[ -\delta\eta\sigma_{a,xf} K_I(u_x^j) + \sigma_{a,m} K_I(w_m^j)\big] + \beta\nabla\delta\eta \cdot \nabla\eta \Big\} d\mathbf{x}, \qquad (3.67) \\
&\Phi'_\sigma[\eta, \sigma_{a,xf}](\delta\sigma_{a,xf}) \\
&= \int_\Omega \sum_{j=1}^{J} z_j \Xi\big[\delta\sigma_{a,xf}(1-\eta) K_I(u_x^j) + \sigma_{a,x}^\eta K_I(v_x) + \sigma_{a,m} K_I(v_m)\big] d\mathbf{x} \\
&\quad + \beta \int_\Omega \nabla\delta\sigma_{a,xf} \cdot \nabla\sigma_{a,xf} d\mathbf{x}, \qquad (3.68)
\end{aligned}$$

*where the residual $z_j = \Xi\big[\sigma_{a,x}^\eta K_I(u_x^j) + \sigma_{a,m} K_I(u_m^j)\big] - H_j$, $w_m$ is the unique solution to (3.20), and $(v_x, v_m)$ is the unique solution to (3.22).*

We can therefore employ gradient-based minimization techniques to minimize the functional (3.66). Here we use the limited memory version of the BFGS quasi-Newton method that we implemented in [86]. This method requires only the gradients of the objective functional which we derived in Corollary 3.4.3. To simplify the computation of these gradients numerically,

we apply the adjoint state technique. We denote by $(q_x^j, q_m^j)$ the unique solution to the following adjoint transport system:

$$\begin{array}{rcll} -\mathbf{v}\cdot\nabla q_x^j + \sigma_{t,x} q_x^j &=& \sigma_{s,x} K_\Theta(q_x^j) + \Xi\sigma_{a,x}^\eta z_j + \eta\sigma_{a,xf} K_I(q_m^j), & \text{in } X \\ -\mathbf{v}\cdot\nabla q_m^j + \sigma_{t,m} q_m^j &=& \sigma_{s,m} K_\Theta(q_m^j) + \Xi\sigma_{a,m} z_j, & \text{in } X \\ q_x^j(\mathbf{x},\mathbf{v}) = 0, && q_m^j(\mathbf{x},\mathbf{v}) = 0 & \text{on } \Gamma_+. \end{array} \tag{3.69}$$

It is then straightforward to show that

$$\begin{aligned} &\Phi'_\eta[\eta,\sigma_{a,xf}](\delta\eta) \\ &= \int_\Omega \Big\{ \sum_{j=1}^J \delta\eta\sigma_{a,xf} K_I(u_x^j)\big[ -\Xi z_j + K_I(q_m^j)\big] + \beta\nabla\delta\eta\cdot\nabla\eta \Big\} d\mathbf{x}, \end{aligned} \tag{3.70}$$

$$\begin{aligned} &\Phi'_\sigma[\eta,\sigma_{a,xf}](\delta\sigma_{a,xf}) \\ &= \int_\Omega \sum_{j=1}^J \delta\sigma_{a,xf} K_I(u_x^j)\big[\Xi(1-\eta)z_j + \eta K_I(q_m) - K_I(q_x)\big] d\mathbf{x} \\ &\quad + \beta\int_\Omega \nabla\delta\sigma_{a,xf}\cdot\nabla\sigma_{a,xf} d\mathbf{x}. \end{aligned} \tag{3.71}$$

Therefore, to compute gradients of the $\Phi$ at $(\eta, \sigma_{a,xf})$, we only need to solve a set of $J$ forward transport systems (3.1) and a set of $J$ adjoint transport systems (3.69). We can then evaluate the gradients in any given direction $(\delta\eta, \delta\sigma_{a,xf})$ according to (3.70) and (3.71).

It is obvious that this optimization-based nonlinear reconstruction method can be used also to reconstruct a single coefficient. To only reconstruct $\eta$, we only need to set the gradient with respect to $\sigma_{a,xf}$ to zero and vice versa.

## 3.5 Numerical Experiments

We now present some numerical reconstructions using synthetic interior data. We restrict ourselves to two-dimensional settings only to simplify the computation.

The spatial domain of the reconstruction is the square $\Omega = (-1, 1) \times (-1, 1)$. All the transport equations in $\Omega \times \mathbb{S}^1$ are discretized angularly with the discrete ordinate method and spatially with a first-order finite element method on triangular meshes. In all the simulations in this section, reconstructions are performed on a finite element mesh consisting of about 2000 triangles and a discrete ordinate set with 64 directions. For the absorption and scattering coefficients that are known, we take

$$\sigma_{a,xi} = \sigma_{a,m} = \sigma_a^b \left(2 - (\lfloor 2x \rfloor + \lfloor 2y \rfloor \mod 2)\right), \tag{3.72}$$

$$\sigma_{s,x} = \sigma_{s,m} = \sigma_s^b \left(1 + (\lfloor 2x \rfloor + \lfloor 2y \rfloor \mod 2)\right), \tag{3.73}$$

where $\lfloor \cdot \rfloor$ represents the floor operation, $\sigma_a^b$ and $\sigma_s^b$ are respectively the base level absorption and scattering coefficients. In all the cases below, we set $\sigma_a^b = 0.1$. The value of $\sigma_s^b$ varies from case to case and will be given below; see Fig. 3.1 (i) and (ii) for plots of the two coefficients. The scattering kernel $\Theta$ is set to be the Henyey-Greenstein phase function [12, 55, 113] which depends only on the product $\mathbf{v} \cdot \mathbf{v}'$.

To generate synthetic data for the nonlinear inversions, we solve the transport system (3.1) with true quantum efficiency $\eta$ and fluorescent absorption coefficient $\sigma_{a,xf}$ and compute $H$ according to (3.3). To generate synthetic

data for linearized inversions, for instance in Experiment 3 below, we use directly the linearized data models, for instance (3.55), with the true coefficient perturbations. This way, we can exclude the linearization error from the data used in the inversion. We do this since our main aim is to test the performance of the reconstruction algorithms, not to check the accuracy of the linearizations. To mimic noisy measurements, we add additive random noise to the synthetic data by multiplying each datum point by $(1+\gamma\times 10^{-2}\texttt{normrnd})$ with `normrnd` a standard Gaussian random variable and $\gamma$ a number representing the noise level in percentage. When $\gamma = 0$, we say the data are noise-free.

To measure the quality of the reconstruction, we use the relative $L^2$ error. This error is defined as the $L^2$ norm of the difference between the reconstructed coefficient and the true coefficient, divided by the $L^2$ norm of the true coefficient and then multiplied by 100.

We performed numerical simulations on the reconstructions of many different coefficients pairs $(\eta, \sigma_{a,xf})$. The qualities of the the reconstructions are very similar. To avoid repetition, we will present only reconstructions for a typical coefficient pair we show in (iii)-(iv) of Fig. 3.1.

**Experiment 1.** In the first set of numerical studies, we consider the reconstruction of the quantum efficiency $\eta$ assuming that the fluorescent absorption coefficient $\sigma_{a,xf}$ is known. We use the Reconstruction Algorithm I presented in Section 3.3.1. We first perform numerical experiments in isotropic medium with two different strengths of scattering coefficients. We show in Fig. 3.2 the

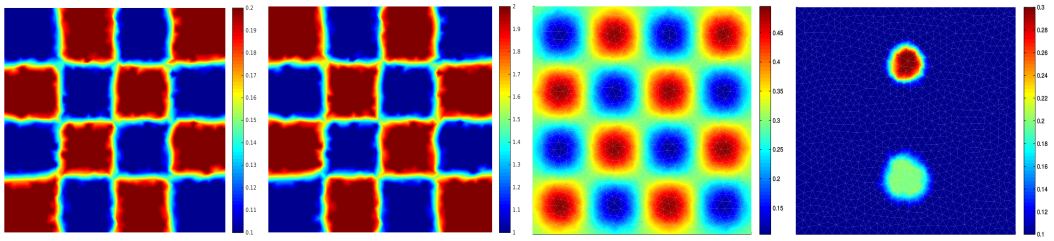

Figure 3.1: From left to right are: (i) the absorption coefficient $\sigma_{a,xi} = \sigma_{a,m}$ defined in (3.72) with $\sigma_a^b = 0.1$, (ii) the scattering coefficient $\sigma_{s,x} = \sigma_{s,m}$ defined in (3.73) with $\sigma_s^b = 2.0$, (iii) the true quantum efficiency $\eta$ to be reconstructed in the numerical experiments, and (iv) the true fluorescence absorption coefficient $\sigma_{a,xf}$ to be reconstructed.

reconstructions of $\eta$ under base scattering $\sigma_s^b = 1.0$. Shown from left to right are respectively the $\eta$ reconstructed using data with noise level $\gamma = 0$, 2, 5 and 10 respectively. The relative $L^2$ errors in the reconstructions are respectively 0.01%, 14.24%, 35.59% and 71.18%. We repeat the simulations for a medium with stronger (but still isotropic) scattering ($\sigma_s^b = 9.0$). The results are shown in Fig. 3.3. The relative $L^2$ errors in this case are 1.04%, 14.84%, 37.02% and 74.02% respectively. If we compare the results in Fig. 3.2 and those in Fig. 3.3, we see that the quality of the reconstructions are almost independent of the scattering strength. This is what we observed in our numerical experiments in other cases as well.

**Experiment 2.** In the second set of numerical studies, we consider the reconstruction of the fluorescent absorption coefficient $\sigma_{a,xf}$ assuming that the quantum efficiency $\eta$ is known. Currently, we do not have a well-established method to construct illuminations sources such that the condition $u_x = K_I(u_x)$

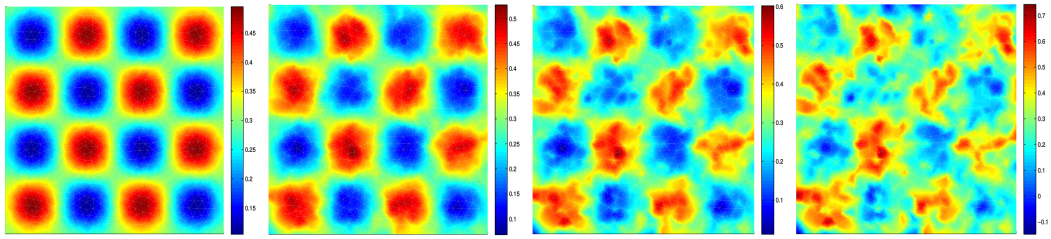

Figure 3.2: The quantum efficiency $\eta$ reconstructed with different types of data. The noise levels in the data used for the reconstructions, from left to right are $\gamma = 0,\ 2,\ 5$ and 10 respectively. The base scattering strength is $\sigma_s^b = 1.0$.

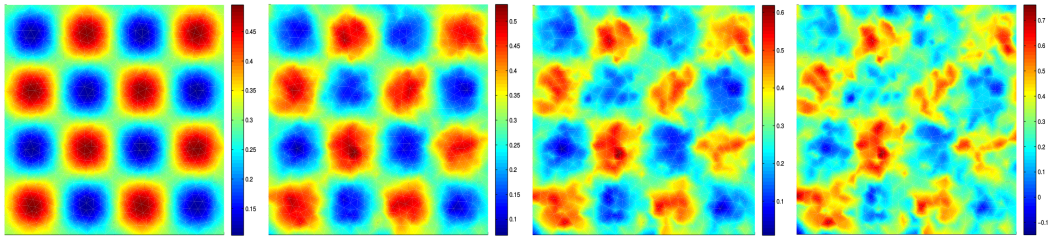

Figure 3.3: Same as in Fig. 3.2 but with base scattering strength $\sigma_s^b = 9.0$.

is satisfied for the transport solution, besides in non-scattering media. We therefore can not use directly the Reconstruction Algorithm II as we commented before. Instead, we use the nonlinear reconstruction algorithm in Section 3.4.4. We show in Fig. 3.4 the reconstructions of $\sigma_{a,xf}$ in an isotropic medium with base scattering strength $\sigma_s^b = 1.0$. Shown from left to right are respectively the reconstructions using data with noise levels $\gamma = 0$, 2, 5 and 10. The relative $L^2$ errors in the four reconstructions are 0.01%, 6.42%,16.06% and 32.12% respectively. In Fig. 3.5, we show the same reconstructions in an anisotropic scattering medium with base scattering strength $\sigma_s^b = 9.0$ and anisotropic factor 0.9. The relative $L^2$ errors are 0.02%,6.70%,16.74% and 33.42%, respectively. We again observed that the reconstructions are of good quality with data contains reasonably low level of random noise.

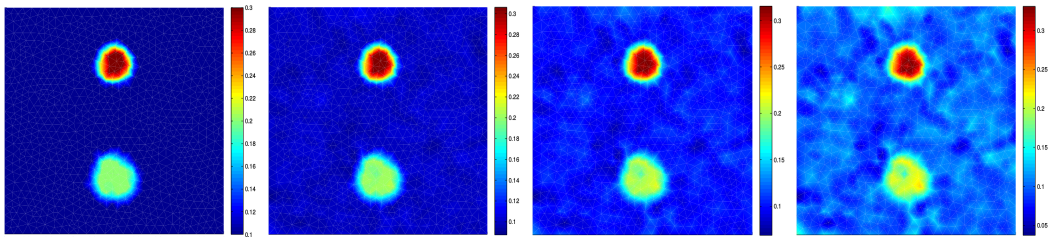

Figure 3.4: The fluorescence absorption coefficient $\sigma_{a,xf}$ reconstructed with different types of data. The noise level in the data used for the reconstructions, from left to right are: $\gamma = 0$ (noise-free), $\gamma = 2$, $\gamma = 5$, and $\gamma = 10$. The base scattering strength is $\sigma_s^b = 1.0$.

**Experiment 3.** In the third set of numerical simulations, we study the simultaneous reconstruction of the coefficients $\eta$ and $\sigma_{a,xf}$ in the linearized setting

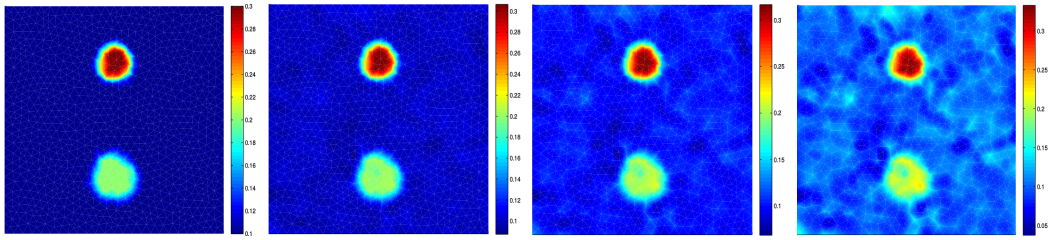

Figure 3.5: Same as in Fig. 3.4 but in a medium of anisotropic scattering with base scattering strength $\sigma_s^b = 9.0$ and anisotropic factor 0.9.

described in Section 3.4.3 using the Reconstruction Algorithm III. The synthetic perturbed data are generated using directly the linearized model (3.55), not the original nonlinear model. Our aim here is to test the stability of the reconstruction, not the accuracy of the linearization. We use data sets collected from four angularly-resolved illuminations supported respectively on the four sides of the boundaries of the domain, pointing toward the interior of the domain. The background scattering strength is $\sigma_s^b = 1.0$. We linearize the problem around the background coefficients:

$$\eta^0 = \frac{1}{|\Omega|}\int_\Omega \eta(\mathbf{x})d\mathbf{x} \quad \text{and} \quad \sigma_{a,xf}^0 = \frac{1}{|\Omega|}\int_\Omega \sigma_{a,xf}(\mathbf{x})d\mathbf{x}.$$

The reconstructions, after adding back the background, are shown in Fig. 3.6. The relative $L^2$ error in the reconstructions using data with noise level $\gamma = 0$, $\gamma = 2$, $\gamma = 5$ and $\gamma = 10$ are respectively $(0.00\%, 0.00\%)$, $(14.65\%, 7.45\%)$, $(37.28\%, 18.77\%)$ and $(75.80\%, 39.04\%)$ respectively. In all reconstructions, we applied the Tikhonov regularization with a small regularization strength that we select by trial and errors. We hope to develop more systematical strategy on regularization in the future.

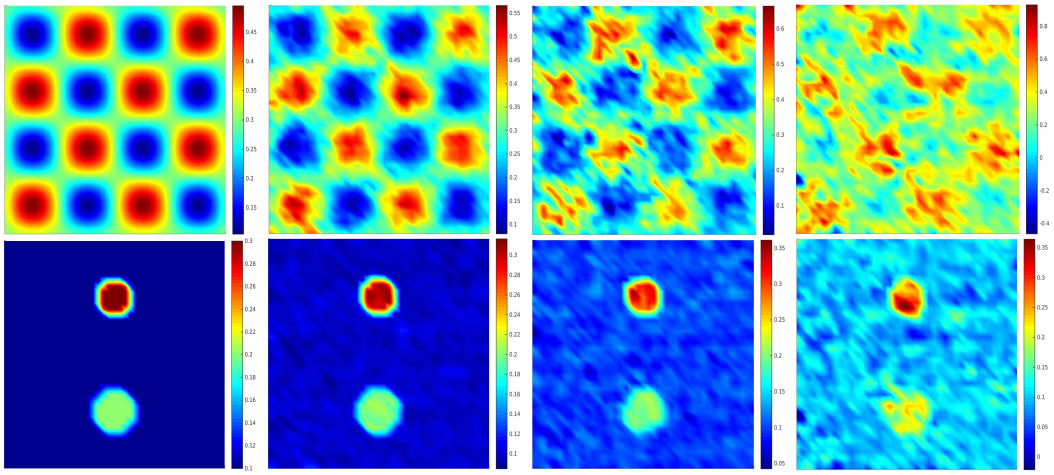

Figure 3.6: Simultaneous reconstructions of the coefficient pair $(\eta, \sigma_{a,xf})$ in the linearized setting with different types of data. The noise level in the data used for the reconstructions are (from left to right): $\gamma = 0$, 2, 5 and 10 respectively. The base scattering strength is $\sigma_s^b = 1.0$.

**Experiment 4.** The last set of numerical simulations are devoted to the simultaneous reconstructions of the coefficient pair $(\eta, \sigma_{a,xf})$ in the fully nonlinear setting. We use the optimization-based reconstruction algorithm developed in Section 3.4.4. The setup is the same as in Experiment 3. We performed reconstructions with data containing various noise levels. When the noise level is too high, we have difficulties to find reasonable initial guesses to make the algorithm converge. We show in Fig. 3.7 reconstructions with data containing a small amount of noise, $\gamma = 0$, 1 and 2 respectively, with the initial guess $(\eta^0, \sigma_{a,xf}^0)$ being the average of the true coefficients inside the domain. The relative $L^2$ error in the reconstructions are respectively $(16.40\%, 8.32\%)$, $(18.26\%, 9.17\%)$ and $(23.26\%, 19.30\%)$ respectively. We again impose weak Tikhonov regularizations in all the reconstructions with the regularization

strengths selected by trial and error. Tuning various parameters in the algorithm could potentially improve the reconstructions results, but we did not pursue in that direction.

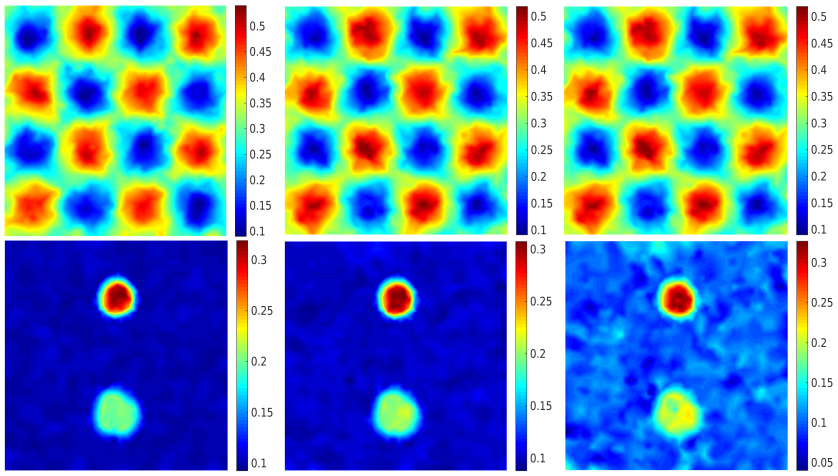


Figure 3.7: Simultaneous reconstruction of the coefficient pair $(\eta, \sigma_{a,xf})$ in the nonlinear setting with different types of data. The noise level in the data used for the reconstructions, from left to right, are respectively $\gamma = 0$, 1 and 2.

## 3.6 Concluding Remarks

We studied in this work a few inverse problems in quantitative fluorescence photoacoustic tomography in the radiative transport regime. We derived some uniqueness and stability results on the reconstruction of the fluorescence absorption coefficient and the quantum efficiency of the medium. In some cases, we were also able to develop efficient numerical reconstruction algorithms. These results complement the results in [92] for the QfPAT problem in the diffusive regime. We showed numerical simulations based on synthetic

data to support the mathematical analysis and demonstrate the performance of some of the reconstruction algorithms.

One important application of the results in this chapter is in X-ray modulated fluorescence tomography (or X-ray luminescence tomography (XLT)) [97]. In XLT, X-rays, instead of NIR photons, are used to excite the molecular markers. The X-ray density $u_x$ and the generated NIR photon densities $u_m$ solve the coupled transport system (3.1) with the scattering term $K_\Theta(u_x) = 0$ since X-rays travel in straight lines without being scattered. The theory and reconstruction methods we developed in this work remain valid in that case. In other words, we can recover stably the fluorescence absorption coefficient using data collected from one X-ray illumination. This would provide a useful alternative to the reconstruction method for XLT in [97].

Even though the QfPAT problem has been analyzed in detail in [92] in the diffusive regime, the developments in this work are still useful in many settings. One well-known example is the application in optical imaging of small animals [56] where the diffusion model is not sufficiently accurate to describe the propagation of NIR photons inside the animals.

Our main research focus in near future is to analyze the uniqueness and stability properties of the simultaneous reconstruction problem, i.e. the problem of reconstructing the pair $(\eta, \sigma_{a,xf})$, in the fully nonlinear setting. This is an unsolved problem even in the diffusive regime [92], although numerical simulations we have so far suggested that uniqueness and stability both hold, at least in the regime where both coefficients are sufficiently large.

# Chapter 4

# Summary and Perspectives

In this dissertation, we studied, mathematically and computationally, two hybrid inverse problems in photoacoustics for molecular imaging: quantiative two-photon PAT and quantitative fluorescence PAT. Our main objective was to reconstruct optical properties of tissues from interior data of absorption energy inferred from ultrasound data.

## 4.1 Summary of Main Results

In Chapter 2, we studied an inverse coefficient problem for a semilinear diffusion equation which models the optical propagation with two-photon absorption in the diffusion regime. We obtained positivity and comparative results on the solutions to the semilinear diffusion equation using standard theory of partial differential equations. Based on these results, we presented uniqueness and stability results on reconstructing the single-photon and two-photon absorption coefficients. We also proposed a direct method for simultaneous reconstruction of the two coefficients. We then studied the problem of reconstructing the diffusion coefficient along with the two optical absorption coefficients in the linearized setting. We obtained uniqueness and stability

based on the construction of CGO solutions and classical results on elliptic systems. We also showed non-uniqueness results on reconstructing the diffusion coefficient, Grüneisen coefficient along with the two optical absorption coefficients. We performed numerical experiments on reconstructing the two optical absorption coefficients to demonstrate the theoretical results. The semilinear equation is discretized using finite element methods in 2-D and solved using a quasi-Newton method based on the variational formulation of the problem. To complement the direct method we proposed, we also performed experiments using optimization based reconstruction method. The optimization algorithm is implemented with limited memory BFGS.

In Chapter 3, we studied an inverse coefficient problem to a system of radiative transport equations with interior data, where we intend to reconstruct the optical absorption coefficient and quantum efficiency of the medium. We obtained uniqueness and stability results for reconstructing a single coefficient. We proposed direct reconstruction method for quantum efficiency. We also obtained direct reconstruction for optical absorption coefficient in the linearized setting. We studied the problem of reconstructing simultaneously the two coefficient in the fully and partially linearized setting and proposed regularized reconstruction methods. We then derived optimization based reconstruction methods in the nonlinear case. For numerical experiments, we discretized the radiative transport equation with discrete ordinate method and finite element method in 2-D. We solved nonlinear optimization problem with a BFGS type quasi-Newton method. Numerical simulations demonstrate that

the inverse problem of recovering a single coefficient in nonlinear setting and two coefficients in linearized setting is stable.

## 4.2 Perspectives on Future Work

The results we obtained in this dissertation are the first ones on these hybrid inverse problems. Many results can be improved and many new directions of research should be pursued to further understand these inverse problems, as well as the physical ability of the corresponding imaging modalities.

On the two-photon PAT inverse problem, it is important to generalize our results on the simultaneous reconstruction of multiple (more than two) parameters to the fully nonlinear setting. Moreover, one should be able to generalize the results in [21] on PAT with multispectral data to the two-photon problem to reconstruct all four coefficients in the model which we have shown that is impossible to do without multispectral data. For applications of two-photon PAT in less diffusive media, it is important to see if we can derive similar uniqueness and stability results for the same problem in the radiative transport regime. A starting point in this direction would be to construct a nonlinear transport model that is similar to the semilinear diffusion model (2.1). From the practical point of view, it is of great importance to develop a computational method for image reconstruction in three-dimensional setting, starting with the measured acoustic data.

On fluorescence PAT, uniquness and stability theory for the simulta-

neous reconstruction of the pair $(\eta, \sigma_{a,xf})$, when both coefficients are large enough, in fully nonlinear setting is still missing, in both the diffusive regime and the transport regime. It is also useful to consider the case where the Grüneisen coefficient is an unknown to be reconstructed as well. In general, we would expect that multispectral data are needed in order to have uniqueness of reconstructions. From the computational point of view, the transport model we have for fPAT is extremely expensive to solve numerically. Therefore, image reconstructions based on iterative schemes are very time-consuming. It would be very important to try to develop fast transport solvers for such inverse problems, for instance following the line of work in [91]. From the application point of view, it is of great interest to develop a mathematical theory for fluorescence PAT with two-photon fluorescence generations. In this case, a quadratic term of the form $\eta\mu[K_I(u_x)]^2$ will need to be added to the right of the second equation in the model (3.1). We expect that the results we developed in the dissertation can be generalized to this problem.

# Bibliography


[1] S. Acosta. Time reversal for radiative transport with applications to inverse and control problems. *Inverse Problems*, 29, 2013. 085014.

[2] V. Agoshkov. *Boundary Value Problems for the Transport Equations*. Birkhauser, Boston, 1998.

[3] V. I. Agoshkov and C. Bardos. Optimal control approach in inverse radiative transfer problems: The problem on boundary function. *ESAIM: Control, Optimisation and Calculus of Variations*, 5:259–278, 2000.

[4] M. Agranovsky, P. Kuchment, and L. Kunyansky. On reconstruction formulas and algorithms for the thermoacoustic tomography. In L. V. Wang, editor, *Photoacoustic Imaging and Spectroscopy*, pages 89–101. CRC Press, 2009.

[5] G. Alessandrini, M. Di Cristo, E. Francini, and S. Vessella. Stability for quantitative photo acoustic tomography with well-chosen illuminations. *Annali di Matematica*, 196:395–406, 2017.

[6] D. Álvarez, P. Medina, and M. Moscoso. Fluorescence lifetime imaging from time resolved measurements using a shape-based approach. *Optics Express*, 17:8843–8855, 2009.

[7] A. Ambrosetti and A. Malchiodi. *Nonlinear Analysis and Semilinear Elliptic Problems*. Cambridge University Press, Cambridge, 2007.

[8] H. Ammari, E. Bossy, V. Jugnon, and H. Kang. Mathematical modelling in photo-acoustic imaging of small absorbers. *SIAM Rev.*, 52:677–695, 2010.

[9] H. Ammari, E. Bossy, V. Jugnon, and H. Kang. Reconstruction of the optical absorption coefficient of a small absorber from the absorbed energy density. *SIAM J. Appl. Math.*, 71:676–693, 2011.

[10] H. Ammari, E. Bretin, V. Jugnon, and A. Wahab. Photo-acoustic imaging for attenuating acoustic media. In H. Ammari, editor, *Mathematical Modeling in Biomedical Imaging II*, volume 2035 of *Lecture Notes in Mathematics*, pages 53–80. Springer-Verlag, 2012.

[11] H. Ammari, J. Garnier, and L. Giovangigli. Mathematical modeling of fluorescence diffuse optical imaging of cell membrane potential changes. *Quarterly of Applied Mathematics*, 72:137–176, 2014.

[12] S. R. Arridge. Optical tomography in medical imaging. *Inverse Probl.*, 15:R41–R93, 1999.

[13] S. R. Arridge and J. C. Schotland. Optical tomography: forward and inverse problems. *Inverse Problems*, 25, 2009. 123010.

[14] M. Badiale and E. Serra. *Semilinear Elliptic Equations for Beginners*. Springer, London, 2011.

[15] G. Bal. Inverse transport theory and applications. *Inverse Problems*, 25, 2009. 053001.

[16] G. Bal. Introduction to Inverse Problems. Department of Applied Physics and Applied Mathematics, Columbia University, 2012.

[17] G. Bal. Hybrid inverse problems and redundant systems of partial differential equations. In P. Stefanov, A. Vasy, and M. Zworski, editors, *Inverse Problems and Applications*, volume 615 of *Contemporary Mathematics*, pages 15–48. American Mathematical Society, 2013.

[18] G. Bal, A. Jollivet, and V. Jugnon. Inverse transport theory of photoacoustics. *Inverse Problems*, 26, 2010. 025011.

[19] G. Bal and K. Ren. Multi-source quantitative PAT in diffusive regime. *Inverse Problems*, 27, 2011. 075003.

[20] G. Bal and K. Ren. Non-uniqueness result for a hybrid inverse problem. In G. Bal, D. Finch, P. Kuchment, J. Schotland, P. Stefanov, and G. Uhlmann, editors, *Tomography and Inverse Transport Theory*, volume 559 of *Contemporary Mathematics*, pages 29–38. Amer. Math. Soc., Providence, RI, 2011.

[21] G. Bal and K. Ren. On multi-spectral quantitative photoacoustic tomography in diffusive regime. *Inverse Problems*, 28, 2012. 025010.

[22] G. Bal and G. Uhlmann. Inverse diffusion theory of photoacoustics. *Inverse Problems*, 26, 2010. 085010.

[23] B. Banerjee, S. Bagchi, R. M. Vasu, and D. Roy. Quatitative photoacoustic tomography from boundary pressure measurements: noniterative recovery of optical absorption coefficient from the reconstructed absorbed energy map. *J. Opt. Soc. Am. A*, 25:2347–2356, 2008.

[24] P. Beard. Biomedical photoacoustic imaging. *Interface Focus*, 1:602–631, 2011.

[25] F. Bouchut and G. Crippa. Uniqueness, renormalization and smooth approximations for linear transport equations. *SIAM J. Math. Anal.*, 38:1316–1328, 2006.

[26] P. Burgholzer, H. Grun, and A. Sonnleitner. Photoacoustic tomography: Sounding out fluorescent proteins. *Nat. Photon.*, 3:378379, 2009.

[27] P. Burgholzer, G. J. Matt, M. Haltmeier, and G. Paltauf. Exact and approximative imaging methods for photoacoustic tomography using an arbitrary detection surface. *Phys. Rev. E*, 75, 2007. 046706.

[28] F. Colombini, G. Crippa, and J. Rauch. A note on two-dimensional transport with bounded divergence. *Comm. Partial Differential Equations*, 31:1109–1115, 2006.

[29] B. T. Cox, S. R. Arridge, and P. C. Beard. Photoacoustic tomography with a limited-aperture planar sensor and a reverberant cavity. *Inverse Problems*, 23:S95–S112, 2007.

[30] B. T. Cox, S. R. Arridge, and P. C. Beard. Estimating chromophore distributions from multiwavelength photoacoustic images. *J. Opt. Soc. Am. A*, 26:443–455, 2009.

[31] B. T. Cox, S. R. Arridge, K. P. Köstli, and P. C. Beard. Two-dimensional quantitative photoacoustic image reconstruction of absorption distributions in scattering media by use of a simple iterative method. *Applied Optics*, 45:1866–1875, 2006.

[32] B. T. Cox, J. G. Laufer, and P. C. Beard. The challenges for quantitative photoacoustic imaging. *Proc. of SPIE*, 7177, 2009. 717713.

[33] B. T. Cox, T. Tarvainen, and S. R. Arridge. Multiple illumination quantitative photoacoustic tomography using transport and diffusion models. In G. Bal, D. Finch, P. Kuchment, J. Schotland, P. Stefanov, and G. Uhlmann, editors, *Tomography and Inverse Transport Theory*, volume 559 of *Contemporary Mathematics*, pages 1–12. Amer. Math. Soc., Providence, RI, 2011.

[34] R. Dautray and J.-L. Lions. *Mathematical Analysis and Numerical Methods for Science and Technology, Vol VI.* Springer-Verlag, Berlin, 1993.

[35] R. J. DiPerna and P.-L. Lions. On the Cauchy problem for Boltzmann equations: global existence and weak stability. *Ann. Math.*, 130:321–366, 1989.

[36] A. Douglis and L. Nirenberg. Interior estimates for elliptic system of partial differential equations. *Comm. Pure Appl. Math.*, 8:503–508, 1955.

[37] P. Elbau, O. Scherzer, and R. Schulze. Reconstruction formulas for photoacoustic sectional imaging. *Inverse Problems*, 28, 2012. 045004.

[38] H. W. Engl, M. Hanke, and A. Neubauer. *Regularization of Inverse Problems*. Kluwer Academic Publishers, Dordrecht, The Netherlands, 1996.

[39] L. C. Evans. *Partial Differential Equations*. American Mathematical Society, Providence, RI, 2010.

[40] D. Finch, M. Haltmeier, and Rakesh. Inversion of spherical means and the wave equation in even dimensions. *SIAM J. Appl. Math.*, 68:392–412, 2007.

[41] D. Finch and Rakesh. The spherical mean operator with centers on a sphere. *Inverse Problems*, 35:S37–S50, 2007.

[42] S. K. Finch, D. Patch, and Rakesh. Determining a function from its mean values over a family of spheres. *SIAM J. Math. Anal.*, 35:1213–1240, 2004.

[43] A. R. Fisher, A. J. Schissler, and J. C. Schotland. Photoacoustic effect for multiply scattered light. *Phys. Rev. E*, 76, 2007. 036604.

[44] H. Gao, S. Osher, and H. Zhao. Quantitative photoacoustic tomography. In H. Ammari, editor, *Mathematical Modeling in Biomedical Imaging II: Optical, Ultrasound, and Opto-Acoustic Tomographies*, volume 2035 of *Lecture Notes in Mathematics*, pages 131–158. Springer, 2012.

[45] H. Gao, H. Zhao, and S. Osher. Bregman methods in quantitative photoacoustic tomography. CAM Report 10-42, UCLA, 2010.

[46] D. Gilbarg and N. S. Trudinger. *Elliptic Partial Differential Equations of Second Order*. Springer-Verlag, Berlin, 2000.

[47] A. Godavartya, E. M. Sevick-Muraca, and M. J. Eppstein. Three-dimensional fluorescence lifetime tomography. *Med. Phys.*, 32:992–1000, 2005.

[48] F. Golse, P.-L. Lions, B. Perthame, and R. Sentis. Regularity of the moments of the solution of a transport equation. *J. Func. Anal.*, 76:110–125, 1988.

[49] W. Greeberg and S. Sancaktar. Solution of the multigroup transport equations in $L^p$ spaces. *J. Math. Phys.*, 17:2092–2097, 1976.

[50] M. Haltmeier. A mollification approach for inverting the spherical mean Radon transform. *SIAM J. Appl. Math.*, 71:1637–1652, 2011.

[51] M. Haltmeier, O. Scherzer, P. Burgholzer, and G. Paltauf. Thermoacoustic computed tomography with large planer receivers. *Inverse Problems*, 20:1663–1673, 2004.

[52] M. Haltmeier, T. Schuster, and O. Scherzer. Filtered backprojection for thermoacoustic computed tomography in spherical geometry. *Math. Methods Appl. Sci.*, 28:1919–1937, 2005.

[53] Q. Han and F. Lin. *Elliptic Partial Differential Equations*. American Mathematical Society, Providence, 1997.

[54] M. Hauray. On two-dimensional Hamiltonian transport equations with $l^p_{\text{loc}}$ coefficients. *Ann. IHP. Anal. Non Lin.*, 20:625–644, 2003.

[55] L. G. Henyey and J. L. Greenstein. Diffuse radiation in the galaxy. *Astrophys. J.*, 90:70–83, 1941.

[56] A. H. Hielscher. Optical tomographic imaging of small animals. *Current Opinion in Biotechnology*, 16:79–88, 2005.

[57] Y. Hristova. Time reversal in thermoacoustic tomography - an error estimate. *Inverse Problems*, 25, 2009. 055008.

[58] Y. Hristova, P. Kuchment, and L. Nguyen. Reconstruction and time reversal in thermoacoustic tomography in acoustically homogeneous and inhomogeneous media. *Inverse Problems*, 24, 2008. 055006.

[59] T. Kato. *Perturbation Theory for Linear Operators*. Springer-Verlag, Berlin, 2013.

[60] A. Kirsch. *An Introduction to the Mathematical Theory of Inverse Problems*. Springer-Verlag, New York, second edition, 2011.

[61] A. Kirsch and O. Scherzer. Simultaneous reconstructions of absorption density and wave speed with photoacoustic measurements. *SIAM J. Appl. Math.*, 72:1508–1523, 2013.

[62] M. V. Klibanov and M. Yamamoto. Exact controllability of the time dependent transport equation. *SIAM J. Control Optim.*, 46:2071–2095, 2007.

[63] P. Kuchment and L. Kunyansky. Mathematics of thermoacoustic tomography. *Euro. J. Appl. Math.*, 19:191–224, 2008.

[64] P. Kuchment and L. Kunyansky. Mathematics of thermoacoustic and photoacoustic tomography. In O. Scherzer, editor, *Handbook of Mathematical Methods in Imaging*, pages 817–866. Springer-Verlag, 2010.

[65] P. Kuchment and D. Steinhauer. Stabilizing inverse problems by internal data. *Inverse Problems*, 28, 2012.

[66] A. T. N. Kumar, S. B. Raymond, A. K. Dunn, B. J. Bacskai, and D. A. Boas. A time domain fluorescence tomography system for small animal imaging. *IEEE Trans. Med. Imag.*, 27:1152–1163, 2008.

[67] L. Kunyansky. Explicit inversion formulae for the spherical mean Radon transform. *Inverse Problems*, 23:373–383, 2007.

[68] Y.-H. Lai, S.-Y. Lee, C.-F. Chang, Y.-H. Cheng, and C.-K. Sun. Nonlinear photoacoustic microscopy via a loss modulation technique: from detection to imaging. *Optics Express*, 22:525–536, 2014.

[69] G. Langer, K.-D. Bouchal, H. Grün, P. Burgholzer, and T. Berer. Two-photon absorption-induced photoacoustic imaging of Rhodamine B dyed polyethylene spheres using a femtosecond laser. *Optics Express*, 21:22410–22422, 2013.

[70] J. Laufer, B. T. Cox, E. Zhang, and P. Beard. Quantitative determination of chromophore concentrations from 2d photoacoustic images using a nonlinear model-based inversion scheme. *Applied Optics*, 49:1219–1233, 2010.

[71] C. Li and L. Wang. Photoacoustic tomography and sensing in biomedicine. *Phys. Med. Biol.*, 54:R59–R97, 2009.

[72] A. V. Mamonov and K. Ren. Quantitative photoacoustic imaging in radiative transport regime. *Comm. Math. Sci.*, 12:201–234, 2014.

[73] M. Mokhtar-Kharroubi, editor. *Mathematical Topics in Neutron Transport Theory: New Aspects*. World Scientific, Singapore, 1997.

[74] L. V. Nguyen. A family of inversion formulas in thermoacoustic tomography. *Inverse Probl. Imaging*, 3:649–675, 2009.

[75] J. M. Ortega. The Newton-Kantorovich theorem. *Amer. Math. Monthly*, 75:658–666, 1968.

[76] G. Paltauf, R. Nuster, M. Haltmeier, and P. Burgholzer. Photoacoustic tomography with integrating area and line detectors. In L. V. Wang,

editor, *Photoacoustic Imaging and Spectroscopy*, pages 251–263. CRC Press, 2009.

[77] G. Y. Panasyuk, Z.-M. Wang, J. C. Schotland, and V. A. Markel. Fluorescent optical tomography with large data sets. *Opt. Lett.*, 33:1744–1746, 2008.

[78] S. K. Patch and O. Scherzer. Photo- and thermo- acoustic imaging. *Inverse Problems*, 23:S1–S10, 2007.

[79] M. S. Patterson and B. W. Pogue. Mathematical model for time-resolved and frequency-domain fluorescence spectroscopy in biological tissues. *Appl. Opt.*, 33:1963–1974, 1994.

[80] A. Pulkkinen, B. T. Cox, S. R. Arridge, J. P. Kaipio, and T. Tarvainen. A Bayesian approach to spectral quantitative photoacoustic tomography. *Inverse Problems*, 30, 2014. 065012.

[81] J. Qian, P. Stefanov, G. Uhlmann, and H. Zhao. An efficient Neumann-series based algorithm for thermoacoustic and photoacoustic tomography with variable sound speed. *SIAM J. Imaging Sci.*, 4:850–883, 2011.

[82] D. Razansky, M. Distel, C. Vinegoni, R. Ma, N. Perrimon, R. W. Köster, and V. Ntziachristos. Multispectral opto-acoustic tomography of deep-seated fluorescent proteins in vivo. *Nature Photonics*, 3:412–417, 2009.

[83] D. Razansky and V. Ntziachristos. Hybrid photoacoustic fluorescence molecular tomography using finite-element-based inversion. *Med. Phys.*, 34:4293–4301, 2007.

[84] K. Ren. Recent developments in numerical techniques for transport-based medical imaging methods. *Commun. Comput. Phys.*, 8:1–50, 2010.

[85] K. Ren. Existence and uniqueness of $L^p$ solutions to a radiative transport system. *Preprint*, 2015.

[86] K. Ren, G. Bal, and A. H. Hielscher. Frequency domain optical tomography based on the equation of radiative transfer. *SIAM J. Sci. Comput.*, 28:1463–1489, 2006.

[87] K. Ren, G. Bal, and A. H. Hielscher. Transport- and diffusion-based optical tomography in small domains: A comparative study. *Applied Optics*, 46:6669–6679, 2007.

[88] K. Ren, H. Gao, and H. Zhao. A hybrid reconstruction method for quantitative photoacoustic imaging. *SIAM J. Imag. Sci.*, 6:32–55, 2013.

[89] K. Ren and R. Zhang. Nonlinear quantitative photoacoustic tomography with two-photon absorption. *SIAM J. Appl. Math.*, 77, 2017.

[90] K. Ren, R. Zhang, and Y. Zhong. Inverse transport problems in quantitative PAT for molecular imaging. *Inverse Problems*, 31, 2015. 125012.

[91] K. Ren, R. Zhang, and Y. Zhong. A fast algorithm for radiative transport in isotropic media. *arXiv:1610.00835*, 2016.

[92] K. Ren and H. Zhao. Quantitative fluorescence photoacoustic tomography. *SIAM J. Imag. Sci.*, 6:2024–2049, 2013.

[93] J. Ripoll and V. Ntziachristos. Quantitative point source photoacoustic inversion formulas for scattering and absorbing media. *Phys. Rev. E*, 71, 2005. 031912.

[94] T. Saratoon, T. Tarvainen, B. T. Cox, and S. R. Arridge. A gradient-based method for quantitative photoacoustic tomography using the radiative transfer equation. *Inverse Problems*, 29, 2013. 075006.

[95] V. A. Solonnikov. Overdetermined elliptic boundary-value problems. *J. Sov. Math.*, 1:477–512, 1973.

[96] V. Y. Soloviev, K. B. Tahir, J. McGinty, D. S. Elson, M. A. A. Neil, P. M. W. French, and S. R. Arridge. Fluorescence lifetime imaging by using time gated data acquisition. *Applied Optics*, 46:7384–7391, 2007.

[97] P. Stefanov, W. Cong, and G. Wang. Modulated luminescence tomography. *Inverse Problems and Imaging*, 9:551–578, 2015.

[98] P. Stefanov and G. Uhlmann. Thermoacoustic tomography with variable sound speed. *Inverse Problems*, 25, 2009. 075011.

[99] D. Steinhauer. A reconstruction procedure for thermoacoustic tomography in the case of limited boundary data. *arXiv:0905.2954*, 2009.

[100] D. Steinhauer. A uniqueness theorem for thermoacoustic tomography in the case of limited boundary data. *arXiv:0902.2838v2*, 2009.

[101] J. Sylvester and G. Uhlmann. Global uniqueness theorem for an inverse boundary value problem. *Ann. Math.*, 125:153–169, 1987.

[102] J. Tervo. On coupled Boltzmann transport equation related to radiation therapy. *J. Math. Anal. Appl.*, 335:819–840, 2007.

[103] J. Tervo and P. Kokkonen. On existence of $L^1$-solutions for coupled Boltzmann transport equation and radiation therapy treatment optimization. *arXiv*, 2014. 1406.3228v1.

[104] J. Tittelfitz. Thermoacoustic tomography in elastic media. *Inverse Problems*, 28, 2012. 055004.

[105] F. Triki. Uniqueness and stability for the inverse medium problem with internal data. *Inverse Problems*, 26, 2010. 095014.

[106] G. J. Tserevelakis, D. Soliman, M. Omar, and V. Ntziachristos. Hybrid multiphoton and optoacoustic microscope. *Opt. Lett.*, 39:1819–1822, 2014.

[107] G. Uhlmann. Electrical impedance tomography and Calderon's problem. *Inverse Problems*, 25, 2009. 123011.

[108] B. E. Urban, J. Yi, V. Yakovlev, and H. F. Zhang. Investigating femtosecond-laser-induced two-photon photoacoustic generation. *J. Biomed. Opt.*, 19, 2014. 085001.

[109] B. Wang, Q. Zhao, N. M. Barkey, D. L. Morse, and H. Jiang. Photoacoustic tomography and fluorescence molecular tomography: A comparative study based on indocyanine green. *Med. Phys.*, 39:2512–2517, 2012.

[110] L. V. Wang. Tutorial on photoacoustic microscopy and computed tomography. *IEEE J. Sel. Topics Quantum Electron.*, 14:171–179, 2008.

[111] L. V. Wang. Photoacoustic tomography: Principles and advances. *Progress in Electromagnetics Research*, 147:1–22, 2014.

[112] Y. Wang, K. Maslov, C. Kim, S. Hu, and L. V. Wang. Integrated photoacoustic and fluorescence confocal microscopy. *IEEE Trans. Biomed. Eng.*, 57:2576–2578, 2010.

[113] A. J. Welch and M. J. C. Van-Gemert. *Optical-thermal Response of Laser Irradiated Tissue*. Plenum Press, New York, 1995.

[114] T. Widlak and O. Scherzer. Stability in the linearized problem of quantitative elastography. *Inverse Problems*, 31, 2015. 035005.

[115] B. L. Willis and C. V. M. van der Mee. Multigroup transport equations with nondiagonal cross-section matrices. *J. Math. Phys.*, 27:1633–1638, 1986.

[116] K. E. Wilson, T. Y. Wang, and J. K. Willmann. Acoustic and photoacoustic molecular imaging of cancer. *J. Nuclear Medicine*, 54:1851–1854, 2013.

[117] P. W. Winter, A. G. York, D. D. Nogare, M. Ingaramo, R. Christensen, A. Chitnis, G. H. Patterson, and H. Shroff. Two-photon instant structured illumination microscopy improves the depth penetration of super-resolution imaging in thick scattering samples. *Optica*, 1:181–191, 2014.

[118] Y. Yamaoka, M. Nambu, and T. Takamatsu. Frequency-selective multiphoton-excitation-induced photoacoustic microscopy (MEPAM) to visualize the cross sections of dense objects. In A. A. Oraevsky and L. V. Wang, editors, *Photons Plus Ultrasound: Imaging and Sensing*. SPIE, 2010. 75642O.

[119] Y. Yamaoka, M. Nambu, and T. Takamatsu. Fine depth resolution of two-photon absorption-induced photoacoustic microscopy using low-frequency bandpass filtering. *Optics Express*, 19:13365–13377, 2011.

[120] Y. Yamaoka and T. Takamatsu. Enhancement of multiphoton excitation-induced photoacoustic signals by using gold nanoparticles surrounded by fluorescent dyes. In A. A. Oraevsky and L. V. Wang, editors, *Photons Plus Ultrasound: Imaging and Sensing*. SPIE, 2009. 71772A.

[121] C. S. Yelleswarapu and S. R. Kothapalli. Nonlinear photoacoustics for measuring the nonlinear optical absorption coefficient. *Optics Express*, 18:9020–9025, 2010.

[122] Z. Yuan, Q. Wang, and H. Jiang. Reconstruction of optical absorption coefficient maps of heterogeneous media by photoacoustic tomography coupled with diffusion equation based regularized Newton method. *Optics Express*, 15:18076–18081, 2007.

[123] R. J. Zemp. Quantitative photoacoustic tomography with multiple optical sources. *Applied Optics*, 49:3566–3572, 2010.